



THE UNIVERSITY *of* EDINBURGH

Edinburgh Research Explorer

Detrital zircon geochronology and related evidence from clastic sediments in the Kyrenia Range, N Cyprus: Implications for the Mesozoic-Cenozoic erosional history and tectonics of southern Anatolia

Citation for published version:

Chen, G, Robertson, AHF & Wu, F 2022, 'Detrital zircon geochronology and related evidence from clastic sediments in the Kyrenia Range, N Cyprus: Implications for the Mesozoic-Cenozoic erosional history and tectonics of southern Anatolia', *Earth-Science Reviews*, vol. 233, 104167.
<https://doi.org/10.1016/j.earscirev.2022.104167>

Digital Object Identifier (DOI):

[10.1016/j.earscirev.2022.104167](https://doi.org/10.1016/j.earscirev.2022.104167)

Link:

[Link to publication record in Edinburgh Research Explorer](#)

Document Version:

Peer reviewed version

Published In:

Earth-Science Reviews

General rights

Copyright for the publications made accessible via the Edinburgh Research Explorer is retained by the author(s) and / or other copyright owners and it is a condition of accessing these publications that users recognise and abide by the legal requirements associated with these rights.

Take down policy

The University of Edinburgh has made every reasonable effort to ensure that Edinburgh Research Explorer content complies with UK legislation. If you believe that the public display of this file breaches copyright please contact openaccess@ed.ac.uk providing details, and we will remove access to the work immediately and investigate your claim.



Highlights

- Detrital zircon U-Pb and related analyses indicate the erosional history of S Anatolia
- The combined data indicate a switch from N to E sources related to Neogene collision
- The zircon and related data support tectonic development along N margin of S Neotethys

Abstract

Triassic to Pleistocene sandstones of the Kyrenia Range, N Cyprus provide an exceptional repository of the erosional history of Anatolia. The Kyrenia Range features in several different tectonic hypotheses of the Eastern Mediterranean region, which are tested here using a combination of new and recently published detrital zircon geochronology, zircon trace-element data and hafnium isotopic data. Minimum detrital zircon ages refine the ages of several formations in the Kyrenia Range. The new data also provide insights into sediment provenance including far-removed sources of Upper Paleozoic zircons, within-plate versus subduction-related sources (e.g., rift; oceanic/continental arc/ophiolite) and Neogene collision-related magmatism. Facies and paleocurrent data indicate a major switch in clastic sediment input from generally southwards to westwards during the Oligocene, which was mainly controlled by the collision of the Arabian promontory with Anatolia, leaving the S Neotethys as an isolated deep-water basin.

The U-Pb zircon age profiles indicate a prominent Late Neoproterozoic population, together with Carboniferous, Permian, Late Cretaceous and Miocene-aged clusters. Pan-African and Grenvillian-aged zircons were ultimately derived from Cadomian continental basement. Basement that rifted from Gondwana during the Triassic later became sources of detritus within Anatolia to the north. Devonian-Carboniferous zircons were originally supplied by active continental margin magmatism in southern Eurasia (Pontides) or

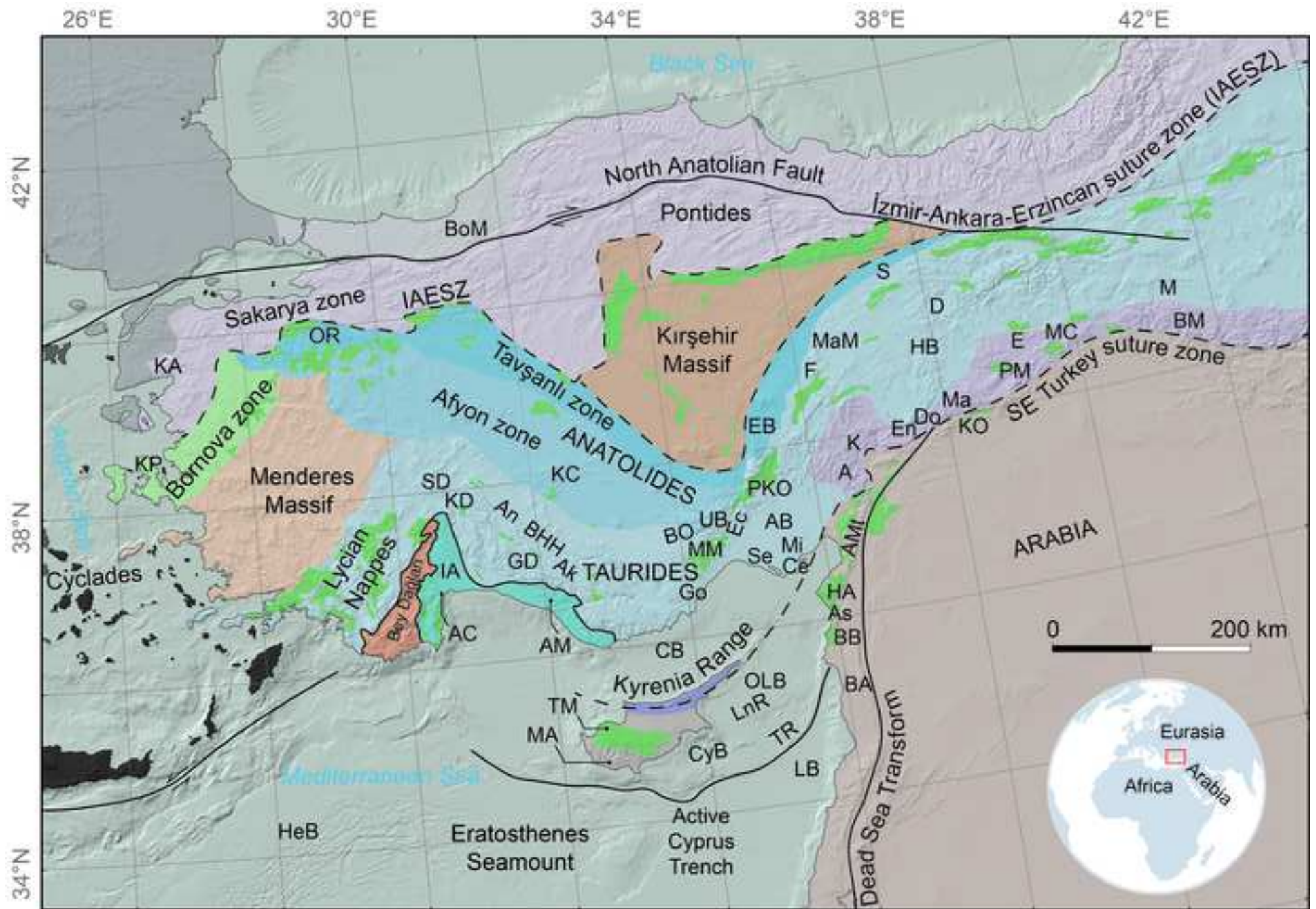
northern Gondwana (Afyon zone of the Anatolides). The proposed explanation is that detrital zircons were sequentially recycled, first to Upper Carboniferous-earliest Permian turbidites (within the Afyon zone to the east), later to Mid-Upper Triassic alluvium and turbidites (within the Taurides to the south), and finally to Triassic-Paleogene clastic sediments as now preserved in the Kyrenia Range. Upper Cretaceous zircons were derived from continental arc granitoids, oceanic arc and/or ophiolitic rocks and related metamorphic rocks, generally to the north of the Kyrenia Range. Paleogene zircons mainly represent late-stage continental margin arc magmatism in SE Turkey. During the Oligocene, the switch from mainly southward sediment supply to mainly westward sediment supply represents dominant input from the S Neotethyan suture zone in SE Turkey. Miocene zircons were mainly derived from post-collisional volcanics in SE Turkey. Paleoriver drainage systems in central/southeast Anatolia largely existed by the Late Miocene in response to collision-related surface uplift, in turn strongly influencing Miocene-Pleistocene zircon provenance in sub-basins within and adjacent to the Kyrenia Range.

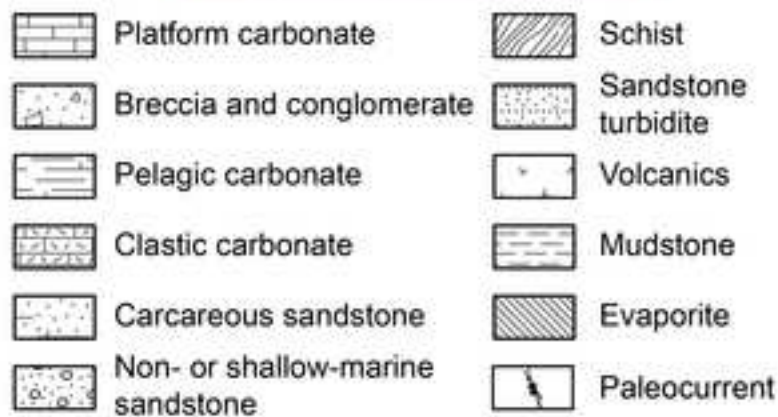
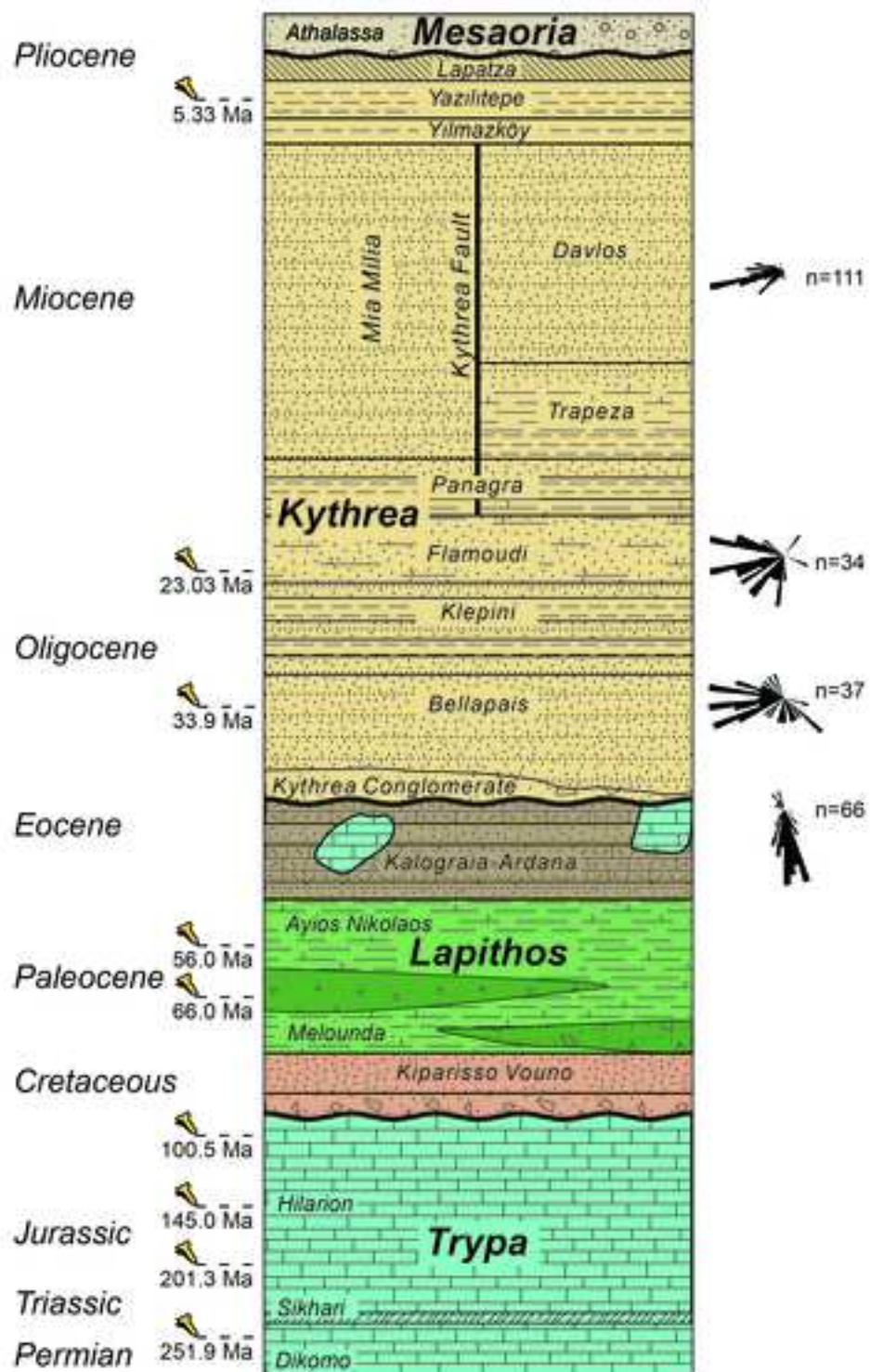
The combined zircon and Hf data, together with assembled geological evidence, are used to discuss three contrasting tectonic hypotheses for the early Mesozoic-Eocene setting of the Kyrenia Range: (1) locally, in the easternmost Mediterranean (i.e., preferred interpretation); (2) far to the south, on the N African passive margin, and (3) far to the north, along (or near) the Eurasian margin. Overall, the present study exemplifies the diversity and

complexity of clastic sediment sources within a developing orogen, with implications for some other regions.

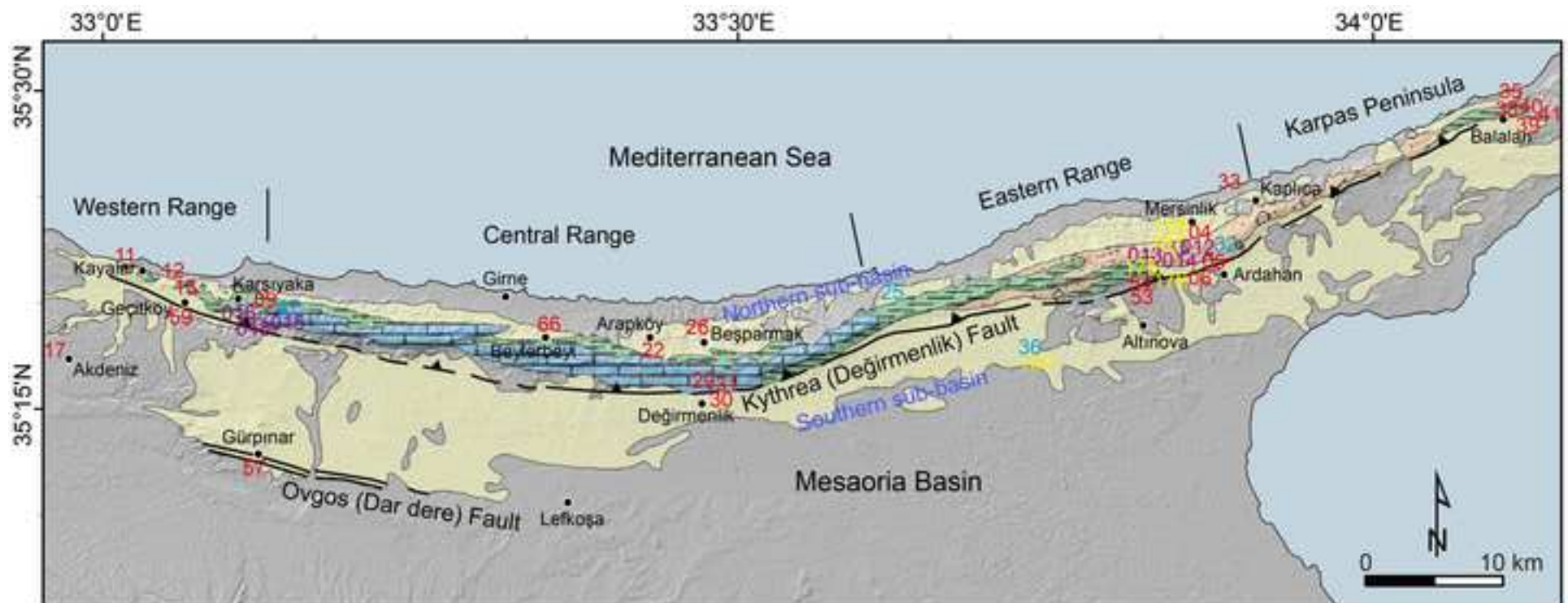
Figure 1

[Click here to access/download;Figure;Fig. 1.jpg](#)









- Pliocene-Quaternary, Shallow-marine and non-marine sediments
 - Late Eocene-Late Miocene, Mainly siliciclastic turbidites and mudrocks, Kythrea Group
 - Middle Eocene, Debris-flow deposits and detached blocks/sheets, Kalograia-Ardana Formation
 - Late Cretaceous-Early Eocene, Pelagic and redeposited carbonates; basaltic and felsic volcanic rocks
 - Triassic-Cretaceous, Shallow-water carbonates (marble and dolomite); minor meta-mudrocks, Trypa Group
- } Lapithos Group
- 47 GC14-series (Chen et al., 2019) 167 SH_CY series (Shaanan et al., 2021) 012 -CY series (Glazer et al., 2021) 09 GC19-series (this study)

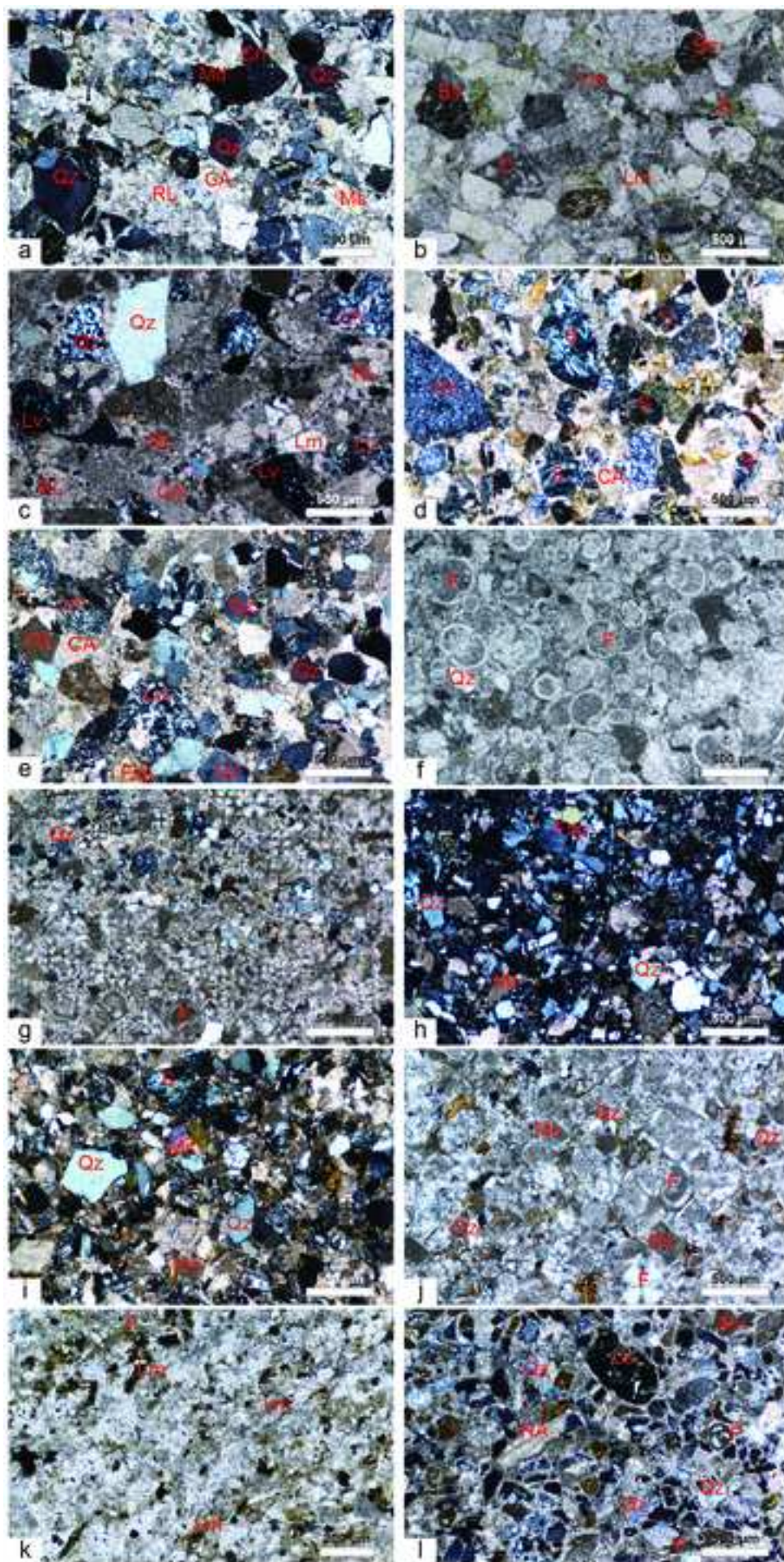




Figure 7

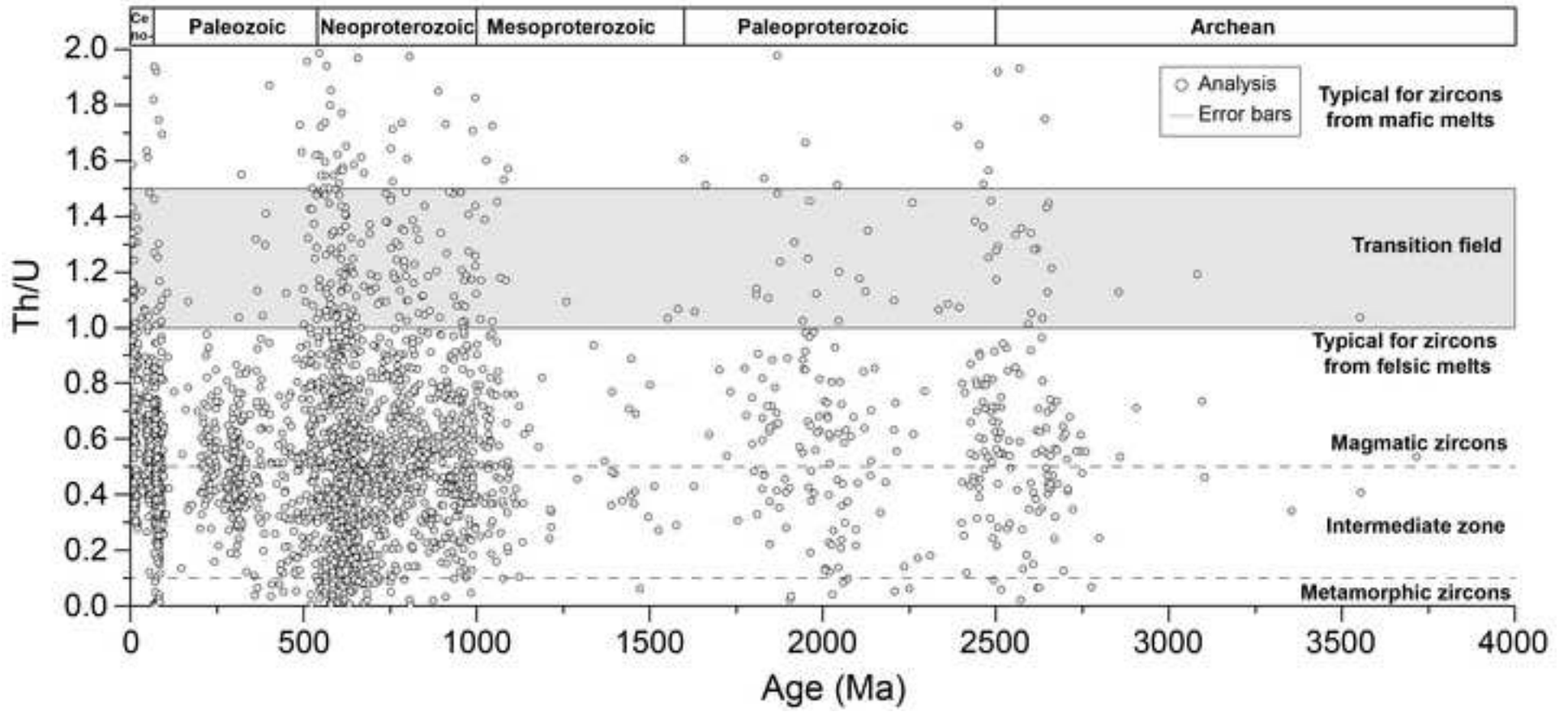


Figure 8

[Click here to access/download;Figure;Fig. 8.jpg](#)

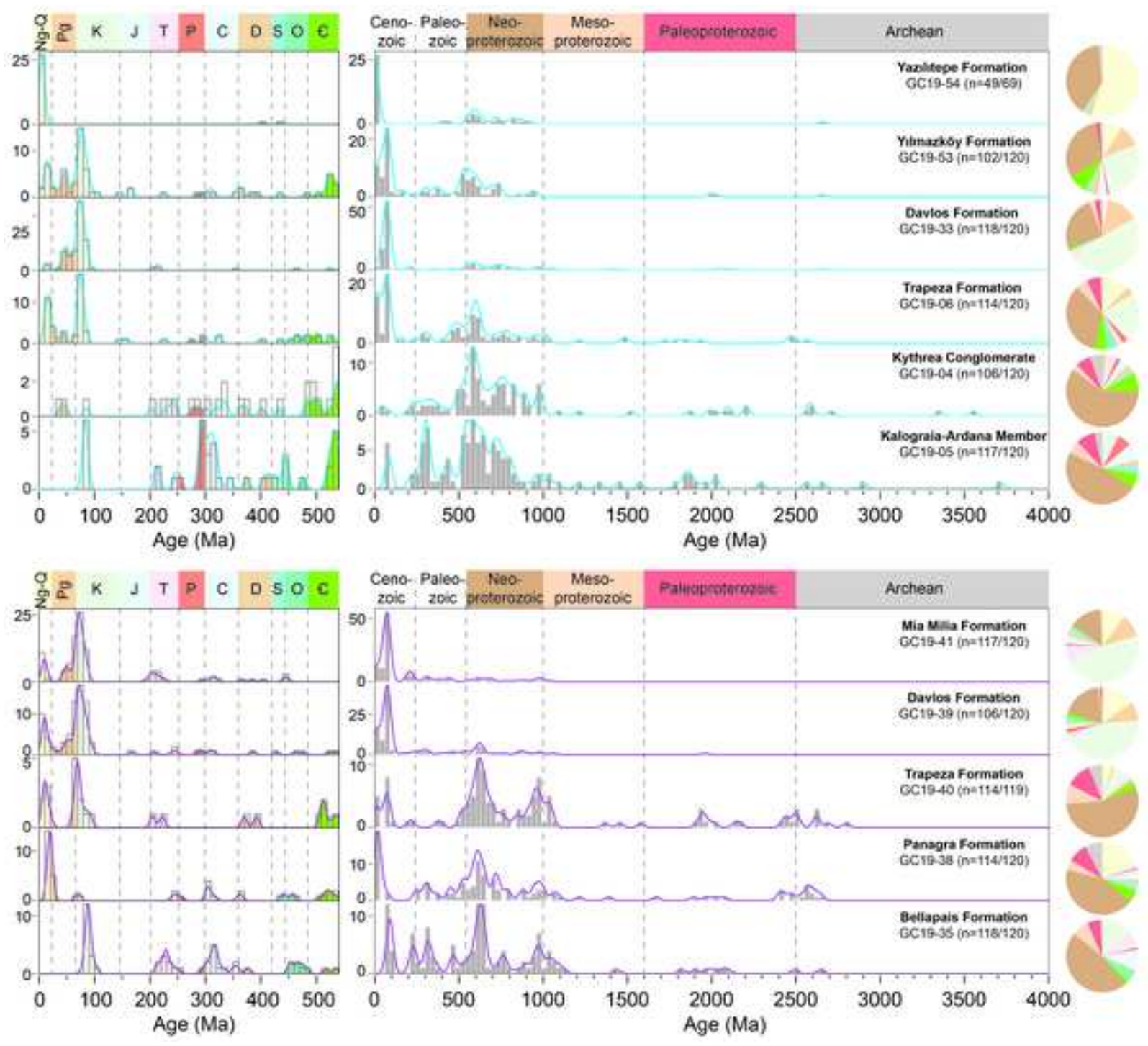
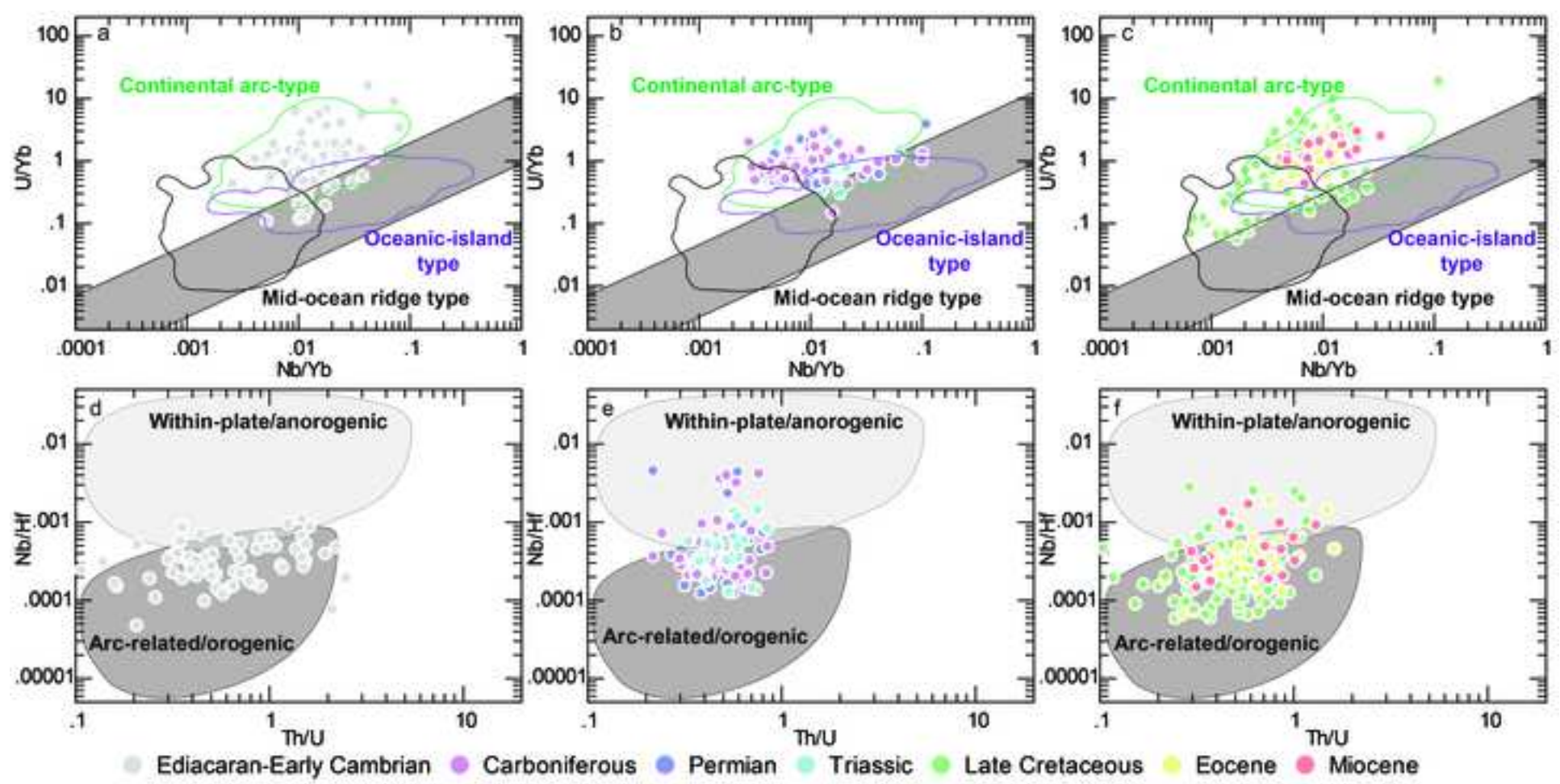
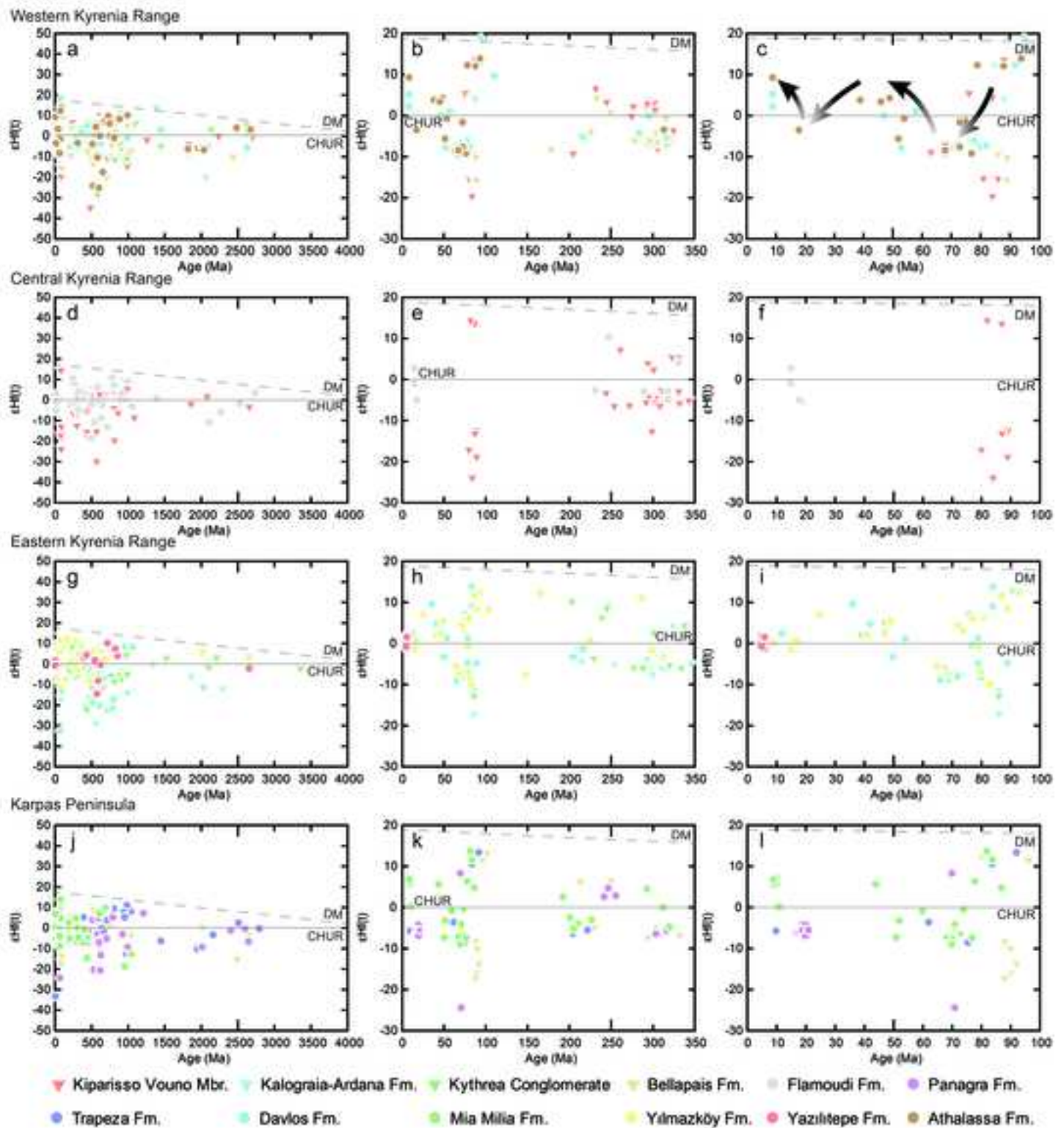
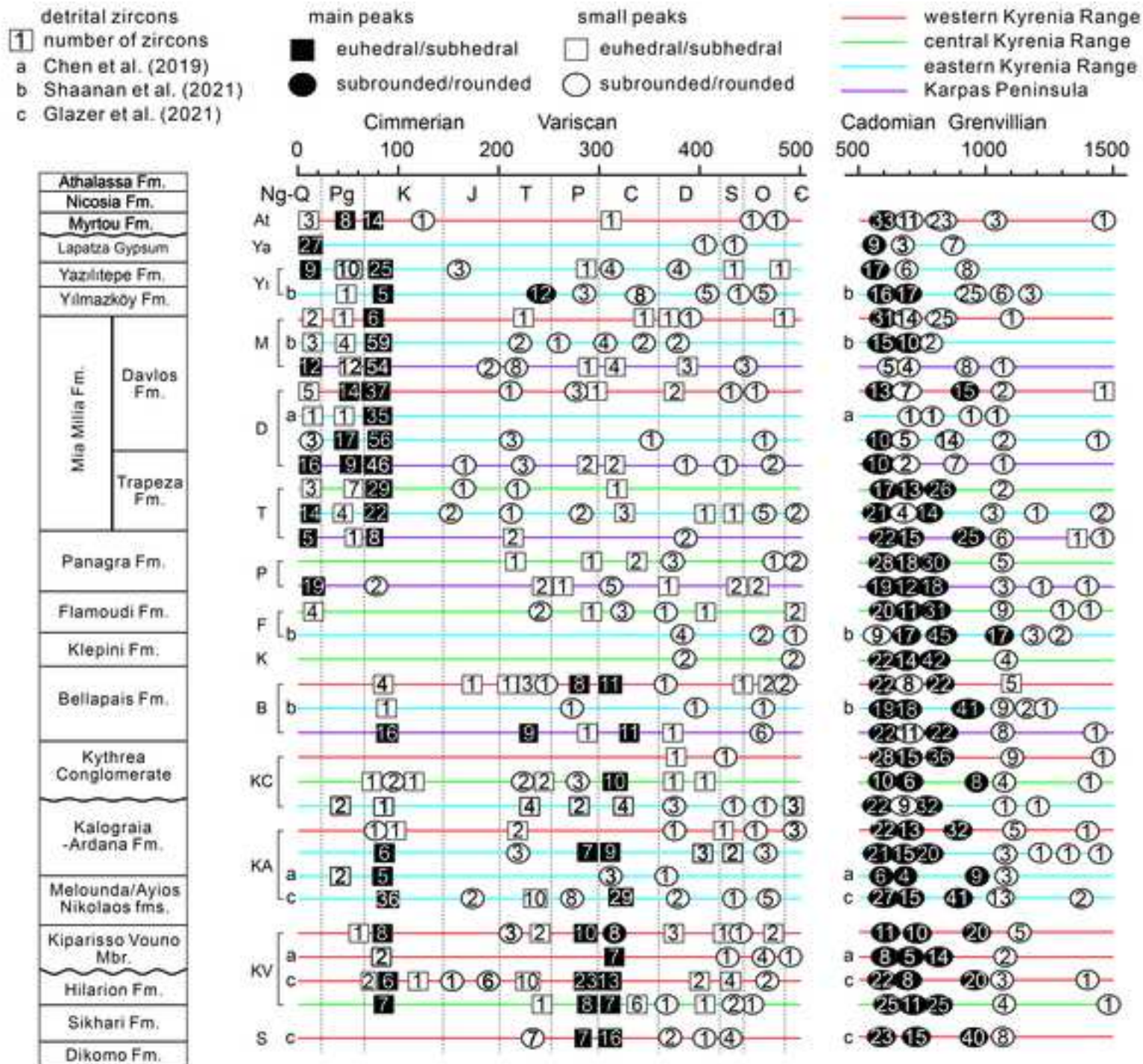
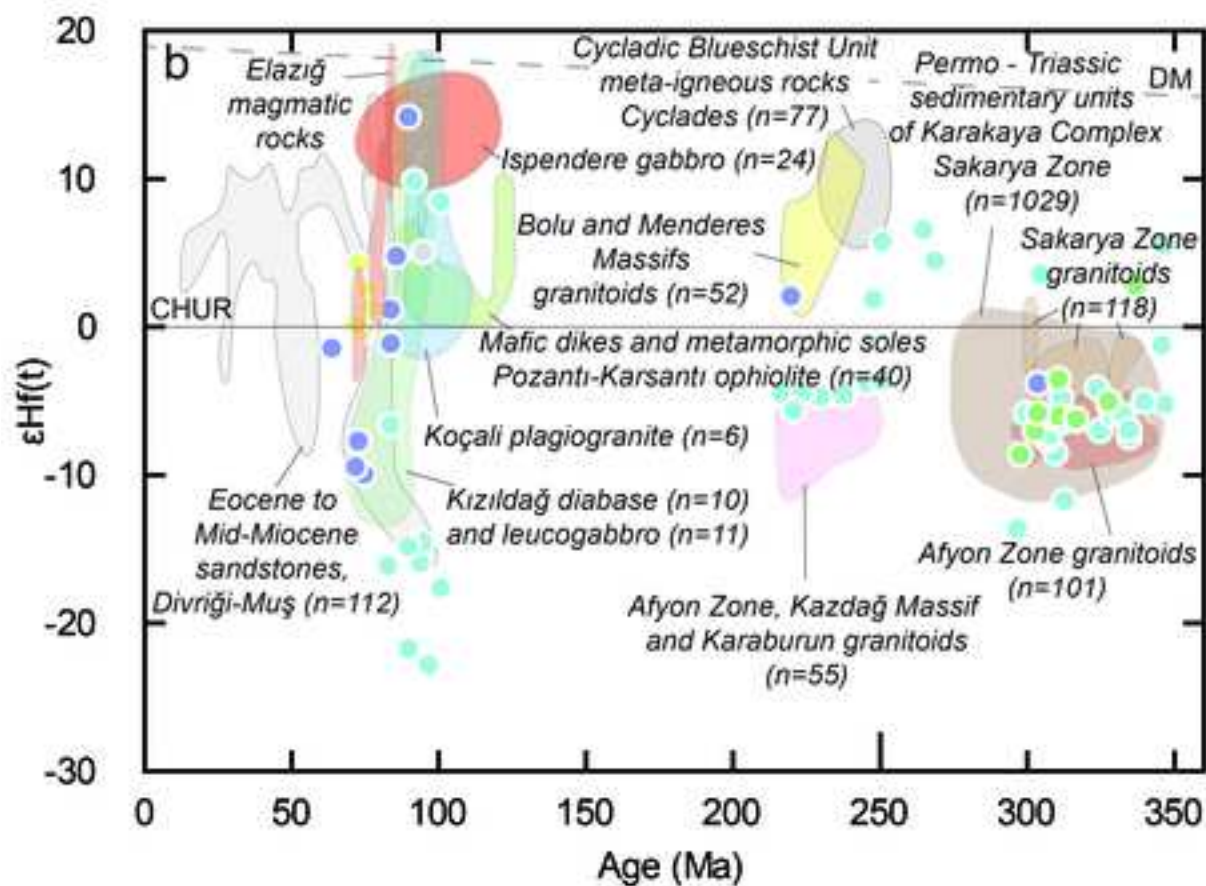
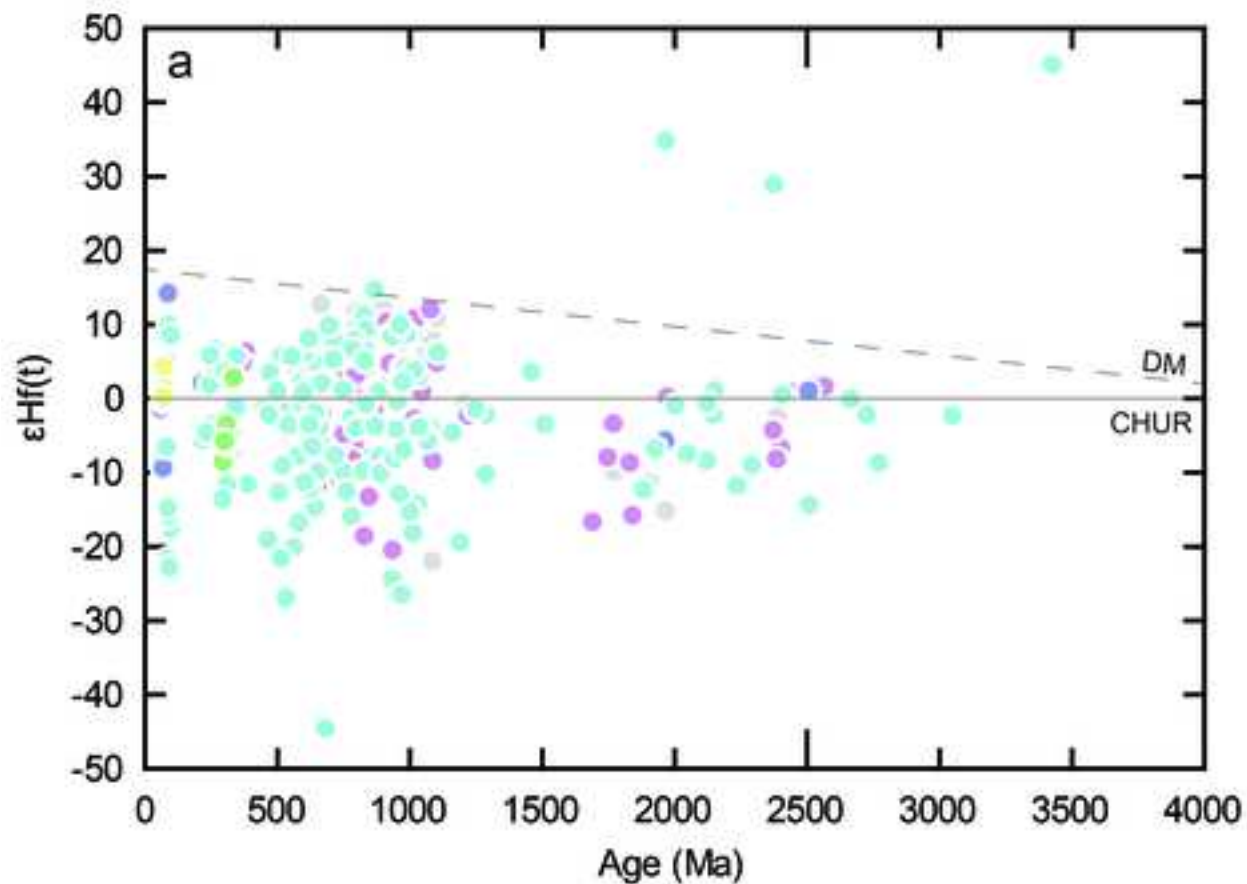


Figure 9

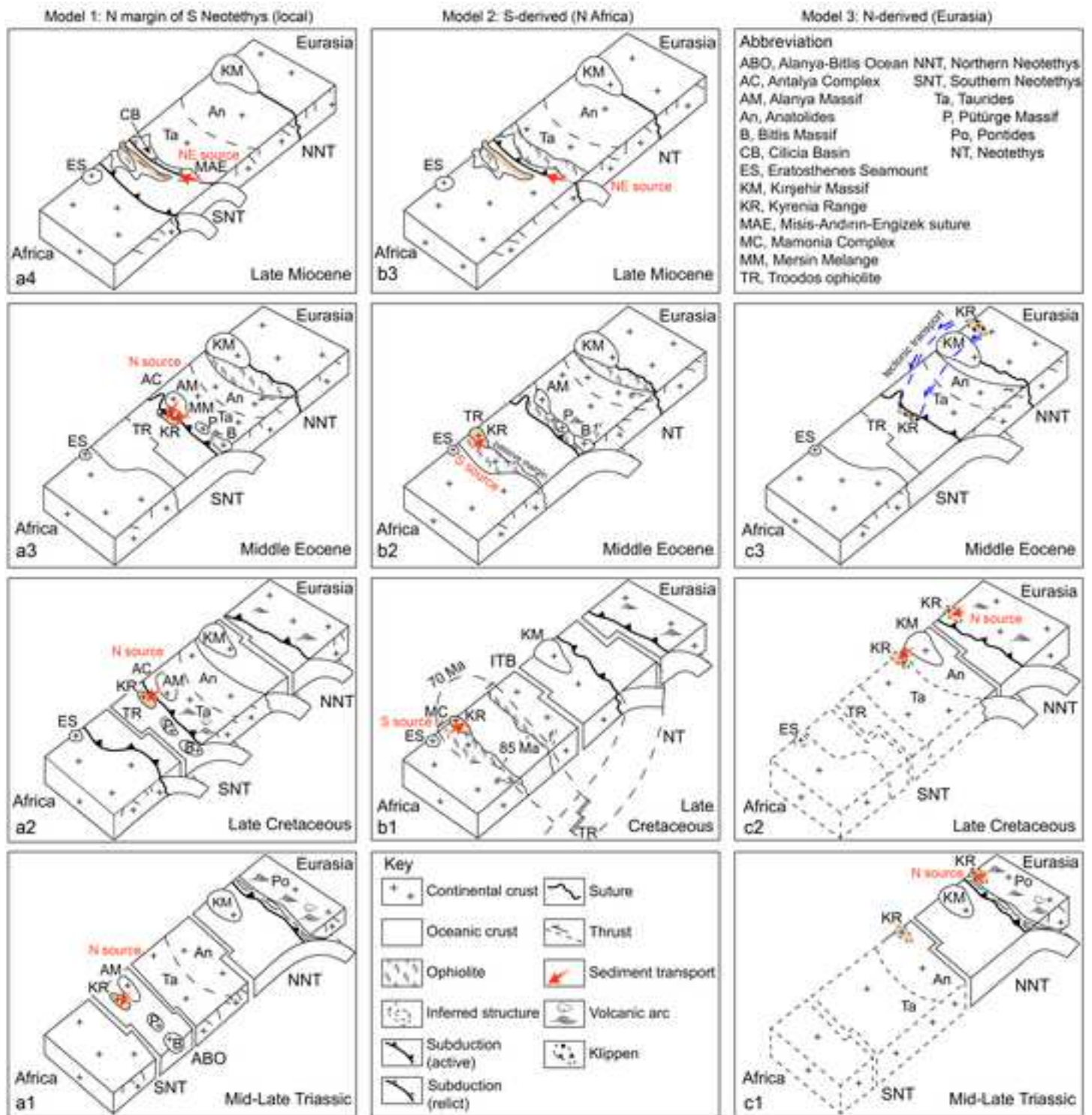








- Sikhari Formation
- Rhyolite block
- Kalograia-Ardana Formation
- Bellapais Formation
- Flamoudi Formation
- Mia Milia Formation



Declaration of interests

The authors declare that they have no known competing financial interests or personal relationships that could have appeared to influence the work reported in this paper.

The authors declare the following financial interests/personal relationships which may be considered as potential competing interests:

1
2
3
4
5
6
7
8
9
10
11
12
13
14
15
16
17
18
19
20
21
22
23
24
25
26
27
28
29
30
31
32
33
34
35
36
37
38
39
40
41
42
43
44
45
46
47
48
49
50
51
52
53
54
55
56
57
58
59
60
61
62
63
64
65

1 Detrital zircon geochronology and related evidence from clastic sediments in the
2 Kyrenia Range, N Cyprus: implications for the Mesozoic-Cenozoic erosional
3 history and tectonics of southern Anatolia

4

5 Guohui Chen^{a,b}, Alastair H. F. Robertson^c, Fu-yuan Wu^b

6

7 ^a School of Earth Sciences and Engineering, Hohai University, Nanjing 210098,
8 China

9 ^b State Key Laboratory of Lithospheric Evolution, Institute of Geology and
10 Geophysics, Chinese Academy of Sciences, Beijing 100029, China

11 ^c School of GeoSciences, University of Edinburgh, Grant Institute, West Mains
12 Road, Edinburgh EH9 3JW, UK

13

14

15 Corresponding author: Guohui.Chen@live.cn

16

17 Highlights

- 18 • Detrital zircon U-Pb and related analyses indicate the erosional history of S
19 Anatolia
- 20 • The combined data indicate a switch from N to E sources related to Neogene
21 collision
- 22 • The zircon and related data support tectonic development along N margin of S
23 Neotethys

1
2
3
4
5
6
7
8
9
10
11
12
13
14
15
16
17
18
19
20
21
22
23
24
25
26
27
28
29
30
31
32
33
34
35
36
37
38
39
40
41
42
43
44
45
46
47
48
49
50
51
52
53
54
55
56
57
58
59
60
61
62
63
64
65

24 Abstract

25 Triassic to Pleistocene sandstones of the Kyrenia Range, N Cyprus provide an
26 exceptional repository of the erosional history of Anatolia. The Kyrenia Range
27 features in several different tectonic hypotheses of the Eastern Mediterranean
28 region, which are tested here using a combination of new and recently published
29 detrital zircon geochronology, zircon trace-element data and hafnium isotopic data.
30 Minimum detrital zircon ages refine the ages of several formations in the Kyrenia
31 Range. The new data also provide insights into sediment provenance including far-
32 removed sources of Upper Paleozoic zircons, within-plate versus subduction-
33 related sources (e.g., rift; oceanic/continental arc/ophiolite) and Neogene collision-
34 related magmatism. Facies and paleocurrent data indicate a major switch in clastic
35 sediment input from generally southwards to westwards during the Oligocene,
36 which was mainly controlled by the collision of the Arabian promontory with
37 Anatolia, leaving the S Neotethys as an isolated deep-water basin.

38 The U-Pb zircon age profiles indicate a prominent Late Neoproterozoic
39 population, together with Carboniferous, Permian, Late Cretaceous and Miocene-
40 aged clusters. Pan-African and Grenvillian-aged zircons were ultimately derived
41 from Cadomian continental basement. Basement that rifted from Gondwana during
42 the Triassic later became sources of detritus within Anatolia to the north. Devonian-
43 Carboniferous zircons were originally supplied by active continental margin
44 magmatism in southern Eurasia (Pontides) or northern Gondwana (Afyon zone of
45 the Anatolides). The proposed explanation is that detrital zircons were sequentially
46 recycled, first to Upper Carboniferous-earliest Permian turbidites (within the Afyon

1
2
3
4
5
6
7
8
9
10
11
12
13
14
15
16
17
18
19
20
21
22
23
24
25
26
27
28
29
30
31
32
33
34
35
36
37
38
39
40
41
42
43
44
45
46
47
48
49
50
51
52
53
54
55
56
57
58
59
60
61
62
63
64
65

47 zone to the east), later to Mid-Upper Triassic alluvium and turbidites (within the
48 Taurides to the south), and finally to Triassic-Paleogene clastic sediments as now
49 preserved in the Kyrenia Range. Upper Cretaceous zircons were derived from
50 continental arc granitoids, oceanic arc and/or ophiolitic rocks and related
51 metamorphic rocks, generally to the north of the Kyrenia Range. Paleogene
52 zircons mainly represent late-stage continental margin arc magmatism in SE
53 Turkey. During the Oligocene, the switch from mainly southward sediment supply
54 to mainly westward sediment supply represents dominant input from the S
55 Neotethyan suture zone in SE Turkey. Miocene zircons were mainly derived from
56 post-collisional volcanics in SE Turkey. Paleoriver drainage systems in
57 central/southeast Anatolia largely existed by the Late Miocene in response to
58 collision-related surface uplift, in turn strongly influencing Miocene-Pleistocene
59 zircon provenance in sub-basins within and adjacent to the Kyrenia Range.

60 The combined zircon and Hf data, together with assembled geological
61 evidence, are used to discuss three contrasting tectonic hypotheses for the early
62 Mesozoic-Eocene setting of the Kyrenia Range: (1) locally, in the easternmost
63 Mediterranean (i.e., preferred interpretation); (2) far to the south, on the N African
64 passive margin, and (3) far to the north, along (or near) the Eurasian margin.
65 Overall, the present study exemplifies the diversity and complexity of clastic
66 sediment sources within a developing orogen, with implications for some other
67 regions.

68
69 Keywords: Eastern Mediterranean, Kyrenia Range, U-Pb zircon dating, Hf isotopic

1
2
3
4
5
6
7
8
9
10
11
12
13
14
15
16
17
18
19
20
21
22
23
24
25
26
27
28
29
30
31
32
33
34
35
36
37
38
39
40
41
42
43
44
45
46
47
48
49
50
51
52
53
54
55
56
57
58
59
60
61
62
63
64
65

70 analysis, sediment provenance, tectonic synthesis

71

72 1. Introduction

73 Provenance analysis of clastic sedimentary rocks, especially detrital zircon U-Pb
74 geochronology and related analysis, provide important information concerning the
75 erosional history of continents and their tectonic development including rifting,
76 subduction and collision on variable scales (e.g., Cawood et al., 2012; Gehrels,
77 2014).

78 The Kyrenia Range in the north of Cyprus (Fig. 1) developed in response to
79 successive rift, passive margin, active margin and collisional processes during
80 opening and closure of a Neotethyan ocean basin (Robertson and Woodcock,
81 1986). Each one of these tectonic phases provided an erosional record that is
82 investigated here using zircon geochronology and related data, especially Lu-Hf
83 isotopic analysis. Where continents border ocean basins much detritus runs off
84 into the deep sea, where it can be studied by deep-sea drilling at relatively shallow
85 depths (several km) (e.g., Clift, 2002). Good examples in the modern oceans
86 include the detrital record of the Himalayan region preserved within the Bengal Fan
87 (Bay of Bengal) (e.g., Tripathy et al., 2014; Pickering et al., 2020; Bretschneider et
88 al., 2021) and also farther west within the Indus Fan (Arabian Sea) (Clift et al.,
89 2002; Yu et al., 2019; Kumar et al., 2020).

90 Following Triassic rifting to form a Neotethyan ocean basin, the Kyrenia Range
91 documents passive margin development, followed by a switch to active margin and
92 collisional settings from Late Triassic to Recent (Robertson and Woodcock, 1986;

1
2
3
4
5
6
7
8
9
10
11
12
13
14
15
16
17
18
19
20
21
22
23
24
25
26
27
28
29
30
31
32
33
34
35
36
37
38
39
40
41
42
43
44
45
46
47
48
49
50
51
52
53
54
55
56
57
58
59
60
61
62
63
64
65

93 Robertson et al., 2012a, 2014). The range runs parallel to the developing Tethyan
94 collision zone for ca. 150 km and has been uplifted from the deep Mediterranean
95 Sea during the Pleistocene (Palamakaumbura et al., 2016), providing access to a
96 lengthy Triassic-Pleistocene erosional record. Ideally, detrital zircon
97 geochronology allows unique provenances to be identified (e.g., Gehrels, 2004).
98 However, the situation is more complex where erosional detritus is supplied and
99 mixed from successive tectonic settings over a large region. In the Eastern
100 Mediterranean region, erosional detritus potentially was supplied from multiple
101 ocean basins, which may be challenging to recognised. The possibility of zircon
102 recycling through different tectonic settings over a long time period needs to be
103 considered. The present study provides a case history of zircon provenance in a
104 tectonically complex region, where all aspects of the regional geology need to be
105 taken into account in the interpretation.

106 Recently published zircon U-Pb geochronology for different time intervals in
107 the Kyrenia Range confirms a close linkage with the geological development of
108 Turkey (Chen et al., 2019; Shaanan et al., 2021; Glazer et al., 2021). Three
109 contrasting tectonic hypotheses have been proposed for the tectonic development
110 of the Kyrenia Range, which will be tested and developed here using a combination
111 of zircon geochronology, trace-element analysis and Lu-Hf analysis, together with
112 existing geological evidence mainly from the Kyrenia Range and Anatolia. The first
113 hypothesis is that the Kyrenia Range represents the northern continental margin
114 of the Southern Neotethys (McCay and Robertson, 2012; Robertson et al., 2012a,
115 2014; Barrier et al., 2018). The second hypothesis is that the Kyrenia Range

1
2
3
4
5
6
7
8
9
10
11
12
13
14
15
16
17
18
19
20
21
22
23
24
25
26
27
28
29
30
31
32
33
34
35
36
37
38
39
40
41
42
43
44
45
46
47
48
49
50
51
52
53
54
55
56
57
58
59
60
61
62
63
64
65

116 represents part of the southern passive margin of the Mesozoic Tethyan ocean
117 (i.e., N Africa) and then was transferred to the southern margin of Eurasia (S
118 Anatolia) during the Neogene (McPhee and van Hinsbergen, 2019). The third
119 hypothesis is that the Kyrenia Range is grossly allochthonous and was transported
120 hundreds of km southwards during the Eocene from an initial position along, or
121 near, the Eurasian continental margin (Glazer et al., 2021). The provenance of
122 detrital zircons, especially their Upper Paleozoic fraction is a key to evaluating the
123 above three contrasting tectonic hypotheses.

124 Here, we present a large body of new detrital zircon evidence from Upper
125 Cretaceous to Pliocene sandstones (24 samples) from the Kyrenia Range. We
126 compare data from four transects along the range to help identify specific
127 provenances. We compare our new results with existing U-Pb detrital zircon data
128 (10 samples) (Chen et al. 2019; Shaanan et al., 2021; Glazer et al., 2021), and
129 utilise new (n=684) and existing (n=319) hafnium isotopic data. We also use zircon
130 trace element data, particularly to help discriminate intra-plate versus convergent
131 plate magmatic sources.

132 Our specific objectives for the Kyrenia Range are: (1) to test paleontologically
133 determined ages; (2) to infer provenance for different time slices from Middle-Late
134 Triassic to Pleistocene; (3) to investigate how provenance has changed through
135 time; (4) to further help interpret tectonic development of Tethys in the easternmost
136 Mediterranean region; (5) to test the three different tectonic hypotheses for the
137 Kyrenia Range in its regional tectonic setting, and (6) to consider the wider
138 implications of our preferred interpretation.

2. Geological setting and tectonostratigraphy of the Kyrenia Range

The island of Cyprus, located in the eastern Mediterranean, is made up of three tectonic terranes: the Troodos Massif in the centre, the Mamonia Complex in the west and the Kyrenia Range in the north (Fig. 1). The Kyrenia Range is characterised by a narrow, elongate topographic ridge (up to 5 km wide × 160 km long × 1.0 km high) that lies between the Troodos Massif to the south and the Cilicia Basin to the north, with the Tauride Mountains of southern Turkey farther north (Fig. 1). The Troodos Massif comprises an Upper Cretaceous, supra-subduction zone-type ophiolite (92-90 Ma; Mukasa and Ludden, 1987), overlain by an Upper Cretaceous to Recent deep-marine to shallow-marine and non-marine sedimentary cover (e.g., Robertson, 1990). The Mamonia Complex is dominated by highly deformed Upper Triassic to Lower Cretaceous sedimentary and igneous rocks, interpreted as a remnant of a deep-marine rifted passive continental margin (e.g., Robertson and Woodcock, 1979; Torley and Robertson, 2018). The easternmost Mediterranean including the Kyrenia Range was strongly affected by rifting that began in the Late Permian, continued during the Early-Middle Triassic and culminated in continental breakup to form oceanic crust during Late Triassic (Robertson and Woodcock, 1979; Şengör and Yılmaz, 1981; Robertson and Dixon, 1984; Garfunkel, 1998). The Kyrenia Range can be interpreted, either as a microcontinent capped by a small carbonate platform or as part of a larger regional, continental unit and carbonate platform (e.g., Robertson et al., 2012a; Barrier et al., 2018; van Hinsbergen et al., 2020).

1
2
3
4
5
6
7
8
9
10
11
12
13
14
15
16
17
18
19
20
21
22
23
24
25
26
27
28
29
30
31
32
33
34
35
36
37
38
39
40
41
42
43
44
45
46
47
48
49
50
51
52
53
54
55
56
57
58
59
60
61
62
63
64
65

162

163 2.1 Late Paleozoic-Mesozoic

164 The oldest rocks exposed in the Kyrenia Range are Upper Paleozoic blocks of
165 carbonate rock that are exposed in a sedimentary melange (olistostrome) in the
166 eastern part of the Range. No basal contact is exposed and entire lithostratigraphy
167 of the Kyrenia Range is inferred to be allochthonous (Baroz, 1979; Robertson and
168 Woodcock, 1986).

169 The intact succession, which is mainly exposed in the central and western part
170 of the Kyrenia Range, is characterised by platform carbonate rocks of the Trypa
171 (Tripa) Group¹, comprising the Dikomo (Dikmen), Sikhari (Kaynakköy) and Hilarion
172 (Hileryon) formations (Fig. 2) (Henson et al., 1949; Ducloz, 1972; Baroz, 1979;
173 Robertson and Woodcock, 1986). The Trypa Group is deformed into thrust sheets
174 and blocks without any overall intact succession (Fig. 3a-b); also, the dominant
175 carbonate rocks are variably recrystallised to marble and dolomite, hindering fossil
176 age determination. The Dikomo Formation, which lacks supporting paleontological
177 age data (Ducloz, 1972), comprises finely laminated calcilutite and silty marl, which
178 is mostly recrystallised to grey, blue and white schistose marble. The overlying
179 Sikhari Formation is laterally variable, comprising sugary textured dolostones,
180 minor quartz and rare diagenetic feldspar, together with chert nodules. The
181 formation is dark grey to black owing to a high content of organic carbon. A Triassic
182 age is inferred based on lithological comparisons with similar dolomitic shelf facies

¹ For simplicity, we use the traditional stratigraphy for the formation names (more recent Turkish equivalents are mentioned initially). However, we use current Turkish names for settlements (previously used names are mentioned initially).

1
2
3
4 183 in the Taurides and elsewhere in the eastern Mediterranean region, and by the
5
6 184 presence of Mesozoic ostracods (Ducloz, 1972). The conformably overlying
7
8
9 185 Hilarion Formation comprises highly recrystallised, brecciated limestones,
10
11 186 dolomites and marbles, with poorly preserved sedimentary structures including
12
13
14 187 planar and cross-lamination (Ducloz, 1972; Baroz, 1979; Robertson and
15
16 188 Woodcock, 1986). The Hilarion Formation is dated as Jurassic-Early Cretaceous
17
18
19 189 based on neritic macrofossils; e.g., the corals *Lovcenipora*, *Diplocoenia* and
20
21 190 *Cryptocoeuia* and the hydrozoan *Ellipsactinia* (Henson et al., 1949); also present
22
23
24 191 is the branched sclerosponge *Cladocoropsis mirabilis* that is particularly abundant
25
26 192 in the Late Jurassic (Baroz, 1979). The Hilarion Formation ends with a major
27
28
29 193 structural and metamorphic break during which the Trypa Group underwent
30
31 194 greenschist-facies metamorphism involving burial to ca. 5 km to 7 km (Baroz, 1979;
32
33
34 195 Robertson and Woodcock, 1986). Detritus from the Trypa Group occurs in
35
36 196 transgressive Maastrichtian sediments of the Lapithos (Lapta) Group, placing a
37
38 197 pre-Maastrichtian upper age limit on the Hilarion Formation (Fig. 3c). The contact
39
40
41 198 between the Trypa Group and the Lapithos Group is characterise by small,
42
43 199 discontinuous thrust slices of ophiolitic rocks, chert, marble and meta-volcanic
44
45 200 rocks (Ducloz, 1972; Baroz, 1979); these are interpreted as ophiolitic melange and
46
47
48 201 retain indications of HP/LT metamorphism (Glazer et al., 2021).
49

50 202 The Mesozoic carbonate platform (Trypa Group) was deformed, brecciated,
51
52
53 203 recrystallised and metamorphosed to greenschist facies, together with the
54
55 204 emplacement of small volumes of ophiolitic melange (with HP/LT metamorphic
56
57
58 205 relics), prior to Campanian-Maastrichtian transgression (Kiparisso Vouno
59
60
61
62
63
64
65

1
2
3
4
5
6
7
8
9
10
11
12
13
14
15
16
17
18
19
20
21
22
23
24
25
26
27
28
29
30
31
32
33
34
35
36
37
38
39
40
41
42
43
44
45
46
47
48
49
50
51
52
53
54
55
56
57
58
59
60
61
62
63
64
65

206 (Alevkaya Tepe) Member). The Upper Cretaceous the emplacement-related
207 structure is overprinted and mainly obliterated by the later deformation events. The
208 primary deformation and metamorphism are interpreted to related to regional
209 subduction, which was followed by rapid exhumation and marine transgression
210 (Robertson and Woodcock, 1986; Robertson et al., 2012b; Maffione et al., 2017;
211 McPhee and van Hinsbergen, 2019; Glazer et al., 2021).

212
213 2.2 Latest Cretaceous-Middle Eocene

214 The Lapithos Group comprises basal carbonate breccias, pelagic carbonates,
215 basic volcanics, calcareous sandstones and sandy carbonates (Figs. 2, 3c;
216 Supplementary Figure S1), which are dated as Campanian to Early Eocene based
217 mainly on planktonic foraminifera (Ducloz, 1972; Baroz, 1979; Hakyemez et al.,
218 2000; Robertson et al., 2012b). Two structurally different units are present. The
219 first unit is the Upper Campanian Fourkovouno (Selvilitepe) Formation. This crops
220 out as thrust slices mainly in the western Kyrenia Range, comprising marine water-
221 lain felsic tuffs and subaqueous felsic debris-flow deposits (Moore, 1960; Baroz,
222 1979; Huang et al., 2007; Robertson et al., 2012b; Chen and Robertson, 2021b).
223 Uranium-lead radiometric dating has yielded an age of ca. 74 Ma (Late Campanian)
224 (Chen and Robertson, 2021b; Glazer et al., 2021). The second unit, which is
225 located at a higher structural position, is the Kiparisso Vouno (Alevkaya Tepe)
226 Member of the Melounda (Mallıdağ) Formation (Lapithos Group) (Supplementary
227 Figure S1a). This lithostratigraphic unit is locally exposed near the base of the
228 Melounda Formation in the western and central Kyrenia Range (Baroz, 1979;

1
2
3
4
5
6
7
8
9
10
11
12
13
14
15
16
17
18
19
20
21
22
23
24
25
26
27
28
29
30
31
32
33
34
35
36
37
38
39
40
41
42
43
44
45
46
47
48
49
50
51
52
53
54
55
56
57
58
59
60
61
62
63
64
65

229 Robertson and Woodcock, 1986; Robertson et al., 2012b). The Kiparisso Vouno
230 Member is dated as Late Campanian-Maastrichtian based on planktic foraminifera;
231 e.g., *Rugoglobigerina sp.* and *Globotruncanita stuarti* (Robertson et al., 2012b).
232 These clastic sediments are conformably overlain by basaltic and pelagic
233 carbonate units (also within the Melounda Formation), which are dated as
234 Maastrichtian using planktic foraminifera and calcareous nannofossils (Baroz,
235 1979; Hakyemez et al., 2000; Hakyemez and Özkan-Altiner, 2007; Robertson et
236 al., 2012b, 2014). The succession continues upwards without a break into the
237 Ayios Nikolaos (Yamaçköy) Formation (Fig. 2; Supplementary Figure S1b), which
238 is dated as Paleocene-Middle Eocene, again using planktonic foraminifera and
239 calcareous nannofossils (Hakyemez et al., 2000; Hakyemez and Özkan-Altiner,
240 2007; Robertson et al., 2012b). The succession continues transitionally within the
241 Kalograia-Ardana (Bahçeli–Ardahan) Formation, which is mainly exposed in the
242 eastern Kyrenia Range (Fig. 4; Supplementary Figure S1c-d) (Baroz, 1979;
243 Robertson and Woodcock, 1986; Hakyemez et al., 2000; Robertson et al., 2014).
244 The lower part of the formation is mainly sandstone turbidites and mudrocks, which
245 pass upwards into thicker-bedded turbidites, debris-flow deposits. Associated
246 large-scale mass-transport units (‘olistostromes’) encompass blocks and
247 dismembered thrust sheets; these include Permian neritic carbonates (Kantara
248 Limestone) and ophiolitic rocks, mainly serpentinite (Ducloz, 1972; Baroz, 1979;
249 Robertson and Woodcock, 1986; Hakyemez et al., 2000; Robertson et al., 2014).
250 Marls in the lower part of the Kalograia-Ardana Formation are dated as Middle
251 Eocene using planktonic foraminifera (e.g., *Acarinina bullbrookii* and

1
2
3
4 252 *Globigerinatheka* sp.) and calcareous nannofossils (e.g., *Coccolithus pelagicus*
5
6
7 253 and *Discoaster saipanesis*) (Baroz, 1979; Hakyemez et al., 2000; Robertson and
8
9 254 Woodcock, 1986; Robertson et al., 2014).

10
11 255 According to most authors, there is a major Mid-Eocene unconformity (Ducloz,
12
13
14 256 1972; Baroz, 1979; Robertson and Woodcock, 1986; Robertson et al., 2014;
15
16 257 Robertson and Kinnaird, 2016) that separates the underlying units (other than
17
18 258 some frontal thrust slices of felsic volcanic rocks) from the Upper Eocene to Upper
19
20
21 259 Miocene non-marine to deep-marine siliciclastic sandstones and mudstones of the
22
23 260 Kythrea (Değirmenlik) Group (Weiler, 1970; McCay and Robertson, 2012;
24
25
26 261 Robertson et al., 2012b, 2014; Robertson and Kinnaird, 2016). Evidence for
27
28 262 Eocene compressional deformation has been reported from many parts of the
29
30
31 263 Kyrenia Range, especially the northern flanks, where highly deformed older units
32
33 264 are unconformably overlain by much less deformed younger units (Robertson and
34
35
36 265 Kinnaird, 2016). There is also evidence of similar-aged deformation in SE
37
38 266 Turkey/Anatolia to the north, notably the Amanos Mountains (e.g., Yilmaz, 1993;
39
40
41 267 Robertson et al., 2006, 2016; Boulton and Robertson, 2008; Duman et al., 2017).
42
43 268 The unconformity in the Kyrenia Range has been suggested to record initial
44
45 269 suturing (continental collision) of the S Neotethys in the easternmost
46
47
48 270 Mediterranean region, or far-field effects of suturing of the N Neotethys in central
49
50
51 271 Anatolia (Robertson et al., 2014). Alternatively, Glazer et al. (2021) relate the
52
53 272 inferred Mid-Eocene structural break in the Kyrenia Range to the emplacement of
54
55 273 the entire Permian to Lower Eocene stratigraphy as a vast allochthonous body that
56
57
58 274 transported from far to the north (see below). On the other hand, McPhee and van
59
60
61
62
63
64
65

1
2
3
4
5
6
7
8
9
10
11
12
13
14
15
16
17
18
19
20
21
22
23
24
25
26
27
28
29
30
31
32
33
34
35
36
37
38
39
40
41
42
43
44
45
46
47
48
49
50
51
52
53
54
55
56
57
58
59
60
61
62
63
64
65

275 Hinsbergen (2019) interpret all of the post-Upper Cretaceous deformation as Late
276 Miocene and instead infer continuous passive margin deposition from the time of
277 Upper Cretaceous deformation and metamorphism until the Upper Miocene
278 thrusting. The Mid-Eocene 'olistostromes' of the Kalograia-Ardana Formation were
279 explained by mass transport down a passive margin.

280

281 2.3 Late Eocene-Late Miocene

282 The Lapithos Group is unconformably overlain, or in fault contact with, an Upper
283 Eocene-Upper Miocene siliciclastic succession known as the Kythrea Group (Fig.
284 3d-e; Supplementary Figure S2-S3). In the north, the succession unconformably
285 overlies various older units within the Kyrenia Range (Fig. 3b). Within the Mesaoria
286 Basin to the south (Fig. 3d-e), where the Kythrea Group is folded and imbricated,
287 the total thickness is estimated utilising borehole evidence as up to 4000 m (Weiler,
288 1970; Cleintuar et al., 1977; Baroz, 1979; Hakyemez et al., 2000; Harrison et al.,
289 2004; McCay, 2010; McCay et al., 2013).

290 Where exposed on the northern and southern flanks of the Kyrenia Range,
291 the Kythrea Group is mainly composed of conglomerates (near basal), sandstone
292 turbidites, bioclastic calciturbidites, mudstones, claystones and minor tuffaceous
293 sediments. The formations present, both within the Kyrenia Range and the
294 Mesaoria Basin to the south, are the Upper Eocene-Oligocene Kythrea (Büyüktepe)
295 Conglomerate Member, the Upper Eocene-Oligocene Bellapais Formation, the
296 Upper Oligocene Klepini (Arapköy) Formation, the Upper Oligocene Flamoudi
297 (Tirmen) Formation, the Lower Miocene Panagra (Geçitköy) Formation, the

1
2
3
4
5
6
7
8
9
10
11
12
13
14
15
16
17
18
19
20
21
22
23
24
25
26
27
28
29
30
31
32
33
34
35
36
37
38
39
40
41
42
43
44
45
46
47
48
49
50
51
52
53
54
55
56
57
58
59
60
61
62
63
64
65

298 Middle-Upper Miocene Trapeza (Esentepe) Formation, the Upper Miocene Davlos
299 (Kaplica) Formation, the Lower to Upper Miocene Mia Milia (Dağyolu) Formation,
300 the Upper Miocene Yılmazköy Formation, the Upper Miocene Yazılıtepe Formation
301 and the Upper Miocene Lapatza (Mermertepe) Gypsum (Fig. 2; Supplementary
302 Figure S2-S3). The Yılmazköy and Yazılıtepe formations have been introduced to
303 represent the lithological variation in the Upper Miocene succession (Hakyemez et
304 al., 2000). Comprehensive descriptions and interpretations of all of these
305 formations are given by Baroz (1979), Robertson and Woodcock (1986) and
306 McCay and Robertson (2012). The dating is mainly based on a combination of
307 planktonic foraminifera, calcareous nannofossils and strontium isotope
308 stratigraphy (Baroz and Bizon, 1974; Baroz, 1979; Hakyemez et al., 2000; McCay
309 et al., 2013). Facies evidence indicates that the Upper Eocene-Upper Miocene
310 basin to the south of the Kyrenia Range was divided into northern and southern
311 sub-basins by an E-W trending, inferred syn-sedimentary fault lineament (Kythrea
312 Fault; Fig. 4) that was mainly active during the Middle to Late Miocene (McCay
313 and Robertson, 2012, 2013).

314 Intense thrust imbrication affected the Kyrenia Range during the Late
315 Miocene-Early Pliocene, with deformation locally continuing during the Pleistocene
316 (Calon et al., 2005a, b; McCay and Robertson, 2012, 2013; Robertson and
317 Kinnaird, 2016; McPhee and van Hinsbergen, 2019). Dominantly southward
318 thrusting strongly affected the structure of the southern flank of the range and there
319 is evidence of northward backthrusting along the northern flank of the range
320 (Robertson and Kinnaird, 2016). The unconformity at the base of the Pliocene

1
2
3
4 321 succession is likely to relate to the collision of the Tauride and North African
5
6 322 (Arabian) continents in the eastern Mediterranean region (Robertson and
7
8
9 323 Woodcock, 1986; McCay and Robertson, 2013; McPhee and van Hinsbergen,
10
11 324 2019).

12
13
14 325

15 16 326 2.4 Pliocene-Pleistocene

17
18
19 327 The Messinian Lapatza Gypsum is unconformably overlain by the Pliocene-
20
21 328 Pleistocene shallow-marine Mesaoria (Mesarya) Group. Adjacent to the Kyrenia
22
23
24 329 Range, the Mesaoria Group is mainly marls and siltstones with subordinate
25
26 330 sandstones and conglomerates. There are three formations: the Myrtou (Çamlıbel)
27
28 331 Formation, the Nicosia (Lefkosa) Formation and the Athalassa (Gürpınar)
29
30
31 332 Formation (Baroz, 1979; Robertson and Woodcock, 1986; McCay and Robertson,
32
33 333 2012; Palamakumbura and Robertson, 2016). The youngest deposits exposed in
34
35
36 334 the Kyrenia Range are mainly non-marine, and to lesser extent shallow-marine
37
38 335 facies that document Pleistocene uplift and glacio-eustatic sea-level change
39
40
41 336 (Palamakumbura and Robertson, 2016; Palamakumbura et al., 2016).

42
43 337 The collision of the Eratosthenes Seamount with the Cyprus trench to the
44
45
46 338 south of Cyprus is interpreted to have strongly influenced the uplift of both the
47
48 339 Troodos Massif and the Kyrenia Range (Fig. 1) (Robertson, 1998; Kempler, 1998;
49
50
51 340 Reiche and Hübscher, 2015; Feld et al., 2017; Ring and Pantazides, 2019).

52
53 341

54 55 342 3. Sampling and Methods

56
57
58 343 New detrital U-Pb zircon isotopic data were obtained from 24 samples of Upper
59
60
61
62
63
64
65

1
2
3
4 344 Cretaceous to Upper Pliocene-Pleistocene sandstones, as exposed in four
5
6 345 selected transects: i.e., western (n=7), central (n=6) and eastern (n=6) Kyrenia
7
8 346 Range and the Karpas Peninsula (n=5) (Fig. 4). Rare Pleistocene sandstones
9
10 347 were sampled only in the western range. Also, Upper Cretaceous sandstone is not
11
12 348 exposed in the Karpas Peninsula. The sample locations, with GPS coordinates,
13
14 349 are listed in Supplementary Tables 1-2. Comparative data are available from
15
16 350 previous spot sampling (Chen et al., 2019) and for one transect in the eastern
17
18 351 range (Fig. 4) (Shaanan et al., 2021; Glazer et al., 2021).

23 352 The methods used in this study are all tried and tested, as described in the
24
25 353 supplementary publication, which includes all of the data for the Cyprus samples
26
27 354 and for analytical standards (see Supplementary Table S1-S3). In outline, the U-
28
29 355 Pb isotopic and trace element analysis of the zircons were carried out
30
31 356 synchronously by laser ablation-inductively coupled plasma-mass spectrometry
32
33 357 (LA-ICP-MS) at the Institute of Geology and Geophysics, Chinese Academy of
34
35 358 Sciences, following the methods of Xie et al. (2008) and Wu et al. (2020). *In situ*
36
37 359 Hf isotope ratio analysis was carried out on the same zircon grains, using the MC
38
39 360 (Multicollector)-ICP-MS at Wuhan Sample Solution Analytical Technology Co., Ltd,
40
41 361 using the operating conditions and analytical methods as described by Hu et al.
42
43 362 (2012). The International Chronostratigraphic Chart of the International
44
45 363 Commission on Stratigraphy (Cohen et al., 2021) was used for the timescale.

52 364

55 365 4. Results

57 366 Below, we summarize the U-Pb, Hf isotope and trace element data for the detrital
58
59
60
61
62
63
64
65

1
2
3
4 367 zircons studied. We also note relevant textural features (e.g., roundness) and
5
6 368 comment on the Th/U ratios that are indicative of igneous or metamorphic source
7
8
9 369 rocks. Generally, zircons with Th/U <0.1 are attributed to a metamorphic origin,
10
11 370 whereas those with Th/U >0.5 are of a magmatic origin (e.g., Rubatto, 2002; Corfu
12
13
14 371 et al., 2003; Hoskin and Schaltegger, 2003; Teipel et al., 2004; Linnemann et al.,
15
16 372 2011; Xiang et al., 2011). In addition, we summarize the petrography of the
17
18
19 373 samples from each formation within the four transects studied. We also summarise
20
21 374 the main paleontological age data for each formation, in relation to the minimum
22
23 375 ages of the analysed detrital zircons. The full data base is recorded in
24
25
26 376 Supplementary Tables 1-5.

27 28 377 4.1. Kiparisso Vouno Member

29
30
31 378 Two samples of medium- to coarse-grained sandstones were analysed from the
32
33 379 Upper Cretaceous Kiparisso Vouno Member. Sample GC19-09 was collected from
34
35
36 380 2.5 km southeast of Karşıyaka, western Kyrenia Range (Fig. 4; Supplementary
37
38 381 Figure S1a). Sample GC19-66 is from 600 m north of Beylerbeyi, central Kyrenia
39
40
41 382 Range. Both sandstones are poorly sorted and contain angular to sub-angular
42
43 383 grains of quartz (mainly monocrystalline) and plagioclase, together with abundant
44
45
46 384 metamorphic rock fragments (mainly muscovite schist), with trace amounts of
47
48 385 basalt, radiolarian chert and mudstone (Table S4) (Fig. 5a).

49
50
51 386 Sample GC19-09 has predominantly Precambrian (61%; Table S5), especially
52
53 387 Neoproterozoic U-Pb ages (35%). This age group is dominantly Tonian (17%) with
54
55 388 peaks at ca. 930 Ma, followed by Ediacaran (9%) and Cryogenian (8%) (Fig. 6;
56
57
58 389 Table S5). Only a small number of zircons (4%) lie between 1.0 Ga and 1.6 Ga.

1
2
3
4 390 Paleoproterozoic and Archean zircons (mostly rounded; Supplementary Figure S4)
5
6 391 are common (ca. 10%). There are also a significant number of Phanerozoic zircons
7
8
9 392 (39%); i.e., Early Permian (8%; peaking at 297 Ma) and Late Cretaceous (5%;
10
11 393 peaking at 85 Ma). The youngest zircon has an age of 63 ± 2 Ma (Table S5), slightly
12
13
14 394 younger than the Late Campanian-Maastrichtian biostratigraphic age of the
15
16 395 Kiparisso Vouno Member (Robertson et al., 2012b).

17
18
19 396 Sample GC19-66 similarly contains abundant Precambrian zircons (69%),
20
21 397 mainly Ediacaran (22%), Cryogenian (10%) and Tonian (22%). The
22
23 398 Neoproterozoic ages peak at 606 Ma and 916 Ma, slightly different from those of
24
25
26 399 sample GC19-09. A smaller number of zircons (3-8%) are older than 1.0 Ga. The
27
28
29 400 Phanerozoic zircons (31%), which are mostly euhedral (Supplementary Figure S4),
30
31 401 have similar age peaks to sample GC19-09 for the Early Permian, at 295 Ma (n=7)
32
33 402 and also for the Late Cretaceous, at 89 Ma (n=7). Late Carboniferous zircons peak
34
35
36 403 at 301 Ma (n=7). The youngest concordant zircon, which is subhedral
37
38 404 (Supplementary Figure S4), yielded an age of 80 ± 9 Ma (Campanian) (Table S5),
39
40
41 405 consistent with the Late Campanian-Maastrichtian biostratigraphic age of the
42
43 406 Kiparisso Vouno Member based on planktic foraminifera within associated pelagic
44
45 407 carbonates, including *Rugoglobigerina* sp., *R. scotti*, *Globotruncana falsostuarti*,
46
47
48 408 *Gansserina gansseri*, *Contusotruncana fornicata*, *C. contusa*, *Abatomphalus*
49
50 409 *mayaroensis* (Bolli) and *Globotruncanita stuartiformi* (Robertson et al., 2012b).

51
52
53 410 In the two sandstones from the Kiparisso Vouno Member, only 3% of the
54
55 411 zircon grains have Th/U <0.1 (Fig. 7; Supplementary Figure S5), representing
56
57
58 412 metamorphic zircons. These grains are Late Devonian (n=1), Ediacaran (n=2),
59
60
61
62
63
64
65

1
2
3
4 413 Cryogenian (n=2) and Tonian (n=1). Most of the zircon population (58%) has Th/U
5
6 414 ratios > 0.5 that are typical of magmatic zircons. 97% of the zircons have Th/U
7
8
9 415 <1.5, indicative of derivation from felsic and/or intermediate melts.
10

11 416

12 13 14 417 4.2. Kalograia-Ardana Formation

15
16 418 One sample (GC19-11) was analysed from a normal-graded sandstone turbidite,
17
18 419 3 km NW of Kayalar, western Kyrenia Range (Fig. 4). In addition, a coarse-grained
19
20
21 420 sandstone (debris-flow deposit; GC19-05) was sampled from 1 km NW of Ardahan,
22
23 421 eastern Kyrenia Range (Supplementary Figure S1c). Both sandstones include
24
25 422 abundant grains of ophiolite-related rock (serpentinite, chert and basalt) (Fig. 5b),
26
27
28 423 terrigenous material (quartz, muscovite and sedimentary lithic fragments) (Table
29
30 424 S4) and there are also calcareous bioclasts including the planktonic foraminifera
31
32
33 425 *Acarinina bullbrooki*, *A. praetopilensis*, *Turborotalia frontosa*, *Igorina*
34
35 426 *broedermanni*, *Morozovelloides crassatus* and *M. coronatus*, and also the large
36
37
38 427 foraminifera, *Orbitoclypeus ramaraoi*, *Alveolina* cf. *A. ellipsoidalis*, *Chapmanina*
39
40 428 sp. and *Sphaerogypsina globulus* that together date the maximum age range of
41
42
43 429 the formation as Eocene (Ypresian-Bartonian). Nannofossil dating yielded mainly
44
45 430 similar ages (Robertson et al., 2014).
46
47

48 431 Sample GC19-11 contains detrital zircons with mainly Precambrian ages (85%,
49
50 432 Table S5). Neoproterozoic zircons dominate (61%) (Fig. 6), with major Ediacaran
51
52 433 (596 Ma; n=13) and Tonian (909 Ma; n=9) age peaks. Paleoproterozoic zircons
53
54 434 (14%) have an age peak at 1824 Ma (n=7). Archean zircons are scarce (3%). For
55
56
57
58 435 the Paleozoic, the main age peak is Early Cambrian (522 Ma, n=6). The youngest
59
60
61
62
63
64
65

1
2
3
4 436 zircon is 85 Ma (Santonian), much older than the planktonic foraminiferal age of
5
6
7 437 Middle Eocene (Baroz, 1979; Robertson et al., 2014).
8

9 438 Sample GC19-05 contains less abundant Precambrian zircons (64%, Table
10
11 439 S5) (Fig. 8). The dominant Neoproterozoic age group (48%) includes 18%
12
13
14 440 Ediacaran, 13% Cryogenian and 17% Tonian grains. Trace-to-minor amounts of
15
16 441 Mesoproterozoic-Archean zircons (3-9%) are present, with an age peak at 1857
17
18
19 442 Ma (n=7). Phanerozoic zircons (34%) have peaks of Early Cambrian (535 Ma; n=9),
20
21 443 Early Permian (295 Ma; n=7) and Late Cretaceous (85 Ma; n=6) ages. The
22
23
24 444 youngest detrital zircon, which is subhedral (Supplementary Figure S4), yielded an
25
26 445 age of 80 Ma (Campanian) (Table S5), older than the paleontologically dated age
27
28
29 446 (Robertson et al., 2014).
30

31 447 Overall, 52% of the analysed zircons have Th/U ratios >0.5, suggesting a
32
33 448 magmatic origin (see Supplementary Figure S5); 96% of the zircons have Th/U
34
35
36 449 <1.5, suggesting felsic and/or intermediate-composition igneous source rocks.
37
38 450 Only 4% of the analysed grains with Th/U <0.1 have Devonian (n=1), Silurian (n=1),
39
40
41 451 Cambrian (n=1) and Precambrian (n=6) ages, indicative of a metamorphic origin.
42

43
44 452

45 453 4.3. Kythrea Conglomerate

46
47
48 454 Three sandstones were sampled from the Kythrea Conglomerate Member at the
49
50
51 455 base of the Kythrea Group. Sample GC19-13 is from Geçitköy Gorge, western
52
53 456 Kyrenia Range (Fig. 4). Sample GC19-29 was collected 1.5 km NE of Değirmenlik,
54
55
56 457 central Kyrenia Range. Sample GC19-04 is from 1 km south of Mersinlik, eastern
57
58 458 Kyrenia Range (Supplementary Figure S2b). These sandstones are poorly sorted,
59
60
61
62
63
64
65

1
2
3
4 459 with angular to sub-rounded grains, largely serpentinite and carbonate, cemented
5
6 460 by calcite spar (see Fig. 5c) (Table S4). Interestingly, the sandstone matrix of the
7
8
9 461 conglomerate contains more serpentinite than the conglomerate itself, which is rich
10
11 462 in limestone and basic igneous clasts. This probably reflects the soft, friable nature
12
13
14 463 of the serpentinite. The mostly non-marine Kythrea Conglomerate, lacks
15
16 464 diagnostic fossils although its age is inferred to be Late Eocene-Oligocene from its
17
18
19 465 position between the unconformably underlying Eocene (Ypresian-Bartonian)
20
21 466 Kalograia-Ardana Formation and the overlying Upper Eocene-Oligocene Bellapais
22
23 467 Formation (Baroz and Bizon, 1974; Hakyemez et al., 2000; McCay et al., 2013). In
24
25
26 468 addition, a Late Eocene age has been obtained from planktonic foraminifera in two
27
28
29 469 samples of marl near the top of the unit in the western Kyrenia Range (Baroz and
30
31 470 Bizon, 1974; Baroz, 1979).

32
33 471 Sample GC19-13 contains abundant Precambrian detrital zircons (93%),
34
35 472 characterised by Ediacaran (606 Ma; n=13) and Tonian (920 Ma; n=7) ages.
36
37
38 473 Stenian (9%), Paleoproterozoic and Archean zircons are scarcer (9% and 8%,
39
40
41 474 respectively), with ages peaking at 2486 Ma (n=6). Paleozoic zircons (7%) peak in
42
43 475 the Early Cambrian (519 Ma; n=8) (Fig. 6). Two grains yielded Devonian and
44
45
46 476 Silurian ages. The youngest zircon age is Late Devonian (372 Ma) (Table S5),
47
48
49 477 much older than the inferred Late Eocene-Oligocene age (Baroz and Bizon, 1974;
50
51 478 Hakyemez et al., 2000; McCay et al., 2013).

52
53 479 A restricted number (n=70) of detrital zircons analysed in sample GC19-29
54
55 480 yielded 58% Precambrian ages, with peaks in the Ediacaran (617 Ma; 15%) and
56
57
58 481 Tonian (966 Ma; 13%). 8% of the zircons have a Stenian age. A few of the zircons
59
60
61
62
63
64
65

1
2
3
4 482 of >1.6 Ga (n=7) are well rounded. The dominant Paleozoic age peak is late
5
6 483 Carboniferous (310 Ma; n=7) (Fig. 6). The youngest age is Maastrichtian (72 Ma)
7
8
9 484 (Table S5), compared to the paleontologically dated Late Eocene age (Baroz and
10
11 485 Bizon, 1974; Hakyemez et al., 2000; McCay et al., 2013).

12
13
14 486 Sample GC19-04 has abundant Precambrian detrital zircons (75%) with
15
16 487 dominant age peaks at 578 Ma (n=12) and 743 Ma (n=8), together with 8%
17
18 488 Cryogenian, 7% Paleoproterozoic and 6% Archean grains, whereas Stenian grains
19
20 489 are scarce (n=3). For the Paleozoic (19%), the main age peaks are Cambrian (538
21
22 490 Ma; n=7) and Early Ordovician (483 Ma; n=5) (Fig. 8). One subhedral zircon grain
23
24 491 (see Supplementary Figure S4) yielded an age of 39 ± 1 Ma (Late Eocene) (Table
25
26 492 S5), which is compatible with the inferred Late Eocene-Oligocene paleontological
27
28 493 and strontium isotope ages (Baroz and Bizon, 1974; McCay et al., 2013).

29
30
31 494 For the three Kythrea Conglomerate samples, the Th/U ratios are >0.5 in 48%
32
33 495 of the analysed zircons, <1.5 in 97% of the zircons, and <0.1 in 5% of the zircons
34
35 496 (see Supplementary Figure S5). Zircons with Th/U <0.1 have Early Devonian (n=1),
36
37 497 Neoproterozoic (n=9), Stenian (n=1), Paleoproterozoic (n=1) and Archean (n=3)
38
39 498 ages.
40
41
42
43
44
45
46
47

48 500 4.4. Bellapais Formation

49
50 501 Two sandstones were sampled from the transitionally overlying marine Bellapais
51
52 502 Formation, one from the western Kyrenia Range (GC19-12) and the other from the
53
54 503 Karpas Peninsula (GC19-35) (Fig. 4). These sandstones have moderately to well
55
56 504 sorted, angular to rounded grains. They are compositionally similar to the
57
58
59
60
61
62
63
64
65

1
2
3
4 505 sandstone matrix of the Kythrea Conglomerate, with abundant igneous and
5
6 506 sedimentary lithic fragments (see Fig. 5d). However, quartz is more abundant (5-
7
8
9 507 15%; Table S4) whereas feldspar is rare. The Bellapais Formation is dated as Late
10
11 508 Eocene-Oligocene based on a combination of planktonic foraminifera (e.g.,
12
13 509 *Globorotalia opima opima*, *Paragloborotalia opima*, *Globoquadrina venezuelana*
14
15
16 510 and *Globigerina ouachitaensis*), calcareous nannofossils (e.g., *Cyclicargolithus*
17
18 511 *abisectus*) and strontium isotope data (Baroz and Bizon, 1974; Hakyemez et al.,
19
20 512 2000; McCay et al., 2013).

21
22
23 513 Sample GC19-12 contains mainly Precambrian zircons (64%), grouping in the
24
25 514 Neoproterozoic (45%) (Table S5); i.e., Ediacaran (19%) and Tonian (19%) peaking
26
27 515 at 610 Ma (n=13). The dominant Mesoproterozoic zircons are Stenian (4%); 15%
28
29 516 of these >1.6 Ga ages (mostly rounded grains) peak at 2619 Ma (n=6). Paleozoic
30
31 517 zircons (27%) mainly cluster in the Early Permian (282 Ma peak; n=5), late
32
33 518 Carboniferous (321-301 Ma; n=10) and Early Cambrian (528 Ma peak; n=6) (Fig.
34
35 519 6). The youngest age is 86 Ma (Santonian), in contrast to the Late Eocene-
36
37 520 Oligocene depositional age (Baroz and Bizon, 1974; Hakyemez et al., 2000;
38
39 521 McCay et al., 2013).

40
41 522 For sample GC19-35, zircon populations group in the Ediacaran (19%),
42
43 523 Cryogenian (9%), Tonian (19%), Stenian (8%) and Mesoproterozoic (6%), together
44
45 524 with significant Carboniferous (9%), Triassic (8%) and Cretaceous (14%) age
46
47 525 groups (Fig. 8). The youngest zircon is Campanian (80 ± 1 Ma) (Table S5), much
48
49 526 older than the previously reported Late Eocene-Oligocene strontium isotopic and
50
51 527 paleontological ages (Baroz and Bizon, 1974; McCay et al., 2013).
52
53
54
55
56
57
58
59
60
61
62
63
64
65

1
2
3
4 528 Only 3% of the zircon grains have Th/U ratios <0.1 (i.e., of metamorphic origin)
5
6 529 (see Supplementary Figure S5); these are mainly Neoproterozoic (n=5), together
7
8
9 530 with a few Late Devonian (n=1), Paleoproterozoic (n=1) and Archean (n=1) grains.
10
11 531 57% of the zircons have Th/U >0.5 (i.e., of magmatic origin); 96% of these grains
12
13
14 532 have Th/U <1.5, indicative of felsic and/or intermediate-composition magmatic
15
16 533 rocks.
17
18
19 534

21 535 4.5. Klepini Formation

23 536 One sample of coarse-grained sandstone (GC19-22) was sampled from a rare
24
25
26 537 interval of mainly medium to thick-bedded, lenticular sandstones and mudstones
27
28
29 538 within the mainly fine-grained Klepini Formation in the central Kyrenia Range, 200
30
31 539 m south of Arapköy (Fig. 4; Supplementary Figure S2d-e). Angular to well-rounded
32
33 540 quartz grains and lithic clasts, mainly carbonates, occur in a micritic matrix (see
34
35
36 541 Fig. 5e) (Table S4). Other lithic fragments are mainly serpentinite, with lesser
37
38
39 542 amounts of muscovite schist. The depositional age of the Klepini Formation is Late
40
41 543 Oligocene based on nannofossils indicative of biozones MNP25-MNN1 (Late
42
43 544 Oligocene), strontium isotope stratigraphy (McCay et al., 2013) and planktonic
44
45 545 foraminifera (e.g., *Globigerina ciperoensis* and *Paragloborotalia opima*) (Baroz
46
47
48 546 and Bizon, 1974; Baroz, 1979).

50 547 The zircon populations mainly cluster in the Neoproterozoic (66%), with
51
52
53 548 Ediacaran (19%), Cryogenian (12%) and Tonian (36%) components. Subordinate
54
55 549 age groups occur in the Paleoproterozoic (17%) and Archean (7%). Paleozoic (8%)
56
57
58 550 zircons are rare, mainly Cambrian (n=7) and Devonian (n=2) (Fig. 6). The youngest
59
60
61
62
63
64
65

1
2
3
4 551 age is Late Devonian (373 Ma) (Table S5).

5
6 552 Th/U ratios are typically >0.1 (99%) (see Supplementary Figure S5); of these,
7
8 553 69% of the zircons have Th/U ratios >0.5 (i.e., of magmatic origin). Th/U <0.1
9
10
11 554 occurs in one grain (no. 86; 2249 Ma) (i.e., of metamorphic origin).
12
13

14 555

15 16 556 4.6. Flamoudi Formation

17
18
19 557 One sample of thick-bedded sandstone turbidite (GC19-31) was collected from the
20
21 558 Flamoudi Formation, 1.8 km NE of Değirmenlik, central Kyrenia Range (Fig. 4).
22

23 559 The Flamoudi Formation is mainly medium to fine-grained calcareous sandstone
24
25
26 560 and marl (Supplementary Figure S2f). The sample collected has a mixed
27

28
29 561 assemblage of planktic and benthic foraminifera, together with subordinate sub-
30
31 562 angular, to rounded quartz and carbonate grains, with a sparite cement (Fig. 5f)
32

33 563 (Table S4). The age of the Flamoudi Formation is Late Oligocene-Burdigalian,
34

35
36 564 based on the occurrence of nannofossil biozones MNP25-MNN1 (Chattian-
37
38 565 Aquitanian) and strontium isotope data. However, one sample contained

39
40 566 *Catapsydrax dissimilis*, *Paragloborotalia mayeri*, '*Paragloborotalia*' *kugleri* and
41
42 567 *Globigerina ciperoensis*, indicating a Langhian age (McCay et al., 2013).
43

44
45 568 Neoproterozoic (54%) zircons dominate, with age peaks in the Ediacaran
46
47 569 (18%) (613 Ma; n=9) and Tonian (27%) (812 Ma; n=9). Minor fractions occur in the
48
49

50 570 Stenian (10%), Paleoproterozoic (10%) and Archean (9%). Trace to minor
51
52 571 populations cluster in the Cambrian (7%), Devonian (2%), Carboniferous (3%),
53

54
55 572 Permian (1%) and Triassic (2%) (Fig. 6). A minor Neogene zircon fraction, mostly
56
57 573 euhedral (Supplementary Figure S4), ranges from 19 to 15 Ma (Burdigalian-
58
59
60
61
62
63
64
65

1
2
3
4 574 Langhian). The youngest age is 15 Ma (Langhian) (Table S5), in agreement with
5
6 575 one sample that was dated using planktonic foraminifera (McCay et al., 2013; see
7
8
9 576 above); this Langhian age is considerably younger than the Aquitanian-Burdigalian
10
11 577 age range suggested by some earlier work (Baroz, 1979; Hakyemez et al., 2000).

12
13
14 578 Th/U ratios of <0.1 occur in six zircons, either Ediacaran ($n=5$) or
15
16 579 Paleoproterozoic ($n=1$) (see Supplementary Figure S5). 67% of the zircon grains
17
18 580 have $\text{Th/U} >0.5$ (i.e., of magmatic origin). 25% of zircons have $\text{Th/U} >1.5$, indicative
19
20
21 581 of a mafic igneous origin, with ages of Miocene ($n=2$), Carboniferous ($n=2$),
22
23 582 Cambrian ($n=3$) and Precambrian ($n=21$).

24
25
26 583

27 28 584 4.7. Panagra Formation

29
30 585 Two samples of medium-grained sandstone turbidites were collected from the
31
32
33 586 Panagra Formation, which is dominated by pale grey hemipelagic marl, with
34
35
36 587 distinctive reddish-coloured intervals (Supplementary Figure S3a). The first
37
38 588 sample (GC19-30) is from 1.5 km NE of Değirmenlik, central Kyrenia Range, and
39
40
41 589 the second (GC19-38) from 200 m N of Balalan, Karpas Peninsula (Fig. 4). These
42
43 590 sandstones have angular to rounded grains, mainly composed of monocrystalline
44
45
46 591 quartz and redeposited micritic fragments (see Fig. 5g) (Table S4). The Panagra
47
48 592 Formation is dated as mainly Burdigalian-Langhian based on strontium isotope
49
50
51 593 stratigraphy and planktonic foraminifera (e.g., *Globigerinoides trilobus*,
52
53 594 *Praeorbulina* sp., *Praegloborotalia siakensis* and *Globorotalia mayeri*) (McCay et
54
55 595 al., 2013), longer ranging than the initially inferred Langhian age (Baroz and Bizon,
56
57
58 596 1974).

1
2
3
4 597 Sample GC19-30 contains abundant Neoproterozoic zircons (68%) with
5
6 598 Ediacaran (25%) (606 Ma; n=18) and Tonian (27%) (954 Ma; n=13) age peaks.
7
8
9 599 Cryogenian zircons are less abundant (16%). Minor zircon fractions occur in the
10
11 600 Mesoproterozoic (5%), Paleoproterozoic (8%) and Archean (6%) (Fig. 6). There
12
13
14 601 are also minor zircon fractions with Cambrian (n=5), Ordovician (n=1), Devonian
15
16 602 (n=3), Carboniferous (n=2), Permian (n=1) and Triassic (n=1) ages. The youngest
17
18
19 603 is 219 Ma (Table S5), much older than the inferred Burdigalian-Langhian
20
21 604 depositional age.

22
23 605 Sample GC19-38 contains relatively less abundant Precambrian zircons (64%)
24
25 606 that are dominantly Neoproterozoic (43%); i.e., Ediacaran (17%), Cryogenian (11%)
26
27 607 and Tonian (18%). Minor zircon fractions of Mesoproterozoic (mainly Stenian, 4%),
28
29 608 Paleoproterozoic (9%) and Archean (8%) ages are also present. Concordant
30
31 609 Phanerozoic zircons are Cambrian (n=6), Ordovician (n=2), Silurian (n=2),
32
33 610 Devonian (n=2), Carboniferous (n=5), Permian (n=1), Triassic (n=2) and
34
35 611 Cretaceous (n=2) (Fig. 8). There is also a significant Neogene zircon fraction,
36
37 612 mostly euhedral grains (Supplementary Figure S4), with a major age peak at 20
38
39 613 Ma (Burdigalian; n=18). The 17 Ma (Burdigalian) age of the youngest zircon (Table
40
41 614 S5) is consistent with preferred Sr isotopic and planktonic foraminifera age data
42
43 615 (see above).

44
45 616 The zircons typically have relatively high Th/U ratios (see Supplementary
46
47 617 Figure S5); >0.1 in 96% and >0.5 in 59% (i.e., of magmatic origin). Only 4% of
48
49 618 these zircons have Th/U <0.1; i.e., Late Cretaceous (n=1), Ediacaran-Cryogenian
50
51 619 (n=8) and Archean (n=1). 5% of the Permian (n=1), Carboniferous (n=1),
52
53
54
55
56
57
58
59
60
61
62
63
64
65

1
2
3
4 620 Ordovician (n=1) and Neoproterozoic (n=8) grains have Th/U >1.5, indicative of a
5
6 621 mafic origin.

7
8
9 622

10 11 623 4.8. Trapeza Formation

12
13
14 624 Three sandstone turbidites were collected from the Trapeza Formation, which is
15
16 625 interbedded with cream-coloured marls (Supplementary Figure S3b); i.e., 2.0 km
17
18 626 NW of Beşparmak, central Kyrenia Range (GC19-26); 600 m W of Ardahan,
19
20 627 eastern Kyrenia Range (GC19-06); and 800 m E of Balalan in the Karpas
21
22 628 Peninsula (GC19-40) (Fig. 4). These sandstones are well-sorted, medium-grained
23
24 629 and contain sub-rounded to rounded grains, mainly quartz, calcite and serpentinite
25
26
27
28 630 (see Fig. 5h) (Table S4). The Trapeza Formation is dated as Langhian-Tortonian,
29
30 631 based on strontium isotopes, planktonic foraminifera (e.g., *Paragloborotalia mayeri*
31
32 632 and *Globorotalia menardii*) and the occurrence of nannofossil biozones MNN7a-
33
34 633 MNN11a (McCay et al., 2013), in part slightly older than the initially inferred
35
36 634 Serravallian-Tortonian age based on planktonic foraminifera (Baroz and Bizon,
37
38 635 1974; Baroz, 1979).

39
40
41
42
43 636 Sample GC19-26 includes a major Neoproterozoic age group; i.e., Ediacaran
44
45 637 (15%), Cryogenian (11%) and Tonian (23%). Other zircons are >1.0 Ga (n=13),
46
47 638 together with Mesoproterozoic (2%), Paleoproterozoic (5%) and Archean (4%)
48
49
50 639 ages. The younger zircon fractions group in the Cretaceous, with peaks at 70 and
51
52 640 82 Ma (Campanian-Maastrichtian). Zircons of Cambrian (n=3), Carboniferous
53
54 641 (n=1), Triassic (n=1) and Jurassic (n=1) ages are rare. There are also minor
55
56
57 642 Paleogene (n=7) and Neogene (n=3) age groups (Fig. 6). The youngest
58
59
60
61
62
63
64
65

1
2
3
4 643 concordant age is 9 Ma (Tortonian) (Table S5).
5

6 644 Sample GC19-06 has Ediacaran (18%), Tonian (12%), Mesoproterozoic (6%)
7
8 645 and Paleoproterozoic (7%) age groupings. Phanerozoic ages are relatively
9
10 646 abundant (54%), with major Campanian (75 Ma) and Burdigalian (16 Ma) age
11
12 647 groups. There are also subordinate Cambrian (5%) and Ordovician zircons (4%).
13
14 648 A few grains (typically $n < 4$) fall within other age ranges (Fig. 8). The youngest
15
16 649 zircon is Tortonian (11 Ma) (Table S5).
17
18
19
20

21 650 Sample GC19-40 contains abundant Precambrian detrital zircons, with major
22
23 651 age peaks at Ediacaran (615 Ma, 19%), Tonian (954 Ma, 22%), Paleoproterozoic
24
25 652 (1946 Ma, 11%) and Archean (2495 Ma, 6%). Trace to minor zircon fractions
26
27 653 include Cambrian ($n=4$), Devonian ($n=2$), Late Cretaceous ($n=8$) and Neogene
28
29 654 ($n=5$). The youngest zircon is Tortonian (9 Ma) (Table S5). The Tortonian ages of
30
31 655 the three samples analysed are consistent with the maximum age range (11-9 Ma),
32
33 656 as inferred from Sr isotopic and planktonic foraminiferal dating (see above).
34
35
36
37

38 657 In the three Trapeza Formation samples, only 2% of the zircons have Th/U
39
40 658 < 0.1 , (i.e., of metamorphic origin), namely Late Cretaceous ($n=1$), Neoproterozoic
41
42 659 ($n=5$) and Mesoproterozoic ($n=1$) (see Supplementary Figure S5). 56% of the
43
44 660 zircon population has Th/U > 0.5 (i.e., of magmatic origin). 96% of the zircons have
45
46 661 Th/U < 1.5 , consistent with derivation from felsic and/or intermediate-composition
47
48 662 magmas.
49
50
51
52

53 663

54 664 4.9. Davlos Formation

55
56
57 665 Three samples were collected from very thick-bedded, massive sandstones of the
58
59
60
61
62
63
64
65

1
2
3
4 666 Davlos Formation (Supplementary Figure S3c-d). Sample GC19-59 is from 500 m
5
6 667 SW of Geçitköy, sample GC19-33 from a coastal exposure, 2.0 km NW of Kaplıca
7
8 668 (Supplementary Figure S3c) and sample GC19-39 from 800 m E of Balalan (Fig.
9
10 4). These sandstones contain abundant poorly sorted grains of quartz and
11 669 redeposited micritic fragments, together with igneous and metamorphic lithics,
12 670 mostly serpentinite and muscovite schist (see Fig. 5i) (Table S4). The Davlos
13 671 Formation contains few dateable microfossils. However, a Tortonian age has been
14 672 inferred, based on planktonic foraminifera (e.g., *Globorotalia acostaensis* and
15 673 *Orbulina universa*) (Baroz, 1979; McCay et al., 2013).
16 674

17 675 Sample GC19-59 is dominated by detrital zircon clusters of Late Cretaceous
18 676 (n=37) and Paleogene (n=14) ages, with major peaks at 72 Ma (Maastrichtian) and
19 677 53 Ma (Early Eocene) (Fig. 6). Older grains are largely Neoproterozoic (31%), with
20 678 age peaks at ca. 622 Ma (n=10) and 942 Ma (n=6). Paleoproterozoic and Archean
21 679 ages are sparse; i.e., 6% and 2%, respectively. The youngest age peak (which is
22 680 also the minimum age) is ca. 9 Ma (Tortonian; n=5) (Table S5), consistent with the
23 681 Tortonian age based on planktonic foraminifera.
24 682

25 683 Sample GC19-33 is dominated by Phanerozoic ages (69%), the majority of
26 684 the zircon grains (64%) yield Late Cretaceous (47%) or younger ages (17%).
27 685 Upper Cretaceous grains, which are generally subhedral to euhedral
28 686 (Supplementary Figure S4), include three age peaks: 72 Ma (n=32), 79 Ma (n=19)
29 687 and 84 Ma (n=14). Paleogene zircons are subordinate, mainly dated as 53-47 Ma,
30 688 and there are a few Miocene grains (16-12 Ma; n=3). Scattered Paleozoic grains
31 (3%) include Cambrian (n=1), Ordovician (n=1) and Carboniferous (n=1) ages. A
32
33
34
35
36
37
38
39
40
41
42
43
44
45
46
47
48
49
50
51
52
53
54
55
56
57
58
59
60
61
62
63
64
65

1
2
3
4 689 single Triassic cluster (n=2) peaks at 211 Ma (n=2) (Fig. 8). There is also a
5
6 690 Neoproterozoic age cluster, with the main age groups being Ediacaran (n=10) and
7
8
9 691 Tonian (n=14). The youngest zircon age is 12 Ma (Serravallian; n=2) (Table S5),
10
11 692 slightly older than the depositional age (preferred Tortonian) based on planktonic
12
13
14 693 foraminifera (Baroz, 1979; McCay et al., 2013).

15
16 694 Sample GC19-39 is dominated by Neoproterozoic zircons (18%), whereas
17
18 695 Mesoproterozoic and Archean grains are rare. Phanerozoic ages (80%) are
19
20
21 696 broadly scattered, with Late Cretaceous (83-69 Ma; n=46) dominating. Minor
22
23 697 Paleogene grains range from 58-31 Ma (n=9) (Fig. 8). The youngest 14 ages
24
25 698 overlap with statistical uncertainties but imply a Tortonian youngest age cluster (ca.
26
27
28 699 10 Ma), which is consistent with the paleontologically determined age (Baroz, 1979;
30
31 700 McCay et al., 2013).

32
33 701 Zircons from the western Kyrenia Range (GC19-59) have Th/U >0.1 (see
34
35 702 Supplementary Figure S5). In contrast, some of the grains from the eastern
36
37
38 703 Kyrenia Range (GC19-33; n=3) and the Karpas Peninsula (GC19-39; n=2), of Late
39
40 704 Cretaceous (82-74 Ma; n=3), Ordovician (n=1) and Ediacaran (n=1) ages, have
41
42 705 Th/U <0.1. 46% of the zircons have Th/U >0.5 (i.e., of magmatic origin). Only 1%
43
44 706 of the grains, with ages of 46 Ma, 524 Ma and 791 Ma, have Th/U >1.5, suggesting
45
46
47 707 a mafic origin.

48
49
50 708

51 52 53 709 4.10. Mia Milia Formation

54
55 710 Two sandstones were sampled from the Mia Milia Formation in the Mesaoria Basin,
56
57
58 711 dominated by folded and imbricated sandstone turbidites and mudstones
59
60
61
62
63
64
65

1
2
3
4 712 (Supplementary Figure S3e-g). Sample GC19-57, a thin to medium-bedded
5
6 713 sandstone turbidite, was collected from a roadcut 700 m S of Gürpınar, western
7
8
9 714 Kyrenia Range. Sample GC19-41, also a sandstone turbidite, came from 1.5 km
10
11 715 E of Balalan in the Karpas Peninsula (Fig. 4). These sandstones are mainly
12
13 716 composed of igneous rock fragments (e.g., serpentinite), sedimentary rock
14
15 717 fragments (e.g., redeposited micritic grains), together with biogenic material (e.g.,
16
17 718 foraminifera) (see Fig. 5j) (Table S4). Quartz grains are relatively common,
18
19 719 whereas felspar is rare. The Mia Milia Formation is dated as Burdigalian-Tortonian
20
21 720 based on planktonic foraminifera (e.g., *Globoturbotalita nepenthes*), calcareous
22
23 721 nanofossils and Sr isotopic analyses (McCay et al., 2013), more long-ranging
24
25 722 than the previously inferred Serravallian-Tortonian age range (Baroz and Bizon,
26
27 723 1974; Baroz, 1979; Hakyemez et al., 2000).

28
29
30
31
32
33 724 Zircons in sample GC19-57 are mainly Neoproterozoic; i.e., Ediacaran (29%),
34
35 725 Cryogenian (14%) and Tonian (23%), together with minor fractions of
36
37 726 Paleoproterozoic (9%) and Archean (8%) ages. Paleozoic zircons mainly cluster
38
39 727 in the Cambrian (n=3), Ordovician (n=1), Devonian (n=2) and Carboniferous (n=1)
40
41 728 (Fig. 6). There is a minor Late Cretaceous fraction (6%). The youngest zircon,
42
43 729 which is euhedral (Supplementary Figure S4), yielded an age of 10 Ma (Tortonian;
44
45 730 n=2) (Table S5).

46
47
48
49
50 731 In contrast, sample GC19-41 is dominated by Mesozoic zircons (75%), with
51
52 732 Triassic (7%), Cretaceous (46%), Paleogene (10%) and Neogene (10%) age
53
54 733 peaks. There is a relatively continuous scatter of Ordovician to Permian ages
55
56 734 (n=<3, generally) (Fig. 8). There are also minor Neoproterozoic zircon fractions of
57
58
59
60
61
62
63
64
65

1
2
3
4 735 Ediacaran (4%), Cryogenian (3%) and Tonian (7%) ages. The youngest zircon is
5
6 736 9 Ma (Tortonian; n=6). The minimum Tortonian ages of the two samples analysed
7
8
9 737 (Table S5) are consistent with the previously reported depositional age range
10
11 738 (Baroz and Bizon, 1974; Baroz, 1979; Hakyemez et al., 2000).

12
13
14 739 52% of the zircons analysed have Th/U >0.5, while 97% are <1.5, suggestive
15
16 740 of derivation from felsic and/or intermediate magmas. 4% of the zircons, of Late
17
18 741 Cretaceous (73 Ma; n=1), Silurian (n=1), Cambrian (n=1), Neoproterozoic (n=6)
19
20
21 742 and Paleoproterozoic (n=1) ages, have Th/U <0.1 (i.e., of metamorphic origin) (see
22
23 743 Supplementary Figure S5).

24
25
26 744

27 28 745 4.11. Yılmazköy and Yazılıtepe Formations

29
30
31 746 The Yılmazköy Formation, which is equivalent to the upper marl unit of the
32
33 747 previously defined Davlos Formation (Baroz, 1979), is mainly marl, mudstone and
34
35 748 sandstone (Supplementary Figure S3h). The overlying Yazılıtepe Formation, which
36
37
38 749 is equivalent to the lower marl unit of the traditional Lapatza Formation (e.g.,
39
40
41 750 Necdet and Anıl, 2006) comprises marl, limestone and sandstone, overlain by
42
43 751 Messinian evaporite. Two thin-bedded, medium-grained gypsiferous sandstones
44
45 752 with common small quartz, metamorphic lithic and biogenic grains (see Fig. 5k)
46
47
48 753 were collected from 1.8 km NW of Altınova, eastern Kyrenia Range (Fig. 4;
49
50
51 754 Supplementary Figure S3h). The Yılmazköy Formation has been dated as
52
53 755 Tortonian using planktonic foraminifera (e.g., *Orbulina universa* and
54
55 756 *Globoturborotalita nepenthes*), calcareous nannofossils and Sr isotopes
56
57
58 757 (Hakyemez et al., 2000; McCay et al., 2013). The Yazılıtepe Formation is dated as
59
60
61
62
63
64
65

1
2
3
4 758 Tortonian-Messinian based on planktonic foraminifera, calcareous nannofossils
5
6 759 and Sr isotopes (McCay et al., 2013), a longer age range than previously inferred
7
8
9 760 for this interval based on the planktonic foraminifera, *Neogloboquadrina*
10
11 761 *acostaensis* and *Neogloboquadrina humerosa* (Baroz, 1979).

12
13
14 762 In sample GC19-53, from the Yılmazköy Formation, Precambrian ages cluster
15
16 763 in Ediacaran (17%), Cryogenian (6%) and Tonian (8%), together with rare
17
18
19 764 Paleoproterozoic to Archean ages (<2%). Cambrian zircons form a significant age
20
21 765 population (n=9). Ordovician to Jurassic grains are scattered (15%). Prominent
22
23
24 766 age groups occur at 78-71 Ma (Campanian-Maastrichtian) and 16 Ma (Burdigalian)
25
26 767 (Fig. 8). Minor Paleogene grains (n=10), peak at 48 Ma (n=4). The youngest zircon
27
28
29 768 age is ca. 9 Ma (Tortonian; n=2) (Table S5), consistent with the Tortonian
30
31 769 depositional age data (Hakyemez et al., 2000; McCay et al., 2013).

32
33 770 Sample GC19-54, from the overlying Yazılıtepe Formation, has a bimodal
34
35
36 771 cluster of Neoproterozoic (39%) ages, mainly Ediacaran (n=9), Tonian (n=7) and
37
38 772 also Neogene (55%), especially Messinian (n=27). Archean (n=1), Silurian (n=1)
39
40
41 773 and Devonian (n=1) zircon grains are rare (Fig. 8). The weighted age mean of the
42
43 774 youngest zircon cluster (mostly euhedral grains; see Supplementary Figure S4) is
44
45 775 Messinian (5.4 ± 0.1 Ma; n=10) (Table S5), consistent with the Tortonian-Messinian
46
47
48 776 depositional age data (McCay et al., 2013).

49
50 777 The zircons from the Yılmazköy Formation (sample GC19-53) typically have
51
52
53 778 high Th/U ratios (>0.1; 92%). Eight grains have Th/U <0.1, characteristic of
54
55 779 metamorphic zircons (see Supplementary Figure S5). These zircons are Early
56
57
58 780 Paleocene (n=1), Late Cretaceous (83-69 Ma; n=4) and Ediacaran-Cryogenian
59
60
61
62
63
64
65

1
2
3
4 781 (n=3). Four grains, with either Late Cretaceous (89-66; n=3) or Ediacaran (n=1)
5
6 782 ages, have Th/U>1.5, indicative of a mafic magmatic origin. Th/U ratios are >0.1
7
8
9 783 in the zircons from the Yazılıtepe Formation (sample GC19-54) (see
10
11 784 Supplementary Figure S5); of these, 80% have Th/U >0.5, indicative of magmatic
12
13
14 785 zircons. Five grains of Messinian (n=4) and Ediacaran (n=1) ages have Th/U >1.5,
15
16 786 characteristic of mafic melts.
17
18

19 787

21 788 4.12. Athalassa Formation

23 789 The overlying Pliocene marine marls and mudrocks (Myrtou and Nicosia
24
25
26 790 formations) were not sampled for zircon dating in view of their relatively fine grain
27
28
29 791 size. The Athalassa Formation, which depositionally overlies these units, is mainly
30
31 792 carbonate rocks with very few sandstones suitable for zircon dating, although one
32
33 793 sandstone (GC19-17) ca. 400 m W of Akdeniz, western Kyrenia Range (Fig. 4).
34
35
36 794 This sandstone is mainly quartz and sedimentary lithics (e.g., carbonates and
37
38 795 sandstones), together with biogenic material, mostly in the form of benthic
39
40
41 796 foraminifera and calcareous algae (see Fig. 5l) (Table S4). The Athalassa
42
43 797 Formation in the Mesaoria Basin is not well dated because the shallow-marine
44
45
46 798 biota present are mainly long-ranging, although the occurrence of the planktonic
47
48 799 foraminifera, *Globorotalia crassaformis* (Baroz, 1979; Hakyemez et al., 2000) and
49
50
51 800 magnetostratigraphic data (Palamakumbura, 2016; Palamakumbura and
52
53 801 Robertson, 2018) indicate a partly Pliocene age. Correlative shallow-marine
54
55
56 802 carbonates in west Cyprus (Polis graben) are more precisely dated as Late
57
58 803 Pliocene-Early Pleistocene (2.76-1.6 Ma) based on nannofossil and Sr isotope
59
60
61
62
63
64
65

1
2
3
4 804 dating (Balmer et al., 2019).
5

6
7 805 Precambrian zircons in the Athalassa Formation sample have Ediacaran
8
9 806 (28%), Cryogenian (9%), Tonian (20%) and Paleoproterozoic (9%) ages (Fig. 6).
10
11 807 Mesoproterozoic (3%) and Archean (3%) grains are scarce. There are minor
12
13 808 fractions of Cambrian (n=2), Ordovician (n=2) and Carboniferous (n=1) ages.
14
15 809 Mostly euhedral zircons (see Supplementary Figure S4) dominate the Upper
16
17 810 Cretaceous (n=15) and Eocene (54-39 Ma; n=9) fractions. One Lower Miocene
18
19 811 grain is present (18 Ma). The youngest zircon age is ca. 9 Ma (Tortonian; n=2)
20
21 812 (Table S5), much older than the inferred Late Pliocene- Early Pleistocene
22
23 813 depositional age (see above).
24
25
26
27

28 814 Only 3% of the analysed zircons have Th/U <0.1 (i.e., of metamorphic origin),
29
30 815 all of which are Precambrian (see Supplementary Figure S5). 50% of the zircons
31
32 816 have Th/U ratios of 0.5-1.5, typical of zircons from felsic and/or intermediate melts.
33
34 817 Three grains of Ediacaran (n=3), and one grain of Eocene age (48 Ma; n=1) have
35
36 818 Th/U >1.5, indicative of a mafic magmatic origin.
37
38
39
40

41 819

42 43 820 4.13. Zircon trace element geochemistry

44
45 821 The concentrations of trace elements in the zircons analysed are as follows: U, 9-
46
47 822 2994 ppm; Th, 0.8-3102 ppm; Y, 43-15335 ppm; Nb, 0.5-133.2 ppm; Yb, 3.8-
48
49 823 3325.6 ppm; Hf, 5515-17840 ppm; Ta, 0.1-130.1 ppm (Table S2). All of the zircons
50
51 824 are characterised by strong heavy REE enrichment (Ce/Yb<0.5) and have positive
52
53 825 Ce and negative Eu anomalies (Supplementary Figure S6).
54
55
56

57
58 826 For the Ediacaran-Early Cambrian (570-520 Ma), the trace element data are
59
60
61
62
63
64
65

1
2
3
4 827 compatible with a continental magmatic arc origin. For the Carboniferous, most of
5
6 828 the zircon grains (76%) fall within the continental, arc-related orogenic field on the
7
8
9 829 basis of their relatively high U/Yb, Hf/Th but low Th/U ratios (Fig. 9; Supplementary
10
11 830 Figure S4). A smaller number of zircons (24%) are compositionally consistent with
12
13
14 831 a within-plate setting (e.g., rift-related). The scattered Permian and Triassic grains
15
16 832 indicate a range of continental margin arc to intra-plate settings. The trace element
17
18
19 833 ratios (e.g., U/Yb, Nb/Yb) of the Upper Cretaceous grains are highly variable,
20
21 834 consistent with a mixed derivation from both continental arc and ophiolite-related
22
23
24 835 settings (Grimes et al., 2015) (Fig. 9). Specifically, the ophiolite-related zircons (89-
25
26 836 82 Ma) have relatively high Y concentrations (>2000 ppm), high Nb/Hf (>0.001)
27
28
29 837 but low U/Yb (<0.1) ratios (Supplementary Figure S7). The continental arc-related
30
31 838 grains (85-67 Ma) are characterised by relatively low Y values (<2000 ppm), low
32
33
34 839 Nb/Hf (<0.0004) but high U/Yb (>1) ratios (Supplementary Figure S7). The Eocene
35
36 840 and Miocene zircons have mainly continental arc-type trace element compositions.

37
38
39 841

40 842 4.14. Detrital zircon Hf isotope signatures

41
42
43 843 Representative zircons (n=684) from 17 samples dated during this study yielded a
44
45
46 844 total of 684 Lu-Hf isotopic analyses (Table S3). Paleoproterozoic and Archean
47
48
49 845 zircons (n=53) are characterised by a relatively small spread of $\epsilon\text{Hf}(t)$ values,
50
51 846 ranging from -20 to +5 (Fig. 10). The smaller Mesoproterozoic zircon fraction (n=22)
52
53
54 847 shows a bimodal cluster of $\epsilon\text{Hf}(t)$ values, 50% of which are moderately to strongly
55
56 848 juvenile (+2.7 to +13.7), whereas the remainder are relatively evolved (-3.4 to -
57
58 849 13.5). In contrast, Neoproterozoic zircon populations (n=189) have a greater range

1
2
3
4 850 of $\epsilon\text{Hf}_{(t)}$ values (-30 to +11.2).
5

6
7 851 The Lower Cambrian zircons (540-519 Ma) exhibit highly evolved to strongly
8
9 852 juvenile $\epsilon\text{Hf}_{(t)}$ (-24.4 to +9.0), whereas the younger grains are dominated by
10
11 853 evolved $\epsilon\text{Hf}_{(t)}$ (-2.4 to -18.8), together with two positive outliers (+4.1, +7.1) (Fig.
12
13
14 854 10). 83% of the Ordovician to Silurian grains have evolved $\epsilon\text{Hf}_{(t)}$, ranging from near-
15
16 855 chondritic to strongly negative (-35.0). Six grains yield super-chondritic $\epsilon\text{Hf}_{(t)}$ (+0.8,
17
18 856 +7.0). In contrast, Devonian (417-360 Ma) grains have relatively restricted $\epsilon\text{Hf}_{(t)}$ (-
19
20 857 5, +5), with 2 negative and 2 positive outliers. Carboniferous zircons overlap, with
21
22 858 mainly negative $\epsilon\text{Hf}_{(t)}$ (-8, -3), together with 9 positive outliers ranging from +1.4 to
23
24 859 +5.4. Permian (298-254 Ma) zircons have dominantly negative $\epsilon\text{Hf}_{(t)}$ (ca. -6),
25
26 860 together with subordinate juvenile $\epsilon\text{Hf}_{(t)}$ (+1.9 to +11.1).
27
28
29
30

31 861 The Lower Triassic to the lower Upper Triassic (250-232 Ma) zircons have
32
33 862 dominantly juvenile $\epsilon\text{Hf}_{(t)}$, decreasing through time from +10.3 to +2.5 (Fig. 10).
34
35 863 The Upper Triassic zircons mainly have evolved $\epsilon\text{Hf}_{(t)}$ (ca. -5), together with three
36
37 864 positive outliers. Jurassic grains (n=5) are sparse, with scattered $\epsilon\text{Hf}_{(t)}$ from -8.3 to
38
39 865 +12.1. Three Lower Cretaceous (111-102 Ma) zircons have strongly juvenile $\epsilon\text{Hf}_{(t)}$
40
41 866 (+8.2 to +13.1). Cenomanian-Turonian (96-91 Ma) zircons mainly exhibit strongly
42
43 867 positive $\epsilon\text{Hf}_{(t)}$ ranging from +11.4 to +18.7, together with one strongly negative
44
45 868 outlier (-13.8). Coniacian-lower Campanian (90-80 Ma) zircons have $\epsilon\text{Hf}_{(t)}$ values
46
47 869 ranging from around approximately -13 to +12 (spread vertically in Fig. 10). Lower
48
49 870 to mid-Campanian (79-75 Ma) zircons have a smaller spread of $\epsilon\text{Hf}_{(t)}$ values (-9.3
50
51 871 to +7.0). Upper Campanian-lower Maastrichtian (75-70 Ma) zircons are
52
53 872 characterised by dominantly evolved $\epsilon\text{Hf}_{(t)}$ values (ca. -7; 61%), together with three
54
55
56
57
58
59
60
61
62
63
64
65

1
2
3
4 873 positive outliers. Upper Maastrichtian (70-66 Ma) grains are all strongly evolved (-
5
6 874 6 to -10).

7
8
9 875 Lower Paleocene zircons (n=5), ranging from 65-62 Ma, have moderately to
10
11 876 strongly negative $\epsilon\text{Hf}_{(t)}$ (-9.0 to -3.7), followed in progressively younger zircons by
12
13 877 an increase in $\epsilon\text{Hf}_{(t)}$ to -0.9 (60 Ma), and then to +1.0 (58 Ma) (Fig. 10). Lower
14
15 878 Ypresian (54-50 Ma) zircons have mostly evolved $\epsilon\text{Hf}_{(t)}$ (-8 to -0.8) with one positive
16
17 879 outlier (+1.2), whereas all of the middle to upper Eocene (49-39 Ma) grains have
18
19 880 positive, juvenile $\epsilon\text{Hf}_{(t)}$ (+1.9, +5.5). One Oligocene grain has strongly juvenile $\epsilon\text{Hf}_{(t)}$
20
21 881 (+7.0). Aquitanian-Burdigalian (21-16 Ma) grains exhibit moderately evolved $\epsilon\text{Hf}_{(t)}$
22
23 882 (ca. -5). Langhian (15 Ma) zircons have near chondritic to slightly juvenile $\epsilon\text{Hf}_{(t)}$ (-
24
25 883 1 to +2.7). Serravallian-Tortonian (12-9 Ma) zircons have dominantly juvenile $\epsilon\text{Hf}_{(t)}$
26
27 884 (+2 to +9.2), together with two negative outliers. Messinian (6-5 Ma) zircons are
28
29 885 characterised by $\epsilon\text{Hf}_{(t)}$ ranging from -1 to +2 (spread vertically in Fig. 10).
30
31
32
33
34
35
36
37

38 887 5. Previous U-Pb and Lu-Hf zircon data

39
40 888 Interpretation of our new U-Pb and Hf isotopic data is aided by taking account of
41
42 889 published data (Chen et al., 2019), in particular, from a transect in the eastern
43
44 890 Kyrenia Range (Shaanan et al., 2021; Glazer et al., 2021) (see Fig. 4) (Table S1).

45 46 891 5.1. Previous detrital zircon U-Pb ages

47
48 892 The oldest sample, namely a calcschist intercalation within the Sikhari Formation
49
50 893 (Trypa Group), of inferred a Triassic age, is characterised by abundant Ediacaran
51
52 894 (15%), Cryogenian (10%) and Tonian (26%) zircons, together with subordinate
53
54 895 Mesoproterozoic (5%), Paleoproterozoic (10%) and Archean (7%) fractions (Fig.
55
56
57
58
59
60
61
62
63
64
65

1
2
3
4 896 11). Upper Carboniferous zircons (11%) dominate the Paleozoic fraction. There is
5
6
7 897 also a minor Triassic zircon fraction (5%) of inferred magmatic origin (Glazer et al.,
8
9 898 2021). The Triassic radiometric age is consistent with the inferred depositional age
10
11 899 (Ducloz, 1972; Baroz, 1979; Robertson and Woodcock, 1986).

12
13
14 900 Samples from the upper Campanian-Maastrichtian Kiparisso Vouno Member
15
16 901 (n=2) exhibit predominantly Neoproterozoic ages (34-42%), with major
17
18 902 contributions from the Ediacaran (13-15%) and Tonian (13-22%). Paleoproterozoic
19
20 903 and Archean fractions are subordinate: 11-20% and 3-11%, respectively.
21
22 904 Carboniferous (9-11%), Permian (15%), Triassic (7%) and Cenomanian-
23
24 905 Maastrichtian (3-6%) age groups are also present (Fig. 11). Jurassic zircons are
25
26 906 rare (5%) (Chen et al., 2019; Glazer et al., 2021).

27
28
29 907 Samples from the Lower-Middle Eocene Kalograia-Ardana Formation (n=2)
30
31 908 are characterised by significant zircon populations of Neoproterozoic age (37-
32
33 909 46%), together with subordinate Mesoproterozoic (7-9%), Paleoproterozoic (6-7%)
34
35 910 and Archean (3-5%) fractions. There are also Carboniferous (7-13%), Triassic (4-
36
37 911 7%) and Cretaceous (12-16%) fractions, whereas Permian and Paleogene grains
38
39 912 are rare (ca. 4-5%) (Chen et al., 2019; Glazer et al., 2021) (Fig. 11). One sandstone
40
41 913 sample (013-CY of Glazer et al., 2021) that was collected from near a large,
42
43 914 detached block (olistolith) of Upper Paleozoic limestone (Kantara Limestone) in
44
45 915 the eastern range has relatively abundant Carboniferous grains (17%). Some of
46
47 916 the detached blocks are dated as Permian based on large foraminifera (Ducloz et
48
49 917 al., 1972), although a Carboniferous age for some of the blocks may be possible
50
51 918 (see Robertson et al., 2014).

1
2
3
4
5
6
7
8
9
10
11
12
13
14
15
16
17
18
19
20
21
22
23
24
25
26
27
28
29
30
31
32
33
34
35
36
37
38
39
40
41
42
43
44
45
46
47
48
49
50
51
52
53
54
55
56
57
58
59
60
61
62
63
64
65

919 One sample from the Upper Eocene-Oligocene Bellapais Formation is
920 dominated by Precambrian zircons (90%), with major peaks of Ediacaran (15%),
921 Cryogenian (14%), Tonian (33%) and Paleoproterozoic (17%) ages. Additional
922 pronounced age clusters occur in the Mesoproterozoic at 1846 Ma (n=5) and the
923 Cambrian at 531 Ma (Shaanan et al., 2021) (Fig. 11).

924 One sample from the Upper Oligocene-Burdigalian Flamoudi Formation has
925 Precambrian zircons of 677 Ma, 805 Ma and 1043 Ma. Dominant Paleoproterozoic
926 zircons peak at 1836 Ma and 2442 Ma. Minor fractions occur in the Cambrian (3%),
927 Ordovician (1%) and Devonian (3%) (Shaanan et al., 2021) (Fig. 11).

928 One sample from the Tortonian Davlos Formation has Upper Cretaceous
929 zircon grains (84-74 Ma; 83%), together with minor Neoproterozoic (7%), Eocene
930 (2%) and Miocene (2%) fractions (Chen et al., 2019).

931 One sample from the Burdigalian-Tortonian Mia Milia Formation has mainly
932 Cretaceous (52%), Ediacaran (13%) and Cryogenian (9%) zircons, together with
933 minor fractions of Paleoproterozoic (4%) and Archean (3%) ages. Paleozoic
934 zircons mainly cluster in the Cambrian (2%), Devonian (2%) and Carboniferous
935 (5%) and there are also minor Paleogene (4%) and Neogene (3%) fractions
936 (Shaanan et al., 2021).

937 The one sample previously analysed from the Tortonian Yılmazköy Formation
938 has prominent Neoproterozoic (45%) and Paleoproterozoic (12%) zircons.
939 Phanerozoic ages (32%) are scattered, with early Carboniferous (6%), Late
940 Triassic (9%) and Late Cretaceous (4%) maximum probabilities (Shaanan et al.,
941 2021) (Fig. 11).

1
2
3
4 942

5
6 943 5.2. Previous detrital zircon Lu-Hf isotopic data

7
8
9 944 Previous zircon analysis of 8 samples yielded a total of 319 Lu-Hf isotope
10 analyses (Table S3): Triassic Sikhari Formation (n=9), Upper Cretaceous rhyolite
11 945 block (n=13), Lower-Middle Eocene Kalogaria-Ardana Formation (n=187), Upper
12 946 Eocene-Oligocene Bellapais Formation (n=44), Upper Oligocene-Burdigalian
13 947 Flamoudi Formation (n=49) and the Burdigalian-Tortonian Mia Milia Formation
14 948 (n=17) (Shaanan et al., 2021; Glazer et al., 2021) (Fig. 12).
15 949

16 950 Most of the Paleoproterozoic and Archean zircons exhibit negative $\epsilon\text{Hf}(t)$ (-16.8
17 951 to -0.2). A few zircons (n=8) have slightly positive (near chondritic) $\epsilon\text{Hf}(t)$ (+0.1 to
18 952 +1.7). The Neoproterozoic zircons (n=140) have both negative (-44.7 to -0.2) and
19 953 positive (+0.5 to +14.6) $\epsilon\text{Hf}(t)$.
20

21 954 Most of the Cambrian (535-502 Ma) zircons (6 out of 8) exhibit negative $\epsilon\text{Hf}(t)$
22 955 (-27.0 to -2.0) with the remainder being positive $\epsilon\text{Hf}(t)$ (+0.9 to +5.6). The
23 956 Ordovician detrital zircons (476-453 Ma) have mainly negative $\epsilon\text{Hf}(t)$ (-19.2 to -1.6).
24 957 A few Devonian zircons (n=3) have $\epsilon\text{Hf}(t)$ ranging from -11.7 to +6.2. Carboniferous
25 958 (347-300 Ma, n=32) zircons mainly exhibit negative $\epsilon\text{Hf}(t)$ (-11.8 to -1.3), together
26 959 with three positive outliers (+2.7 to +5.5). Permian zircons (n=4) have $\epsilon\text{Hf}(t)$
27 960 between -13.7 and +6.5. Triassic zircons are dominated by negative $\epsilon\text{Hf}(t)$ (-5.7 to
28 961 -3.7), together with three positive outliers (+1.8 to +5.7). Two Lower Cretaceous
29 962 zircons, dated at 101 Ma, yielded both negative and positive $\epsilon\text{Hf}(t)$ (-17.7, +8.4).
30 963 Upper Cretaceous zircons (n=30) have highly variable $\epsilon\text{Hf}(t)$, ranging from strongly
31 964 negative to strongly positive (-22.9 to +14.1). The youngest zircon fraction from the
32
33
34
35
36
37
38
39
40
41
42
43
44
45
46
47
48
49
50
51
52
53
54
55
56
57
58
59
60
61
62
63
64
65

1
2
3
4 965 Upper Cretaceous (77-72 Ma) rhyolite block yielded predominantly near-chondritic
5
6 966 $\epsilon\text{Hf}(t)$ (-0.6, +4.2).
7
8

9 967

10 11 968 6. Discussion

12 13 14 969 6.1. Constraints on depositional age

15
16 970 Below, we compare the minimum detrital zircon ages, as obtained in this and
17
18 971 previous studies (Table S5), with the ages of the stratigraphic units as determined
19
20
21 972 paleontologically and by strontium isotopes.
22

23
24 973 The Sikhari Formation is dated as 240-233 Ma (Ladinian-Carnian) based on
25
26 974 the youngest zircon ages (Table S5) (Glazer et al., 2021). This is similar to the
27
28 975 Middle to Late Triassic age range utilizing large bivalves (megalodontids) and
29
30 976 ostracods (Ducloz, 1972). The U-Pb detrital zircon data also point to a source of
31
32
33 977 nearly-contemporaneous magmatic detritus, probably related to continental rifting
34
35 978 (see Section 6.3).
36
37

38 979 The weighted mean ages of the youngest cluster of two or more grains in
39
40 980 the Kiparisso Vouno Member (of magmatic origin) mainly range from 86-79 Ma
41
42 981 (Santonian-Late Campanian) (Table S5), compared with the Late Campanian-
43
44 982 Maastrichtian depositional age based on planktonic foraminifera and calcareous
45
46 983 nannoplankton (Baroz, et al., 1979; Robertson et al., 2012b). The formation might
47
48 984 therefore have begun to accumulate ca. 3 Ma earlier than as suggested by the
49
50
51 985 biostratigraphic age.
52

53
54 986 Six samples analysed from the Eocene (Ypresian-Bartonian) Kalograia-
55
56
57 987 Ardana Formation yielded the youngest, magmatic zircon U-Pb ages of 88-80 Ma
58
59
60
61
62
63
64
65

1
2
3
4
5
6
7
8
9
10
11
12
13
14
15
16
17
18
19
20
21
22
23
24
25
26
27
28
29
30
31
32
33
34
35
36
37
38
39
40
41
42
43
44
45
46
47
48
49
50
51
52
53
54
55
56
57
58
59
60
61
62
63
64
65

988 (Coniacian-Campanian) (Table S5). However, Middle Eocene (Lutetian), magmatic
989 zircons (45 Ma; n=1) do rarely occur (Chen et al., 2019), in agreement with the
990 Middle Eocene biostratigraphic age. Maastrichtian-Paleogene igneous or
991 metamorphic lithologies were apparently absent from the source area. Whole-rock
992 chemical analyses of clasts of fine to medium-grained basic igneous rocks from
993 the Kalograia-Ardana Formation (mainly altered) range in composition from island
994 arc tholeiite to boninitic, and are interpreted to have an ophiolitic provenance
995 (Robertson et al., 2014). This is dissimilar to the more 'enriched' chemical
996 composition of the fine to medium-grained basic igneous rocks within the
997 underlying Maastrichtian-Lower Eocene Melounda and Ayios Nikolaos formations
998 (Robertson and Woodcock, 1986; Huang et al., 2007; Chen and Robertson,
999 2021b). The provenance of the samples analysed from the Kalograia-Ardana
1000 Formation is therefore unlikely to have included a significant contribution from the
1001 underlying Maastrichtian-Paleogene succession.

1002 The youngest zircon age obtained from the Kythrea Conglomerate sample (of
1003 magmatic origin) in this study is 39 Ma; i.e., Bartonian (late Middle Eocene) (Table
1004 S5), compared to the oldest reported Late Eocene paleontological age (from the
1005 western range). This suggests that the unconformity between the Kalograia-
1006 Ardana Formation and the Kythrea Conglomerate represent a relatively short time
1007 interval (several Ma at most) (see Section 2.2 for significance of the unconformity).

1008 The youngest zircons from the Bellapais Formation (of magmatic origin) range
1009 from 95-80 Ma (Cenomanian-Campanian) (Table S5), compared to the Late
1010 Eocene-Oligocene paleontological age. This suggests that Paleogene zircons

1
2
3
4
5
6
7
8
9
10
11
12
13
14
15
16
17
18
19
20
21
22
23
24
25
26
27
28
29
30
31
32
33
34
35
36
37
38
39
40
41
42
43
44
45
46
47
48
49
50
51
52
53
54
55
56
57
58
59
60
61
62
63
64
65

1011 were absent from the source lithologies. Whole-rock chemical analyses of clasts
1012 of fine to medium-grained basic igneous rocks from the Bellapais Formation are
1013 mainly of near-MORB composition, but with a negative Nb anomaly which
1014 suggests a subduction influence (Robertson et al., 2014); this contrast with the
1015 more 'enriched' composition of the basalts within the underlying succession (see
1016 above). The source of the Bellapais Formation igneous clasts was probably
1017 ophiolitic, similar to those within the Kalograia-Ardana Formation (McCay and
1018 Robertson, 2012; Robertson et al., 2014).

1019 The youngest detrital zircon age of the overlying Upper Oligocene Klepini
1020 Formation is 373 Ma (Late Devonian), suggesting that the inferred absence of
1021 zircon-bearing igneous or metamorphic source rocks of Paleocene age extended
1022 into the early Neogene. The youngest detrital zircon grains of magmatic origin (this
1023 study) in the Chattian-Langhian Flamoudi Formation are dated as 15 ± 1 M
1024 (Langhian). This points to a nearby contemporaneous magmatic source, in
1025 contrast to the underlying Upper Eocene-Oligocene formations. The youngest
1026 zircon age of the overlying Panagra Formation (of magmatic origin) is 17 Ma
1027 (Burdigalian) (Table S5), consistent with its paleontologically inferred Burdigalian-
1028 Langhian age range. Above this, the youngest zircon ages in the Trapeza
1029 Formation are 10.6-9.2 Ma (Tortonian), consistent with the inferred Langhian-
1030 Tortonian paleontological age.

1031 The youngest zircons (of magmatic origin) within the overlying Davlos
1032 Formation are dated as 9 Ma (Tortonian) (Table S5), in agreement with the inferred
1033 Tortonian paleontological age. The Mia Milia Formation has youngest magmatic

1
2
3
4
5
6
7
8
9
10
11
12
13
14
15
16
17
18
19
20
21
22
23
24
25
26
27
28
29
30
31
32
33
34
35
36
37
38
39
40
41
42
43
44
45
46
47
48
49
50
51
52
53
54
55
56
57
58
59
60
61
62
63
64
65

1034 zircon ages of 15-9 Ma (Langhian-Tortonian), which is consistent with its
1035 paleontologically inferred Burdigalian-Tortonian age. The youngest zircons (of
1036 magmatic origin) in the overlying Yılmazköy Formation are 9 Ma (Tortonian), in
1037 agreement with its paleontologically inferred Tortonian age. The youngest zircon
1038 age (of magmatic origin) in the overlying Yazılıtepe Formation is 5.4 ± 1.0 Ma (Late
1039 Messinian) (Table S5). This contrasts with its Tortonian-Messinian age based on
1040 calcareous nannofossils, planktonic foraminifera and strontium isotopes. The
1041 overlying evaporites (Baroz, 1979; Necdet and Anil, 2006; McCay et al., 2013) are
1042 assumed to have accumulated during the Messinian Salinity Crisis (ca. 5.96-5.33
1043 Ma) (e.g., Roveri et al., 2014; Artiaga et al., 2021). Taking account of the 1.0 Ma
1044 total calculated error, the youngest zircon age could be as old as 6.4 Ma, consistent
1045 with the sample's position beneath (rather than within) the evaporites. The Upper
1046 Pliocene-Pleistocene Athalassa Formation has a youngest, magmatic zircon age
1047 of 9 Ma (Tortonian) (Table S5), pointing to an absence of contemporaneous,
1048 igneous or metamorphic detritus.

1049 In summary, the main points from the above discussion of age relations are:

- 1050 (1) There is a nearly-contemporaneous source of Triassic detritus in the
- 1051 Sikhari Formation sample (n=1);
- 1052 (2) There is also a nearly-contemporaneous source of Upper Cretaceous
- 1053 detritus in the Kipassisso Vouno Member samples (n=5);
- 1054 (3) There is an absence of Maastrichtian-Paleogene detritus in the samples
- 1055 from the Middle Eocene Kalograia-Ardana Formation and the Upper Eocene-
- 1056 Oligocene Bellapais Formation;

1
2
3
4
5
6
7
8
9
10
11
12
13
14
15
16
17
18
19
20
21
22
23
24
25
26
27
28
29
30
31
32
33
34
35
36
37
38
39
40
41
42
43
44
45
46
47
48
49
50
51
52
53
54
55
56
57
58
59
60
61
62
63
64
65

1057 (4) Approximately coeval igneous sources existed for all of the samples from
1058 the overlying pre-Pliocene formations, except for the Upper Oligocene Klepini
1059 Formation. However, sandstones are rare in the Klepini Formation and the
1060 available detrital zircon age data could be unrepresentative or relate to local
1061 erosional effects or different depositional pathways.

1062 (5) Upper Pliocene-Pleistocene igneous or metamorphic sources did not
1063 supply the sample analysed from the western Kyrenia Range.

1064

1065 6.2. Age variations along and across the range and through time

1066 An understanding of the above detrital zircon variation can help with interpretation
1067 of provenance and depositional pathways, in relation to the potential source areas.

1068 For the Upper Campanian-Maastrichtian Kiparisso Vouno Member (Fig. 11),
1069 the western range samples are relatively enriched in >1.5 Ga grains (22% and
1070 11%, respectively), whereas the central range sample has relatively more (27%)
1071 Pan-African-aged grains (ca. 750-500 Ma). All of the samples contain abundant
1072 Permian zircons (up to 8%), whereas Carboniferous grains are instead present (up
1073 to 11%) in the central range.

1074 There are no Carboniferous or Permian grains in the overlying Eocene
1075 Kalograia-Ardana Formation sample from the western range, whereas grains of
1076 this age range commonly occur in the eastern range sample (up to 8%).
1077 Cretaceous zircon grains (86-80 Ma) are additionally present in the eastern range
1078 samples (up to 12%). Rare Paleocene-Eocene (61-45 Ma; n=2) zircons also occur
1079 in the eastern range sample (Chen et al., 2019) (Fig. 11).

1
2
3
4
5
6
7
8
9
10
11
12
13
14
15
16
17
18
19
20
21
22
23
24
25
26
27
28
29
30
31
32
33
34
35
36
37
38
39
40
41
42
43
44
45
46
47
48
49
50
51
52
53
54
55
56
57
58
59
60
61
62
63
64
65

1080 The Upper Eocene-Oligocene Kythrea Conglomerate sample from the
1081 western range contains abundant Precambrian grains (93%), compared to the
1082 samples from the central and eastern ranges (58% and 75%, respectively). For the
1083 central and eastern ranges, the zircon abundances are similar to the underlying
1084 Kiparisso Vouno Member and the Kalograia-Ardana Formation. Rare Eocene (47-
1085 39 Ma; n=2) zircon grains are only present in the eastern range sample (GC19-04)
1086 (Fig. 11).

1087 The Upper Eocene-Oligocene Bellapais Formation samples from the western
1088 range and the Karpas Peninsula have abundant Carboniferous and/or Permian
1089 grains (up to 9%), compared to the sample from the eastern range (Fig. 11).
1090 Triassic and Upper Cretaceous grains are additionally present in the Karpas
1091 Peninsula sample (GC19-35), i.e., 8% and 14%, respectively.

1092 The Upper Oligocene-Burdigalian Flamoudi Formation from the eastern range
1093 is characterised by a dominance of Precambrian zircons (93%), whereas the
1094 sample from the central range contains scattered Carboniferous to Triassic zircons,
1095 and also a Lower Miocene (19-15 Ma; 4%) age population.

1096 For the Panagra Formation, Cretaceous grains occur rarely, only in the Karpas
1097 Peninsula sample, together with a Burdigalian age peak (20 Ma; 17%).

1098 For the Trapeza Formation, the sample from the northern sub-basin (Fig. 4) in
1099 the central range includes minor Miocene grains (n=3), whereas the samples from
1100 the southern sub-basin in the eastern range and the Karpas Peninsula (Fig. 11)
1101 have a larger Miocene fraction.

1102 For the Davlos Formation, the samples from the southern sub-basin in the

1
2
3
4
5
6
7
8
9
10
11
12
13
14
15
16
17
18
19
20
21
22
23
24
25
26
27
28
29
30
31
32
33
34
35
36
37
38
39
40
41
42
43
44
45
46
47
48
49
50
51
52
53
54
55
56
57
58
59
60
61
62
63
64
65

1103 western range and the northern sub-basin in the eastern range have similar aged
1104 populations, whereas the Karpas Peninsula sample has an additional Tortonian
1105 peak (13%).

1106 The Mia Milia Formation samples, both from the southern sub-basin, are
1107 dominated by Precambrian grains (84%) in the western range, whereas there are
1108 prominent Upper Cretaceous and Tortonian grains, 46% and 10%, respectively, in
1109 the Karpas Peninsula (Fig. 11).

1110 In summary, for units with more than one sample from different areas the main
1111 differences along and across the range are:

1112 (1) The samples from the western and central ranges include more
1113 Precambrian grains (average 72% and 75%, respectively) than those from the
1114 eastern range and the Karpas Peninsula (average 54% and 48%, respectively). Of
1115 the total zircons analysed, the Neoproterozoic zircon fraction is consistently
1116 dominant, averaging, from west to east along the range: ca. 51%, 55%, 39% and
1117 35%, respectively. The variation in Precambrian zircons is likely to represent
1118 differences in detrital input from the basement or cover of microcontinents located
1119 in southern Anatolia, generally to the north of Cyprus (see section 6.4 for
1120 discussion);

1121 (2) Younger zircons, although generally present, only represent major age
1122 populations in the more easterly samples. For example, Upper Cretaceous and
1123 Miocene grains are more abundant in the eastern range (average 21% and 7%)
1124 and the Karpas Peninsula (22% and 9%) than the western range (8% and 1%) and
1125 the central range (6% and 1%). This probably relates to the occurrence of available

1
2
3
4
5
6
7
8
9
10
11
12
13
14
15
16
17
18
19
20
21
22
23
24
25
26
27
28
29
30
31
32
33
34
35
36
37
38
39
40
41
42
43
44
45
46
47
48
49
50
51
52
53
54
55
56
57
58
59
60
61
62
63
64
65

1126 source rocks within Anatolia generally to the north and northeast of Cyprus (see
1127 section 6.4);

1128 (3) Samples collected from the southern sub-basin (e.g., Trapeza Formation)
1129 include more Miocene zircons than those from the northern sub-basin. This is likely
1130 to represent differences in sediment supply via two distinct drainage systems (see
1131 section 6.4).

1132 In addition to the above variation in zircon ages along the range, there are
1133 significant changes in zircon populations through time (Fig. 11):

1134 (1) Precambrian zircons predominate all of the sandstones analysed, ranging
1135 from 15%-93%. The consistently relatively large Precambrian input indicates that
1136 source rocks of this age, or their erosional products, both located in southern
1137 Anatolia, continued to reach the Kyrenia Range from Triassic to Pleistocene time
1138 (see sections 6.3 and 6.4);

1139 (2) Carboniferous to Permian zircons form significant age populations (up to
1140 22%) in some samples during the Middle Triassic to Oligocene, but are relatively
1141 sparse after the Late Oligocene. This significant change is a key to evaluating the
1142 alternative tectonic hypotheses for the Kyrenia Range (see sections 6.4 and 6.5);

1143 (3) Neogene (21-17 Ma) zircons become more abundant during the Early
1144 Miocene, representing magmatic or metamorphic detrital input from Anatolia
1145 during this time period (see section 6.3);

1146 (4) Upper Cretaceous grains dominate the populations (up to 52%; Shaanan
1147 et al., 2021) during the Middle Miocene, whereas Miocene grains dominate those
1148 of Upper Miocene and younger formations (up to 55% for the Yazılıtepe Formation).

1
2
3
4
5
6
7
8
9
10
11
12
13
14
15
16
17
18
19
20
21
22
23
24
25
26
27
28
29
30
31
32
33
34
35
36
37
38
39
40
41
42
43
44
45
46
47
48
49
50
51
52
53
54
55
56
57
58
59
60
61
62
63
64
65

1149 The differences in the Upper Cretaceous and Miocene zircon populations prompt
1150 a search for suitable paleo-river systems that could have supplied the Upper
1151 Miocene and Pleistocene sediments (see section 6.4).

1152

1153 6.3. Ages of potential zircon sources

1154 6.3.1. Precambrian

1155 The Precambrian zircon age spectra (>540 Ma) is strikingly like that of northeast
1156 Africa and Arabia (e.g., Chen et al., 2019; Shaanan et al., 2021). The Upper
1157 Ediacaran-Lower Cambrian (570-520 Ma) zircon grains can be correlated with the
1158 Andean-type Cadomian magmatism bordering the northern margin of Gondwana
1159 in the Eastern Mediterranean region (Ustaömer et al., 2009, 2012, 2016, 2020;
1160 Zlatkin et al., 2013; Abbo et al., 2015; Gürsu et al., 2017; see below). These zircons
1161 are unlikely to have been derived directly from Gondwana because the marine
1162 Levant basin existed to the southeast of the Kyrenia Range (Fig. 1), at least from
1163 the Late Triassic-Early Jurassic (Gardosh et al., 2010). Also, the deep-marine
1164 Herodotus Basin to the southwest of Cyprus (Fig. 1) possibly originated as early
1165 as the Carboniferous (e.g., Granot, 2016; Golan et al., 2018). Much more likely
1166 sources are from one, or several, microcontinents that are now located within
1167 Turkey to the north (see Ustaömer et al., 2009; Zlatkin et al., 2013; Abbo et al.,
1168 2015; Chen et al., 2019). Cadomian fragments began to rift by the Late Permian
1169 and then spread away from Gondwana towards Eurasia, beginning during the Late
1170 Triassic, thereby opening the Southern Neotethys (e.g., Şengör and Yılmaz, 1981;
1171 Robertson and Dixon, 1984; Garfunkel, 1998; Stampfli and Borel, 2002;

1
2
3
4
5
6
7
8
9
10
11
12
13
14
15
16
17
18
19
20
21
22
23
24
25
26
27
28
29
30
31
32
33
34
35
36
37
38
39
40
41
42
43
44
45
46
47
48
49
50
51
52
53
54
55
56
57
58
59
60
61
62
63
64
65

1172 Göncüoğlu et al., 2004). Consistent with this interpretation, Gondwana-related
1173 zircons occur extensively in the Taurides to the north of the Kyrenia Range.
1174 Examples include the Neoproterozoic basement and Lower Paleozoic siliciclastic
1175 cover of the Menderes Massif, W Turkey (Zlatkin et al., 2013) and the Cadomian
1176 basement and Paleozoic to Triassic cover of the Karacahisar dome, central Turkey
1177 (Abbo et al., 2015) (Fig. 1). Detritus of north Gondwana origin (i.e., NE
1178 Africa/Arabian–Nubian Shield) (Chen et al., 2019) could have been recycled from
1179 Cadomian-aged primary lithologies into Paleozoic cover units throughout the
1180 Taurides. Both primary and secondary (recycled) material could later have been
1181 recycled, for example into the Triassic Sikhari Formation in the Kyrenia Range and
1182 the Mamonia Complex, SW Cyprus (Chen et al., 2019).

1183 A few of the Proterozoic and Archean zircons ($Th/U < 0.1$) are indicative of a
1184 metamorphic origin, especially in samples from the western transects (see Section
1185 4). Suitable sources include the Neoproterozoic high-grade metamorphic
1186 basement in the eastern and central Taurides (Ustaömer et al., 2012; Abbo et al.,
1187 2015; Gürsu et al., 2017), the Precambrian high-grade metamorphic basement of
1188 Menderes Massif in western Anatolia (e.g., Okay, 2001; Özer et al., 2001; Candan
1189 et al., 2011) and/or the Precambrian basement of the Alanya Massif north of
1190 Cyprus (Fig. 1) (Çetinkaplan et al., 2016; Çetinkaplan, 2018; Robertson and Parlak,
1191 2020). The relatively high U/Yb but low Nb/Hf ratios of the Upper Ediacaran-Lower
1192 Cambrian zircons (Fig. 9) are compatible with derivation from the Cadomian
1193 continental magmatic arc that is inferred from outcrops in southern Turkey (Gürsu
1194 and Göncüoğlu, 2005, 2008; Gürsu et al., 2015).

1
2
3
4
5
6
7
8
9
10
11
12
13
14
15
16
17
18
19
20
21
22
23
24
25
26
27
28
29
30
31
32
33
34
35
36
37
38
39
40
41
42
43
44
45
46
47
48
49
50
51
52
53
54
55
56
57
58
59
60
61
62
63
64
65

1195

1196 6.3.2. Paleozoic

1197 Paleozoic zircons form minor, to subordinate age populations in all of the
1198 sandstones analysed, with major peaks in the Cambrian, Carboniferous and
1199 Permian. Compositionally appropriate Lower Cambrian crystalline basement rocks
1200 are represented by Cadomian active margin granitoids along the north-Gondwana
1201 margin (e.g., Bitlis Massif; Ustaömer et al., 2009). Related Cadomian ‘back-arc’
1202 magmatism, of late-stage extensional or post-collisional origin, could also have
1203 supplied zircons (Gürsu and Göncüoğlu, 2005, 2008; Gürsu et al., 2015; Beyarslan
1204 et al., 2016).

1205 Ordovician to Devonian zircons are relatively rare, with Th/U ratios >0.1 and
1206 zonal structures, signifying an igneous origin (Rubatto, 2002). A dominantly
1207 continental arc origin of the zircons analysed is inferred, based on their relatively
1208 high U/Yb, Th/Nb but low Nb/Hf ratios (see Figure S6). Volcanism of this age range,
1209 albeit volumetrically minor, is known in several areas of the Taurides, including the
1210 Orhaneli area, NW Turkey (Okay, 2002; Okay et al., 2008a, b; Özbey et al. 2013),
1211 the Antalya area, SW Turkey and the Feke area, central E Turkey (Göncüoğlu and
1212 Kozlu, 2000; Robertson et al., 2021a) (Fig. 1). However, these volcanics are mainly
1213 basaltic and unlikely to have supplied many zircons (e.g., Watson and Harrison,
1214 1983; Keller et al., 2017).

1215 Carboniferous and Permian zircon populations are well represented in the
1216 Middle Triassic to Oligocene of the Kyrenia Range (Fig. 11). Zircon trace element
1217 compositions are suggestive of mixed continental arc and within-plate (e.g., rift-

1
2
3
4
5
6
7
8
9
10
11
12
13
14
15
16
17
18
19
20
21
22
23
24
25
26
27
28
29
30
31
32
33
34
35
36
37
38
39
40
41
42
43
44
45
46
47
48
49
50
51
52
53
54
55
56
57
58
59
60
61
62
63
64
65

1218 related) settings (see Section 4.13). Potential sources are exposed in both the
1219 Taurides and the Anatolides. Carboniferous granites locally intrude older
1220 lithologies in the Afyon zone of the Anatolides, central W Turkey (Candan et al.,
1221 2016; Ustaömer et al., 2020), although these appear to be volumetrically minor.
1222 Basaltic-intermediate composition volcanics and volcanoclastic sediments are
1223 widely distributed across Tauride-related units in central and eastern Anatolia,
1224 extending at least from the Sultan Dağı in the western central Anatolia to the
1225 Malatya Massif in central eastern Anatolia (Göncüoğlu et al., 2007; Robertson et
1226 al., 2021a) (Fig. 1). Carboniferous magmatism affected the north margin of
1227 Gondwana following the opening of Paleotethys during Late Silurian-Devonian
1228 time (Stampfli and Borel, 2002; Cocks and Torsvik, 2006; Özbey et al., 2013;
1229 Robertson et al., 2021a).

1230 Alternative explanations of the Carboniferous magmatism involve either rifting
1231 of the north-Gondwana continental margin or southward subduction of Paleotethys
1232 (see Robertson et al., 2021a). Carboniferous magmatic rocks also occur in the
1233 Konya Complex of the Anatolides (Afyon zone) (Fig. 1), although being
1234 volumetrically minor and mainly basaltic these are unlikely to have provided many
1235 zircons. In addition, voluminous sandstone turbidites within the Konya Complex
1236 include abundant Precambrian, Carboniferous, and locally also, Devonian zircons
1237 (Löwen et al., 2020; Ustaömer et al., 2020). The Carboniferous zircons are
1238 interpreted by Löwen et al. (2020) to have been derived from the Sakarya zone of
1239 the NW Pontides (Fig. 1). However, Lu-Hf isotopic ratios of the Carboniferous
1240 detrital zircons are dissimilar to those of the zircons of similar age in the NW

1
2
3
4
5
6
7
8
9
10
11
12
13
14
15
16
17
18
19
20
21
22
23
24
25
26
27
28
29
30
31
32
33
34
35
36
37
38
39
40
41
42
43
44
45
46
47
48
49
50
51
52
53
54
55
56
57
58
59
60
61
62
63
64
65

1241 Pontides (Fig. 12), and alternative sources have been suggested farther west; i.e.,
1242 within the north-Aegean region or beyond (Ustaömer et al., 2020).

1243 Small volumes of Permian alkaline volcanic rocks are known in the Taurides,
1244 specifically within the Antalya Complex in the Güzelsu area (N of Cyprus) (Şahin
1245 et al., 2012) and within the Mersin Melange further east (Tekin et al., 2019) (Fig.
1246 1). Also, Permian detrital grains occur in some Triassic Tauride sandstones,
1247 although their source is unclear (Ustaömer et al., 2020). The Permian volcanism
1248 is attributed to rifting of Neotethys (Tekin et al., 2019; Ustaömer et al., 2020;
1249 Robertson et al., 2021b), which is compatible with the relatively high Nb/Hf ratios
1250 of the detrital zircons (see Section 4.13).

1251

1252 6.3.3. Mesozoic

1253 The Kyrenia Range Triassic zircons show a range of continental margin arc to
1254 intra-plate settings (see Section 4.13), consistent with a mixed derivation. Triassic
1255 zircons, generally $n < 4$, were potentially derived from the widespread Triassic
1256 volcanics of the Tauride allochthons, including the Lycian nappes to the NW
1257 (Collins and Robertson, 1998; Sayit et al., 2015), the Antalya Complex directly to
1258 the NW (Robertson and Waldron, 1990; Maury et al., 2008; Robertson and Parlak,
1259 2020; Robertson et al., 2020), the Beyşehir-Hoyran-Hadim (Bözkır) nappes to the
1260 north (Özgül, 1997; Andrew and Robertson, 2002), the Mersin Melange directly to
1261 the north (Parlak and Robertson, 2004; Sayit et al., 2017, 2020), the Andırın region
1262 to the NE (Uzuncimen et al., 2011; Robertson et al., 2016) and the Baer-Bassit
1263 region (N Syria) to the east (Al-Riyami and Robertson, 2002) (Fig. 1). The Triassic

1
2
3
4
5
6
7
8
9
10
11
12
13
14
15
16
17
18
19
20
21
22
23
24
25
26
27
28
29
30
31
32
33
34
35
36
37
38
39
40
41
42
43
44
45
46
47
48
49
50
51
52
53
54
55
56
57
58
59
60
61
62
63
64
65

1264 magmatic rocks of the Antalya, Andırın and Baer-Bassit units relate to rifting of the
1265 Southern Neotethys (e.g., Robertson et al., 2012a). In contrast, the Triassic
1266 magmatic rocks within the Lycian nappes, the Beyşehir-Hoyran-Hadim nappes and
1267 probably also the Mersin Melange relate to rifting of the İzmir-Ankara-Erzincan
1268 ocean (Northern Neotethys) farther north (Özgül, 1984a; Andrew and Robertson,
1269 2002; Göncüoğlu et al., 2003; Parlak and Robertson, 2004). These allochthonous
1270 units were emplaced generally southwards over the Mesozoic Tauride carbonate
1271 platform during latest Cretaceous and Eocene (Özgül, 1997; Mackintosh and
1272 Robertson, 2009). Triassic meta-volcanic rocks (subduction-influenced) occur
1273 further north, within the Afyon zone of the Anatolides (Akal et al., 2012). As a whole,
1274 the Triassic volcanics are basaltic and so are unlikely to have supplied many
1275 zircons.

1276 Jurassic zircons are rarely present in the Upper Cretaceous Kiparisso Vouno
1277 Member, the Middle Eocene Kalograia-Ardana Formation, the Upper Eocene-
1278 Oligocene Bellapais Formation and the Miocene Trapeza, Davlos and Yılmazköy
1279 formations (Fig. 11). The rare zircons analysed (n=3) with low Nb/Hf but high U/Yb
1280 ratios are consistent with a continental arc origin (Fig. 9). Jurassic igneous rocks
1281 are virtually absent from the Mesozoic carbonate platform units of the Taurides and
1282 Anatolides. Jurassic seamount-type volcanics do, however, characterise the
1283 Northern Neotethyan suture zone (İzmir-Ankara-Erzincan suture zone) (e.g., Rojay
1284 et al., 2004; Bortolotti et al., 2018). Middle-Upper Jurassic ophiolites and rare
1285 associated granitoid arc intrusives of the Ankara-Erzincan suture zone further east
1286 are potentially a source of Jurassic zircons (Dilek and Thy, 2006; Rolland et al.,

1
2
3
4
5
6
7
8
9
10
11
12
13
14
15
16
17
18
19
20
21
22
23
24
25
26
27
28
29
30
31
32
33
34
35
36
37
38
39
40
41
42
43
44
45
46
47
48
49
50
51
52
53
54
55
56
57
58
59
60
61
62
63
64
65

1287 2011; Çelik et al., 2013; Sarıfakıoğlu et al., 2017). In Eastern Anatolia, basaltic
1288 rocks are interbedded with Lower to Middle Jurassic deep-marine radiolarites that
1289 were emplaced southwards onto Tauride platform units during the Late Cretaceous
1290 (Robertson et al., 2016, 2021b); these basaltic rocks could also have provided a
1291 southward supply of zircon.

1292 Elsewhere, alkaline/per-alkaline volcanics are interbedded with Middle
1293 Jurassic-Lower Cretaceous radiolarites in Baer-Bassit, N Syria (Al-Riyami and
1294 Robertson, 2002; Al-Riyami et al., 2002) (Fig. 1). Tiny intrusive bodies of this age
1295 range are also present in the Mamonia Complex, SW Cyprus (Fig. 1) (Chan et al.,
1296 2008). In addition, either plume-related (Garfunkel, 1998), or rift-related (Gardosh
1297 et al., 2010), Lower Jurassic volcanics occur in the northern margin of the Levant
1298 platform. Jurassic volcanics are also well represented in the Pontides, northern
1299 Turkey (Altıner et al., 1991; Genç and Tüysüz, 2010; Ustaömer et al., 2013; Okay
1300 et al., 2015; Akdoğan et al., 2018) (Fig. 1). Dismembered Jurassic ophiolites within
1301 the Intra-Pontide suture zone include basaltic extrusive and intrusive rocks (e.g.,
1302 Marroni et al., 2020).

1303 The only Lower Cretaceous zircon analysed, which is characterised by an
1304 enrichment of Y (2288 ppm) and a relatively low U/Yb ratio (0.012), could have an
1305 oceanic crust origin (see Table S2). Lower Cretaceous volcanism is documented,
1306 both within the Inner Tauride suture zone (Robertson et al., 2016) and the Northern
1307 Neotethyan suture zone (farther north), based on paleontological dating of
1308 interbedded deep-sea sediments (e.g., Rojay et al., 2004). However, these
1309 magmatic rocks are unlikely to have contributed many zircons as they are again

1
2
3
4
5
6
7
8
9
10
11
12
13
14
15
16
17
18
19
20
21
22
23
24
25
26
27
28
29
30
31
32
33
34
35
36
37
38
39
40
41
42
43
44
45
46
47
48
49
50
51
52
53
54
55
56
57
58
59
60
61
62
63
64
65

1310 mainly basaltic.

1311 Upper Cretaceous detrital zircon grains dominate the Mesozoic populations
1312 of the Kyrenia Range (see section 6.2). Of these, a few Upper Cretaceous (83-69
1313 Ma) grains from the Yılmazköy Formation, with Th/U ratios (<0.1) (see
1314 Supplementary Figure S5), are of metamorphic origin. Metamorphic zircons form
1315 under a wide range of greenschist, to amphibolite, to blueschist-facies conditions
1316 (e.g., Rubatto, 2002; Dempster et al., 2004; Hay and Dempster, 2009). Cretaceous
1317 greenschist to blueschist facies metamorphic rocks generally to the north of the
1318 Kyrenia Range that might have supplied zircons include the Alanya Massif of S
1319 Turkey (Campanian; 84-75 Ma) (Çetinkaplan et al., 2016), the Upper Paleozoic to
1320 Upper Cretaceous Malatya Metamorphics of E Turkey (Perinçek and Kozlu, 1984;
1321 Robertson et al., 2006, 2021b), the Afyon zone (Maastrichtian, 97-62 Ma)
1322 (Pourteau et al., 2010, 2016) and the Tavşanlı zone (Turonian-Selandian; 92-60
1323 Ma) (Okay et al., 1998, 2020; Sherlock et al., 1999) (Fig. 1).

1324 In addition, the few Upper Cretaceous grains (89-66 Ma) analysed from the
1325 Yılmazköy Formation, with Th/U >1.5 (Supplementary Figure S5), are inferred to
1326 be of mafic origin. Source candidates include numerous Cretaceous basaltic units,
1327 mainly associated with ophiolites and volcanic arc units throughout SE Anatolia
1328 (e.g., Schleiffarth et al., 2018), specifically, Upper Cretaceous ophiolites (92-84 Ma)
1329 and arc-related granitoids (ca. 88-70 Ma) (Parlak, 2006; Karaoğlan et al., 2012,
1330 2013, 2016; Nurlu et al., 2016). The highly variable U/Yb and Nb/Yb zircon ratios
1331 suggest a mixed derivation from both continental arc and ophiolite-related source
1332 (see Section 4.13). In contrast, the Troodos ophiolite to the south is an unlikely

1
2
3
4
5
6
7
8
9
10
11
12
13
14
15
16
17
18
19
20
21
22
23
24
25
26
27
28
29
30
31
32
33
34
35
36
37
38
39
40
41
42
43
44
45
46
47
48
49
50
51
52
53
54
55
56
57
58
59
60
61
62
63
64
65

1333 source of Upper Cretaceous ophiolitic detritus as it remained covered by Upper
1334 Cretaceous to Upper Pliocene marine sediments, as exposed along the southern
1335 margin of the Mesaoria Basin and in deep wells to the south of the Kyrenia Range
1336 (Fig. 4) (e.g., Robertson and Hudson, 1974; Lord et al., 2000; Harrison et al., 2004;
1337 Morag et al., 2016). Uplift and deep erosion of the Troodos Massif did not take
1338 place until the Pleistocene (e.g., Poole and Robertson, 1991; Kinnaird and
1339 Robertson, 2013; Ring and Pantazides, 2019) and, therefore, a supply of detritus
1340 from the Troodos ophiolite or its sedimentary cover to the Kyrenia Range is unlikely.
1341 As a caveat, it should be noted however that the composition of any crust beneath
1342 the Kyrenia Range remains unknown.

1343

1344 6.3.4. Cenozoic

1345 A minor Eocene zircon population in the Kyrenia Range peaks at ca. 53-47 Ma
1346 (Fig. 11). Continental arc-type trace element compositions dominated the zircons
1347 analysed, together with a minor within-plate-type fraction (see Section 4.13).
1348 Eocene volcanic rocks and small related intrusives are present in the Maden
1349 Complex (Fig. 1), as widely exposed across Eastern Anatolia (Aktaş and
1350 Robertson, 1984, 1990, Elmas and Yılmaz, 2003; Erturk et al., 2018). These rocks
1351 are mainly basaltic-andesitic and therefore may not be an important zircon source.
1352 Localised, Lower-Mid Eocene magmatic rocks of alkaline, within-plate type (both
1353 extrusives and intrusives), occur farther north, e.g., in the Hekimhan Basin of
1354 central E Turkey (Fig. 1) (Booth et al., 2014). Other possible sources include calc-
1355 alkaline magmatic rocks, mainly granitoids (e.g., Doğanşehir area; Fig. 1), in SE

1
2
3
4
5
6
7
8
9
10
11
12
13
14
15
16
17
18
19
20
21
22
23
24
25
26
27
28
29
30
31
32
33
34
35
36
37
38
39
40
41
42
43
44
45
46
47
48
49
50
51
52
53
54
55
56
57
58
59
60
61
62
63
64
65

1356 Turkey (Karaođlan et al., 2013; Parlak et al., 2013). Zircons are abundant in these
1357 rocks, although the Eocene granitoids are much less extensive than the Upper
1358 Cretaceous granitoids in the same region (see above).

1359 A few Oligocene grains are present in the Middle-Upper Miocene Trapeza and
1360 Yılmazk y formations of the eastern and central Kyrenia Range (Table S1). Post-
1361 collisional Oligocene volcanism is well documented in W Turkey (Yılmaz, 1989;
1362 Altunkaynak and Gen, 2008; Ersoy et al., 2012) but is rare in central and E Turkey
1363 (Oyan, 2018), closer to the Kyrenia Range.

1364 Miocene zircons, peaking at ca. 20 Ma, 16 Ma and 9 Ma, constitute up to 17%
1365 of the grains analysed in the Middle to Upper Miocene sediments (Table S1) (see
1366 section 6.2). Available zircon trace element compositions are suggestive of mixed
1367 continental arc and within-plate settings (see Section 4.13). Possible sources
1368 include the Neogene, post-collisional volcanic rocks in the southern Kırşehir Block
1369 (Fig. 1), central Anatolia (e.g., Innocenti et al., 1975). Volcanic rocks in this region
1370 range from Early Miocene (21 Ma) to Quaternary (Innocenti et al., 1975; Platzman
1371 et al., 1998; Asan and Kurt, 2011; Schleiffarth et al., 2018). Generally younger (ca.
1372 13 Ma-Holocene) post-collisional magmatic rocks occur farther east, within the
1373 Eastern Anatolia Volcanic Province of E Turkey, Armenia and NE Iran (Innocenti
1374 et al., 1975; Pearce et al., 1990; Keskin et al., 1998), although this is >900 km
1375 northeast of Cyprus. Felsic ignimbrites of the İzmir-Afyon-Isparta volcanic zone in
1376 the Western Anatolian Volcanic Province also have similar radiometric ages; i.e.,
1377 ca. 21-10 Ma (Aquitanian-Tortonian) (e.g., Bing l, 1977; Aydar, 1998; Dilek and
1378 Altunkaynak, 2010). Lower to Middle Miocene (ca. 19-15 Ma) basaltic magmatic

1
2
3
4
5
6
7
8
9
10
11
12
13
14
15
16
17
18
19
20
21
22
23
24
25
26
27
28
29
30
31
32
33
34
35
36
37
38
39
40
41
42
43
44
45
46
47
48
49
50
51
52
53
54
55
56
57
58
59
60
61
62
63
64
65

1379 rocks are widespread in central and eastern Anatolia (e.g., Sivas-Elazığ-Malatya
1380 regions; Fig. 1) (e.g., Arger et al., 2000; Önal et al., 2008; Gürsoy et al., 2011),
1381 mainly as basanites to basaltic andesites, with subordinate rhyolite, rhyolitic dykes,
1382 trachyandesite and basaltic-trachyandesitic dykes (e.g., Arger et al., 2000; Önal et
1383 al., 2008). Much closer sources are mainly restricted to basaltic and andesitic rocks
1384 in the Türkoğlu-Pazarcık area of the Kahramanmaraş region (Fig. 1), which are
1385 dated as 18.6-16.5 Ma (Burdigalian) by the K-Ar method (Arger et al., 2000). Lower
1386 Miocene basaltic extrusive rocks and minor associated dykes occur extensively in
1387 the central and northern Amanos Mountain area (Fig. 1), to the northeast of Cyprus
1388 (Duman et al., 2017). In addition, zircons could have been locally reworked from
1389 tuffaceous intercalations in the underlying Panagra Formation, which have a U-Pb
1390 age of ca. 16.6 Ma (Burdigalian) (Chen and Robertson, 2021a).

1391 Messinian (6-5 Ma) zircon grains are very abundant (55%) in the Yazılıtepe
1392 Formation (Table S5). A relatively proximal source could be airfall tuffs and silicic
1393 extrusives, which are dated as 5.8 Ma by the Ar-Ar method in the Erciyes Basin,
1394 central Turkey (Fig. 1) (Jaffey et al., 2004). Messinian rhyolites and airfall tuffs are
1395 present in the Kırşehir Block, central Anatolia (Aydar et al., 2012). 6.2-5.2 Ma-aged
1396 lavas occur in coastal areas of western Syria (Baniyas-Mt Saphita; Fig. 1) (Sharkov
1397 et al., 1994, 1998; Trifonov et al., 2011). In addition, Messinian ash layers (5.53
1398 Ma) are reported from the central-northern Mediterranean Basin (Cosentino et al.,
1399 2013).

1400

1401 6.3.5. Major zircon sources

1
2
3
4
5
6
7
8
9
10
11
12
13
14
15
16
17
18
19
20
21
22
23
24
25
26
27
28
29
30
31
32
33
34
35
36
37
38
39
40
41
42
43
44
45
46
47
48
49
50
51
52
53
54
55
56
57
58
59
60
61
62
63
64
65

1402 Bearing in mind that felsic rocks, especially intrusives, are the most likely to
1403 have supplied zircons (Watson and Harrison, 1983; Keller et al., 2017), the
1404 following units seem most likely to have contributed large number of zircons to the
1405 Kyrenia Range:

1406 (1) The Precambrian grains were likely recycled from the rifted Cadomian
1407 microcontinental blocks and, or their Paleozoic sedimentary cover in southern
1408 Turkey. The sources were therefore generally to the north rather than from the
1409 Arabian-Nubian Shield directly;

1410 (2) The Upper Ediacaran-Lower Cambrian grains relate to erosion of
1411 Cadomian active margin granitoids (e.g., Bitlis Massif, SE Turkey) that were
1412 intruded along the north-Gondwana margin. After Triassic rifting, these Caromian
1413 zircons were derived generally from the north, in Turkey, possibly following
1414 significant recycling;

1415 (3) Devonian-Carboniferous zircons are likely to have been derived from
1416 Devonian-earliest Permian sandstone turbidites of the Konya Complex (or
1417 equivalents), as located along the northern margin of the Anatolide-Tauride Block
1418 (Afyon zone) in central Anatolia. Another, local source could be from the upper
1419 Carboniferous granitoids in the same area, although, as currently known, these
1420 are volumetrically minor and may not have been exhumed by late Carboniferous
1421 time. Direct derivation from the Upper Paleozoic, S Eurasian active continental
1422 margin is unlikely because in many interpretations Paleotethys intervened (see
1423 discussion in section 6.6);

1424 (4) Upper Cretaceous zircons were derived from coeval arc-related granitoids,

1
2
3
4
5
6
7
8
9
10
11
12
13
14
15
16
17
18
19
20
21
22
23
24
25
26
27
28
29
30
31
32
33
34
35
36
37
38
39
40
41
42
43
44
45
46
47
48
49
50
51
52
53
54
55
56
57
58
59
60
61
62
63
64
65

1425 as widely exposed in SE Turkey;

1426 (5) Eocene zircons came from the arc/back-arc magmatic rocks of the Maden
1427 Complex in SE Turkey;

1428 (6) Neogene zircons were derived from evolved, post-collisional volcanic
1429 products in SE Turkey.

1430

1431 6.4. Sediment pathways

1432 The interpretation of zircon provenance and deposition needs to take account of
1433 available sedimentological evidence, especially paleocurrent data from the
1434 Eocene-Miocene clastic sediments. Northern Cyprus was characterised by
1435 southerly paleocurrents during the Late Eocene-Early Oligocene (Fig. 2), as
1436 indicated by variably developed clast imbrication within the Kythrea Conglomerate
1437 (McCay and Robertson, 2012) (see Supplementary Figure S2). As summarized
1438 above, the combined zircon data indicate that suitable-aged source lithologies
1439 exist generally to the north of Cyprus, including within the Precambrian basement
1440 of the Alanya Massif (Çetinkaplan et al., 2016; Çetinkaplan, 2018), the Antalya
1441 Complex (e.g., Güzelsu area) (Monod, 1977; Robertson et al., 2020), the Mersin
1442 Melange (Parlak and Robertson, 2004; Sayit et al., 2017, 2020) and the Beyşehir-
1443 Hoyran-Hadim (Bözkır) nappes that were emplaced southwards over the Mesozoic
1444 Tauride carbonate platform finally during the Eocene (Özgül, 1997; Andrew and
1445 Robertson, 2002; Mackintosh and Robertson, 2012) (Fig. 1). The clast composition
1446 (including ophiolitic rocks) and the paleocurrent data suggest that the non-marine
1447 Kythrea Conglomerate was supplied generally from the north; i.e., from southern

1
2
3
4
5
6
7
8
9
10
11
12
13
14
15
16
17
18
19
20
21
22
23
24
25
26
27
28
29
30
31
32
33
34
35
36
37
38
39
40
41
42
43
44
45
46
47
48
49
50
51
52
53
54
55
56
57
58
59
60
61
62
63
64
65

1448 Turkey or from the now-submerged crust beneath the Cilicia Basin, rather than
1449 locally from the Kyrenia Range. A further implication is that the deep-water Cilicia
1450 basin post-dates the Kythrea Conglomerate (Robertson and Woodcock, 1986;
1451 McCay and Robertson, 2012).

1452 Our new results also indicate that Precambrian grains have more significant
1453 age populations in the western and central ranges compared to the eastern range
1454 and the Karpas Peninsula (Table S5; see section 6.2). A possible explanation is
1455 that the Precambrian grains were preferentially derived from the basement of the
1456 Alanya Massif generally to the northwest of Cyprus (Fig. 1), whereas Precambrian
1457 basement is absent to the north of the eastern range and the Karpas Peninsula
1458 (MTA, 2011). Consistent with their outcrop distribution, the Alanya Massif and the
1459 equivalent Bitlis and Pütürge massifs (Fig. 1) of SE Turkey have been interpreted
1460 as separate Mesozoic microcontinental blocks rather than as a continuous crustal
1461 unit (e.g., Şengör and Yılmaz, 1981; Robertson and Dixon, 1984; Robertson et al.,
1462 2012a).

1463 The Upper Cretaceous Kiparisso Vouno Member and the Middle Eocene
1464 Kalograia-Ardana Formation include significant populations of Carboniferous-
1465 Permian detrital zircons (see section 6.2) for which there is no obvious source in
1466 Cyprus or the adjacent E Mediterranean region (Chen et al., 2019; Glazer et al.,
1467 2021). One possible explanation, mentioned above (section 6.3), is that the
1468 Carboniferous-Permian zircons were ultimately derived from the Paleotethyan
1469 suture zone to the west of Turkey, where Paleotethys sutured prior to Early
1470 Permian in some interpretations (e.g., Zanchi et al., 2003; Robertson and

1
2
3
4
5
6
7
8
9
10
11
12
13
14
15
16
17
18
19
20
21
22
23
24
25
26
27
28
29
30
31
32
33
34
35
36
37
38
39
40
41
42
43
44
45
46
47
48
49
50
51
52
53
54
55
56
57
58
59
60
61
62
63
64
65

1471 Ustaömer, 2009b; Okay and Topuz, 2017; Robertson, 2022).

1472 Whatever their magmatic source(s), Carboniferous zircons accumulated
1473 along the northern margin of Gondwana (Anatolides) during the late
1474 Carboniferous-earliest Permian, within the Konya Complex and its Mesozoic cover
1475 (Halıcı and Ardıçlı formations), or equivalent units (e.g., Löwen et al., 2020). Once
1476 deposited there, southward recycling became possible, independently of their
1477 original source. Carboniferous-Permian zircons also occur within Middle-Upper
1478 Triassic sandstones of the Taurides, including the Anamas-Akseki platform
1479 (Kasımlar Formation) (Ustaömer et al., 2020) and the Karaburun Peninsula of
1480 Aegean Turkey (Güvercinlik Formation) (Löwen et al., 2017; Ustaömer et al., 2020)
1481 (Fig. 1). The Carboniferous zircons from the Tauride and the Karaburun Peninsula
1482 samples, with characteristic $\epsilon\text{Hf}(t)$ values < -5 , are compatible with a source within
1483 Carboniferous arc-type granites of the Anatolides (Ustaömer et al., 2020), although
1484 other sources are possible. The Carboniferous Kyrenia Range zircons have a
1485 continental arc affinity (see Section 4.13), together with a likely felsic/intermediate-
1486 related magmatic origin (i.e., $\text{Th}/\text{U}=0.22\text{-}0.85$; median 0.47), also mainly negative
1487 $\epsilon\text{Hf}(t)$ ranging from -8 to -3 (see section 4.14), which together suggest
1488 granitic/andesitic source(s), either from Eurasia or from the Anatolides (although
1489 known outcrops there are small).

1490 Relatively common (3-7%) Carboniferous zircons, together with a few
1491 Permian zircons, occur farther south, within the Middle-Upper Triassic sandstones
1492 of the Antalya Complex (Güzelsu area) and reach ca. 18% in some Cretaceous
1493 sandstones in the same area (Chen et al., 2022). Black chert grains are present in

1
2
3
4
5
6
7
8
9
10
11
12
13
14
15
16
17
18
19
20
21
22
23
24
25
26
27
28
29
30
31
32
33
34
35
36
37
38
39
40
41
42
43
44
45
46
47
48
49
50
51
52
53
54
55
56
57
58
59
60
61
62
63
64
65

1494 Middle-Upper Triassic sandstone turbidites in many areas (Gutnic et al., 1979),
1495 including the NE Antalya Complex (Waldron, 1984), the SW Antalya Complex
1496 (Robertson and Woodcock, 1984) and the E Antalya Complex (Alanya window)
1497 (Robertson et al., 2020). In the absence of any stratigraphically underlying (older)
1498 source of black chert (mid-Triassic cherts are reddish coloured), the black chert is
1499 likely to have been derived from Paleotethys to the north. In support, paleocurrents,
1500 measured in mainly Upper Triassic successions (Çayır Formation) exposed in both
1501 the regional autochthon (Geyik Dağı) and the over-riding thrust sheets (Bolkar and
1502 Hadim nappes) (Fig. 1) are southerly directed (Mackintosh and Robertson, 2009).

1503 Upper Paleozoic detrital zircons are unlikely to have been transported far
1504 southwards during the Jurassic-Eocene because developing carbonate platforms,
1505 notably the Bey Dağları, Geyik Dağı and Akseki-Anamas platforms (e.g., Özgül,
1506 1997) (Fig. 1) are likely to have blocked this transport route. Northerly sources
1507 were potentially re-established during the Eocene following the southward over-
1508 thrusting of the Tauride thrust sheets (Beyşehir-Hoyran-Hadim nappes) that
1509 include Triassic sandstones (e.g., Hadim and Bolkar nappes) (Özgül, 1997;
1510 Mackintosh and Robertson, 2013; McPhee et al., 2018). Any additional clastic
1511 sediment supply from northwest of the Bey Dağları carbonate platform (Fig. 1) was
1512 delayed until the Miocene (Hayward and Robertson, 1982).

1513 Of the Kyrenia Range zircons analysed, Devonian grains are relatively rare
1514 (generally <4), similar to the abundance in the Middle-Upper Triassic sandstones
1515 of the Tauride Anamas-Akseki platform (Kasımlar Formation) (Ustaömer et al.,
1516 2020). In contrast, the upper Carboniferous and Triassic sandstones of the

1
2
3
4
5
6
7
8
9
10
11
12
13
14
15
16
17
18
19
20
21
22
23
24
25
26
27
28
29
30
31
32
33
34
35
36
37
38
39
40
41
42
43
44
45
46
47
48
49
50
51
52
53
54
55
56
57
58
59
60
61
62
63
64
65

1517 Karaburun Peninsula contain abundant Devonian zircons that, however, occur only
1518 locally in the Konya Complex (Löwen et al., 2017, 2020). The paucity of Devonian
1519 zircons in the Tauride Triassic and in the Kyrenia Range sandstones is at odds with
1520 the Kyrenia Range being located along the Eurasian continental margin during the
1521 Late Paleozoic-Paleocene (see section 6.6).

1522 In summary, we infer that the Upper Paleozoic detrital zircons of the Kyrenia
1523 Range were mainly derived from Paleotethyan active margin magmatic rocks, with
1524 the ultimate source being located in the N Aegean region or farther west. Zircons
1525 of this age range were eroded and deposited in upper Carboniferous-earliest
1526 Permian sandstone turbidites along the northern margin of Gondwana (Afyon zone,
1527 Anatolides). After Triassic uplift and erosion in the north Upper Paleozoic zircons
1528 were transported southwards within non-marine, shallow-marine and deep-marine
1529 siliciclastic sediments, mainly during Mid-Late Triassic time. After having reached
1530 a southerly position bordering the Southern Neotethys, Carboniferous-Permian
1531 zircon-bearing facies were strongly deformed during the Late Cretaceous
1532 (Campanian-Maastrichtian) and again during the Late Paleocene-Middle Eocene
1533 related to Neotethyan closure. The zircons were then supplied to the relict S
1534 Neotethys (Eastern Mediterranean Sea), including the future Kyrenia Range.

1535 The Oligocene was characterised by a fundamental shift from southward to
1536 westward deep-water gravity flows persisted at least until the Messinian (Fig. 2).
1537 This switch is inferred from abundant paleocurrent data (e.g., flutes, grooves) in
1538 sandstone turbidites from both the northern and the southern flanks of the Kyrenia
1539 Range (Weiler, 1970; McCay and Robertson, 2012) (see Supplementary Figures

1
2
3
4
5
6
7
8
9
10
11
12
13
14
15
16
17
18
19
20
21
22
23
24
25
26
27
28
29
30
31
32
33
34
35
36
37
38
39
40
41
42
43
44
45
46
47
48
49
50
51
52
53
54
55
56
57
58
59
60
61
62
63
64
65

1540 S2-S3). Lithologies of the appropriate ages to supply zircons to the Kyrenia Range
1541 are present throughout the Misis-Andırın-Engizek suture zone (Kelling et al., 1987;
1542 Robertson et al., 2004, 2006) and its eastward extension, the Bitlis suture zone in
1543 SE Turkey (Fig. 1). The suturing resulted from Eocene-Lower Miocene closure of
1544 the Southern Neotethys (e.g., Perinçek and Kozlu, 1984; Aktaş and Robertson,
1545 1984; Yılmaz, 1993; Robertson et al., 2004; Darin et al., 2018).

1546 The Upper Eocene-Oligocene Bellapais Formation was sourced locally,
1547 mainly from the north (Fig. 2), until subsidence of the Cilicia Basin (Fig. 1) between
1548 the Kyrenia Range and Turkey ended this southerly sediment supply, including the
1549 Upper Paleozoic zircons.

1550 Conversely, zircons of Late Cretaceous, Eocene and Miocene ages became
1551 more abundant in progressively younger sediments (see section 6.2). The
1552 prevailing westward paleocurrents (Fig. 2) point to sources in SE Turkey, as noted
1553 above. In eastern Anatolia, metamorphic and volcanic arc rocks were partially
1554 exhumed by the latest Cretaceous based on stratigraphic evidence (Perinçek and
1555 Kozlu, 1984; Robertson et al., 2016, 2021b). There is also evidence of thrusting,
1556 uplift and erosion during the Eocene (e.g., Hekimhan area). Southward thrusting
1557 during the Early-Middle Miocene (related to collision) and then again during the
1558 Late Miocene (related to suture tightening), resulted in uplift and erosion (Okay et
1559 al., 2010; Karaoğlan et al., 2016; Cavazza et al., 2018). The uplift accelerated
1560 erosion into deeper levels of the thrust stack, resulting in longer and deeper fluvial
1561 incision into Upper Cretaceous and Eocene lithologies (e.g., granitoids), coupled
1562 with supply from post-collisional Miocene magmatic rocks, for example, in the

1
2
3
4
5
6
7
8
9
10
11
12
13
14
15
16
17
18
19
20
21
22
23
24
25
26
27
28
29
30
31
32
33
34
35
36
37
38
39
40
41
42
43
44
45
46
47
48
49
50
51
52
53
54
55
56
57
58
59
60
61
62
63
64
65

1563 Sivas-Elazığ-Malatya-Kahramanmaraş region (Fig. 1) (e.g., Arger et al., 2000;
1564 Önal et al., 2008; Gürsoy et al., 2011).

1565 The northeasternmost corner of the Arabian platform was uplifted, related to
1566 continental collision during the Oligocene-Miocene (Boulton, 2009; Duman et al.,
1567 2017), potentially providing an additional source of Precambrian to Miocene
1568 zircons. However, the Precambrian outcrop area is minimal, suggesting that the
1569 Amanos Mountains were not a significant source. The Upper Cretaceous ophiolites
1570 in this area (e.g., Hatay ophiolite) are unlikely to have supplied many zircons as
1571 these are basic-ultrabasic igneous rocks with very few zircons.

1572 Detrital zircon sources from within the uplifted Arabian continent to the east or
1573 southeast of Cyprus are questionable because of the development of several
1574 intervening topographic lineaments (e.g., the Tartus and Amanos-Larnaca ridges)
1575 (Fig. 1) that are likely to have blocked northwestward turbidity current flow (Ben-
1576 Avraham et al., 1995; Robertson, 1998; Calon et al., 2005a; Hardenberg and
1577 Robertson, 2007). Sediments from the onshore Arabian plate areas are likely to
1578 have accumulated mainly within the Outer Latakia Basin, the Cyprus Basin and
1579 the deeper Levant Basin to the SW (Fig. 1).

1580 Given the dominantly westward paleocurrents, the most likely controls of
1581 zircon provenance during the Miocene-Pleistocene are: (1) uplift of SE Anatolia
1582 beginning during Middle-Late Miocene (Jaffey and Robertson, 2005; Okay et al.,
1583 2010; Meijers et al., 2020); (2) development of the Seyhan, Ceyhan and other
1584 regional river catchments as major sediment suppliers to the NE Mediterranean
1585 basin (e.g., Robertson et al., 2019); and (3) development of ca. SW-NE trending

1
2
3
4
5
6
7
8
9
10
11
12
13
14
15
16
17
18
19
20
21
22
23
24
25
26
27
28
29
30
31
32
33
34
35
36
37
38
39
40
41
42
43
44
45
46
47
48
49
50
51
52
53
54
55
56
57
58
59
60
61
62
63
64
65

1586 topographic ridges (e.g., Kyrenia-Misis, Tartus and Amanos-Larnaca ridges) (see
1587 above; Fig. 1) that channelled turbidite distribution towards Cyprus from specific
1588 fluvial inputs.

1589 A recent reconstruction during the Messinian sea-level drawdown (Aksu et al.,
1590 2021) suggests that the Seyhan and Göksu paleorivers could have contributed
1591 much sediment to the Cilicia Basin and the future Kyrenia Range, whereas the
1592 paleo-Ceyhan and Orontes (Asi) river systems carried sediment to the Latakia and
1593 Mesaoria basins (Fig. 1) (e.g., Calon et al., 2005a) farther southwest. A clue to the
1594 Miocene sediment provenance is provided by the contrasting zircon age profiles
1595 of the southern versus northern sub-basins of the Kyrenia Range (see section 6.2).
1596 For the Upper Miocene and Pleistocene sandstones, especially the Middle-Upper
1597 Miocene Trapeza Formation, the southern sub-basin samples are characterised
1598 by a relatively high Cretaceous-Miocene zircon contribution. On the other hand,
1599 the samples from the northerly sub-basin have relatively small Miocene fractions
1600 (see section 6.2). Preliminary zircon geochronological data from Oligocene-
1601 Miocene turbidites in the adjacent Miocene Adana Basin indicate similarities with
1602 the Kyrenia Range northern sub-basin; e.g., relatively sparse Miocene detritus
1603 (Chen et al., 2021). The Adana Basin is transected by the Seyhan River (Fig. 1),
1604 which may have contributed zircons to both of these areas during the Late Miocene.
1605 Conversely, the Misis Basin farther southeast (Fig. 1) shows similarities with the
1606 Kyrenia Range southern sub-basin; e.g., relatively abundant (and constant) Upper
1607 Cretaceous to Miocene detrital input (Chen et al., 2021). The Ceyhan River runs
1608 through the Misis Basin (Fig. 1) and could have contributed zircons to both the

1
2
3
4
5
6
7
8
9
10
11
12
13
14
15
16
17
18
19
20
21
22
23
24
25
26
27
28
29
30
31
32
33
34
35
36
37
38
39
40
41
42
43
44
45
46
47
48
49
50
51
52
53
54
55
56
57
58
59
60
61
62
63
64
65

1609 Misis Basin and the Kyrenia Range southern sub-basin.

1610 Clastic sediment supply to the easternmost Mediterranean Sea was strongly
1611 influenced by the surface uplift of central and southeast Anatolia. Paleogeographic
1612 reconstruction based on leaf, pollen and phytolith data suggests that highlands
1613 existed by the Middle to Late Miocene, for example in the central east region
1614 (Sivas-Adana) of SE Anatolia (e.g., Huang et al., 2019; Meijers et al., 2020). The
1615 uplift triggered a switch from inward-drainage basins to incision and outflow to the
1616 eastmost Mediterranean Sea, for example along the strike-slip controlled Ecemiş
1617 corridor (Fig. 1) (Jaffey and Robertson, 2005). Major drainage catchments became
1618 established (e.g., Seyhan and Göksu paleorivers) and were entrenched during the
1619 Messinian low-stand (Aksu et al., 2021). Further uplift focussed on the Taurus
1620 Mountains took place during the Late Miocene-Pleistocene steepening the
1621 southern margin of the Anatolian plateau (e.g., Cosentino et al., 2012; Schildgen
1622 et al., 2012; Meijers et al., 2020; Racano et al., 2020) and exposing deeper
1623 structural levels to erosion (Chen et al., 2021). Climate and climate change also
1624 affected erosion and fluvial run-off to the ocean (e.g., Harris and Mix, 2002; Molnar,
1625 2004) although more research is needed before the effects of tectonism versus
1626 ‘climate’ can be distinguished in the study region.

1627 In addition, 6-5 Ma grains commonly occur in the eastern range samples,
1628 which contrasts with an absence of Messinian grains in the western range samples
1629 (see section 6.2). The Upper Miocene succession shows a gradual decrease in
1630 sandstone turbidites (still with westerly paleo-flow), whereas mudrocks become
1631 much more abundant, followed by Messinian gypsum. Likely zircon sources

1
2
3
4
5
6
7
8
9
10
11
12
13
14
15
16
17
18
19
20
21
22
23
24
25
26
27
28
29
30
31
32
33
34
35
36
37
38
39
40
41
42
43
44
45
46
47
48
49
50
51
52
53
54
55
56
57
58
59
60
61
62
63
64
65

1632 include airfall tuffs and ignimbrites of central Turkey (Akin et al., 2021). The
1633 absence of airfall zircon grains in the western range samples might represent
1634 localised fallout or sediment reworking by currents or gravity flows.

1635 The Kyrenia Range itself is not likely to have provided many zircons. Only
1636 minor Triassic siliciclastic rocks are present, overlain by the Mesozoic platform
1637 carbonates (mainly marble and dolomite). The Maastrichtian-Middle Eocene felsic
1638 and basic igneous rocks of the Kyrenia Range also contain few zircons (Chen and
1639 Robertson, 2021b) and thus were not a significant zircon source. The structural
1640 and stratigraphical break between the Middle Eocene Kalograia-Ardana Formation
1641 and the transgressive Upper Eocene-Oligocene (Kythrea Conglomerate) was
1642 short-lived (several Ma), without evidence of deep erosion that could have supplied
1643 much siliciclastic sediment. In addition, the geochemistry of igneous blocks and
1644 clasts in both the Middle Eocene Kalograia-Ardana Formation and the Upper
1645 Eocene-Oligocene Bellapais Formation suggests an ophiolitic source, including
1646 boninites that are not present in the Kyrenia Range (Eyüboğlu et al., 2010;
1647 Robertson et al., 2014). As noted above (see section 6.3), the Troodos Massif to
1648 the south is unlikely to have contributed detritus to the Kyrenia Range because it
1649 retained its sedimentary cover until the Pleistocene.

1650

1651 6.5. Differentiation of crustal type using Lu-Hf isotope data

1652 Crustal sources can be specified more clearly when the Lu-Hf isotope data are
1653 taken into account. The dominant strongly negative $\epsilon\text{Hf}(t)$ values of
1654 Paleoproterozoic and Archean detrital zircons from the Kyrenia Range consistently

1
2
3
4
5
6
7
8
9
10
11
12
13
14
15
16
17
18
19
20
21
22
23
24
25
26
27
28
29
30
31
32
33
34
35
36
37
38
39
40
41
42
43
44
45
46
47
48
49
50
51
52
53
54
55
56
57
58
59
60
61
62
63
64
65

1655 suggest a recycled crustal origin. The Mesoproterozoic is characterised by igneous
1656 quiescence in the inferred ultimate provenance area (North Africa/Levant).
1657 Igneous activity resumed towards the end of Stenian time related to the Tonian-
1658 Stenian orogeny, consistent with the occurrence of occasional Stenian-aged
1659 detrital zircons (1193-1031 Ma). In contrast, Neoproterozoic detrital zircons are
1660 characterised by a wide spread of $\epsilon\text{Hf}(t)$ ratios; half of these (52%) show negative
1661 $\epsilon\text{Hf}(t)$ values, which suggests the involvement of ancient crust. The remainder of
1662 the zircon grains are juvenile, with positive $\epsilon\text{Hf}(t)$ (+0.1, +14.6), consistent with
1663 juvenile sources like the Arabian-Nubian Shield (e.g., Ustaömer et al., 2016, 2020).

1664 The Cambrian detrital zircons mainly exhibit negative $\epsilon\text{Hf}(t)$, which suggests
1665 the involvement of ancient crust. The Ordovician and Devonian detrital zircons with
1666 negative $\epsilon\text{Hf}(t)$ values suggest recycled crust formation, together with probable
1667 reworking of juvenile Tonian-Stenian (arc) crust (0.8-1.2 Ga).

1668 Zircon grains of Carboniferous, Permian and Triassic ages suggest a
1669 dominant involvement of melts related to Mesoproterozoic crust, as well as some
1670 grains derived from young juvenile Ediacaran-Tonian crust. However, specific
1671 sources are difficult to identify because the isotopic data for the Carboniferous
1672 zircons overlaps for the Taurides (Aladağ)-Anatolides (e.g., Afyon zone) and the
1673 Pontides (Sakarya zone) (Fig. 12) (Ustaömer et al., 2020).

1674 The Upper Cretaceous (96-91 Ma) zircons with dominantly super-chondritic
1675 $\epsilon\text{Hf}(t)$ (+11.4, +18.7) indicate juvenile magmatic additions, compatible with the
1676 radiometrically dated ophiolites (e.g., Parlak et al., 2013). Subordinate
1677 contemporaneous (Upper Cretaceous) zircons with negative $\epsilon\text{Hf}(t)$ values (-22.9 to

1
2
3
4
5
6
7
8
9
10
11
12
13
14
15
16
17
18
19
20
21
22
23
24
25
26
27
28
29
30
31
32
33
34
35
36
37
38
39
40
41
42
43
44
45
46
47
48
49
50
51
52
53
54
55
56
57
58
59
60
61
62
63
64
65

1678 -14.6) mainly occur in the Kalograia-Ardana Formation (e.g., Glazer et al., 2021).
1679 The analysed samples from the Kalograia-Ardana Formation are rich in detrital
1680 serpentinite of ultramafic ophiolitic origin (Fig. 5b). In contrast, the Upper
1681 Cretaceous (90-66 Ma) detrital zircons, with vertically arrays of $\epsilon\text{Hf}(t)$ values, point
1682 to mixture of juvenile and reworked materials. Upper Cretaceous ophiolites, other
1683 related basaltic rocks (e.g., accretionary melange) and younger volcanic arc units
1684 are possible sources (see section 6.3), all with positive $\epsilon\text{Hf}(t)$ values (Bingöl et al.,
1685 2018; Xin et al., 2021) and highly variable U/Yb and Nb/Yb ratios (see section 4.13).
1686 The strongly negative $\epsilon\text{Hf}(t)$ values could be explained in several different ways: (1)
1687 the involvement of subducted sediments during late-stage ophiolite formation
1688 (Bingöl et al., 2018); (2) the involvement of sub-continental mantle lithosphere
1689 related to an intra-continental rift or narrow ocean (Arenas et al., 2014; Tsikouras
1690 et al., 2021); or (3) the influence of ancient recycled oceanic crust (e.g., Gregory
1691 and Taylor, 1981; Eiler, 2001).

1692 Paleocene-Lower Miocene zircons have increasing $\epsilon\text{Hf}(t)$ values, involving
1693 juvenile materials (e.g., remnant Neotethys) and recycled crustal additions. A
1694 possible decreasing $\epsilon\text{Hf}(t)$ trend during ca. 40-20 Ma could indicate a contribution
1695 related to crustal assimilation in the source magmatic system. A small number of
1696 the 21-16 Ma grains from the Panagra Formation can be attributed to post-
1697 collisional volcanism in western Anatolia (Chen and Robertson, 2021a). The Upper
1698 Miocene grains (Tortonian-Messinian) with near-chondritic to juvenile $\epsilon\text{Hf}(t)$, -5 to
1699 5, are comparable to those of the widespread ignimbrites of Central Anatolia (e.g.,
1700 Akin et al., 2021).

1
2
3
4
5
6
7
8
9
10
11
12
13
14
15
16
17
18
19
20
21
22
23
24
25
26
27
28
29
30
31
32
33
34
35
36
37
38
39
40
41
42
43
44
45
46
47
48
49
50
51
52
53
54
55
56
57
58
59
60
61
62
63
64
65

1701

1702 6.6. Testing alternative models

1703 Three contrasting tectonic models for the tectonic development of the Kyrenia

1704 Range can be tested and developed using the assembled detrital zircon

1705 geochronological data and relevant geological evidence for the Middle Triassic to

1706 Pleistocene siliciclastic sediments.

1707 In model 1 (Fig. 13a), the Kyrenia Range is restored to the northern margin

1708 of the Southern Neotethys, adjacent to southern Turkey. A passive margin setting

1709 existed from Triassic to Cretaceous (Fig. 13a1-a2), followed by a switch to an

1710 active margin or collisional setting related to northward plate convergence from the

1711 Late Cretaceous onwards (Robertson and Woodcock, 1986; McCay and

1712 Robertson, 2012; Robertson et al., 2012a, 2014; Chen et al., 2019). The Cilicia

1713 Basin between Cyprus and Turkey is interpreted as continental crust that subsided

1714 to form a deep sea during accumulation of the Upper Eocene-Oligocene Bellapais

1715 Formation. This model assumes that the Southern Neotethys existed as a

1716 southerly oceanic basin, separated from more northerly Tethyan oceanic basins by

1717 the Tauride microcontinents, which are likely to have been important sediment

1718 contributors to the Kyrenia Range.

1719 In model 1, two distinct provenances existed. The first was characterised by

1720 a general north to south sediment transport during Late Cretaceous-Early

1721 Oligocene (Fig. 13a2-a3). The dominantly Pan-African and Grenvillian zircon

1722 populations were derived from the rifted Cadomian basement (rifted

1723 microcontinents) within Anatolia (e.g., Zlatkin et al., 2013; Abbo et al., 2015; Chen

1
2
3
4
5
6
7
8
9
10
11
12
13
14
15
16
17
18
19
20
21
22
23
24
25
26
27
28
29
30
31
32
33
34
35
36
37
38
39
40
41
42
43
44
45
46
47
48
49
50
51
52
53
54
55
56
57
58
59
60
61
62
63
64
65

1724 et al., 2019). The Upper Cretaceous zircons were derived from continental margin
1725 arc and/or ophiolite-related magmatism within Anatolia (Fig. 13a2). Eocene zircons
1726 associated with serpentinite-derived detritus came from the supra-subduction zone
1727 ophiolites in S Turkey including boninites (e.g., Mersin ophiolite, or equivalent)
1728 (Robertson et al., 2014) (Fig. 13a3). After the Middle Eocene, coarse clastic
1729 transport, associated with similar supra-subduction zone ophiolitic rocks, remained
1730 generally from N to S, as indicated by paleocurrent data (Fig. 2) (McCay and
1731 Robertson, 2012). From Late Oligocene onwards, the major supply of detritus was
1732 from the east (Fig. 2), from the developing Tauride-Arabia collision zone in SE
1733 Turkey. The Eocene and Neogene zircon grains were mainly derived from late-
1734 stage subduction-related magmatism (e.g., Eocene granitoids) and, or evolved
1735 collision-related magmatism in SE Turkey (see Fig. 13a4).

1736 In model 2, the Kyrenia Range is restored as part of the distal, N Africa
1737 continental margin (e.g., Maffione et al., 2017; McPhee and van Hinsbergen, 2019)
1738 (Fig. 13b). The Mesozoic carbonate platform (Trypa Group) represents part of the
1739 North African passive margin, with oceanic crust to the north. The Kyrenia Range,
1740 together with the Mamonia Complex of SW Cyprus, and the Bitlis and Pütürge
1741 continental units of SE Turkey formed parts of the North Africa/Arabia continental
1742 margin (Fig. 13b1). During the Late Cretaceous, supra-subduction zone ophiolites
1743 formed within Neotethys far to the northeast (Maffione et al., 2017). The supra-
1744 subduction zone slab rolled back into pre-existing oceanic gap between North
1745 Africa/Arabia and the Tauride continent. Ophiolites were emplaced by 'radial
1746 invasion', generally northwards onto the Tauride continent and also southwards

1
2
3
4
5
6
7
8
9
10
11
12
13
14
15
16
17
18
19
20
21
22
23
24
25
26
27
28
29
30
31
32
33
34
35
36
37
38
39
40
41
42
43
44
45
46
47
48
49
50
51
52
53
54
55
56
57
58
59
60
61
62
63
64
65

1747 onto the opposing Arabian continent (Maffione et al., 2017). The Troodos ophiolite,
1748 part of the 'invaded' supra-subduction zone oceanic crust, underwent southward
1749 emplacement over the N African continental margin during the Late Cretaceous.
1750 Passive margin-type deposition persisted in the Kyrenia Range during the
1751 Paleogene when the Kyrenia Range remained as part of the North Africa/Arabia
1752 continental margin. Down-margin sliding of olistoliths, took place during the
1753 Eocene (without compressional tectonics) to form the Kalograia-Ardana Formation
1754 (Fig. 13b2). Northward subduction was then activated in the south and this
1755 consumed remaining oceanic crust (Misis ocean) between North Africa/Arabia and
1756 Turkey (Eurasian plate) during the Oligocene-Miocene, culminating in Late
1757 Miocene continental collision (Fig. 13b3) (McPhee and van Hinsbergen, 2019).
1758 Van Hinsbergen et al. (2020) retained the above model of Upper Cretaceous
1759 ophiolite emplacement (Maffione et al., 2017) but re-assigned the Bitlis and
1760 Pütürge continental units to the Taurides rather than to Arabia. This would imply
1761 the existence of a Mesozoic oceanic basin to the south of the Bitlis and Pütürge
1762 continental units.

1763 Some aspects of the detrital zircon provenance are compatible with Model
1764 2, including the ultimate North Africa-Arabia provenance of the Precambrian
1765 zircons and the presence of Upper Cretaceous ophiolite-derived zircons. Also, the
1766 provenance from Oligocene-Recent is similar in both models because northward
1767 subduction/collision and Miocene collision are common to both models.

1768 Several aspects of the detrital zircon provenance are, however,
1769 incompatible with model 2: (1) There is no known source of Carboniferous-Permian

1
2
3
4
5
6
7
8
9
10
11
12
13
14
15
16
17
18
19
20
21
22
23
24
25
26
27
28
29
30
31
32
33
34
35
36
37
38
39
40
41
42
43
44
45
46
47
48
49
50
51
52
53
54
55
56
57
58
59
60
61
62
63
64
65

1770 zircons related to magmatism or metamorphism in the North Africa-Arabia region,
1771 which remained passive during the Late Paleozoic (e.g., Cocks and Torsvik, 2006;
1772 Rolland et al., 2011); (2) The Upper Cretaceous (82-74 Ma) continental arc-type
1773 zircons, with relatively high U/Yb ratios but low Y concentrations (Fig. 9;
1774 Supplementary Figure S7), are explicable by derivation from the continental
1775 margin arc rocks of eastern Anatolia (e.g., Baskil Intrusives) (Chen and Robertson,
1776 2021b). However, there is no known source of such arc-derived zircons within the
1777 North African-Arabia region which remained passive during this time. Eocene
1778 zircons similarly have a ready source in the continental margin arc rocks in eastern
1779 Anatolia (e.g., Doğanşehir area, see above) but are again absent from North
1780 Africa/Arabia.

1781 Some other geological evidence is also incompatible with model 2 including:
1782 (1) The deep Herodotus Basin (Fig. 1) to the SW of Cyprus has been interpreted
1783 as oceanic crust (e.g., Woodside, 1977; Granot, 2016) that separated the North
1784 Africa passive margin from Cyprus, including the Kyrenia Range and the Mamonia
1785 Complex of W Cyprus (Fig. 1). Because this deep-water basin still exists, it is
1786 difficult to interpret the Kyrenia Range as a carbonate platform along the North
1787 Africa/Arabia continental margin, which was instead characterised by carbonate-
1788 evaporite facies (e.g., Sharief, 1986; Davies and Simmons, 2018). Similarly, the
1789 Levant basin farther east was deeply submerged from the Early Jurassic onwards,
1790 with the rifted North African continental margin to the south (Gardosh et al., 2010);
1791 (2) The Mamonia Complex includes Triassic-Cretaceous passive margin-type
1792 sedimentary rocks (e.g., debris-flow deposits) that were derived from a nearby

1
2
3
4
5
6
7
8
9
10
11
12
13
14
15
16
17
18
19
20
21
22
23
24
25
26
27
28
29
30
31
32
33
34
35
36
37
38
39
40
41
42
43
44
45
46
47
48
49
50
51
52
53
54
55
56
57
58
59
60
61
62
63
64
65

1793 continental block and carbonate platform, which is unlikely to correlate with the
1794 rifted North African margin far to the south (Robertson and Woodcock, 1979). The
1795 Mamonia Complex is instead lithologically and temporally similar to the Antalya
1796 Complex (=Antalya nappes) of the Taurides in adjacent SW Turkey (Torley and
1797 Robertson, 2018). The Antalya Complex is widely interpreted as rift/passive margin
1798 lithologies that bordered the southern margin of the Tauride continental block (e.g.,
1799 Woodcock and Robertson, 1977; Poisson, 1977; Şengör and Yılmaz, 1981); (3)
1800 Arc magmatism of Upper Cretaceous and Eocene age in SE Turkey implies
1801 northward subduction, which is incompatible with eastward subduction, as
1802 indicated by the westward oceanic crust 'invasion' hypothesis (see Robertson and
1803 Parlak, 2020). Also, arc magmatism of Oligocene-Miocene age is absent from
1804 southern Turkey but would be expected if significant northward subduction took
1805 place during the Eocene, as in model 2.

1806 In Model 3 (Fig. 13c), the entire Kyrenia Range is allochthonous and was
1807 emplaced from far to the north during the Eocene. The model implies that the entire
1808 Triassic to Eocene of the Kyrenia Range developed along the southern margin of
1809 Eurasia (Fig. 13c1-2) (Glazer et al., 2021). The lithologies making up the Triassic
1810 to Paleogene of Kyrenia Range were thrust southwards over the
1811 Anatolides/Taurides to near their present position during the Mid-Eocene, coeval
1812 with the widely reported southward thrusting in the Kyrenia Range (Fig. 13c3)
1813 (although not accepted in model 2). Carboniferous zircons that are common within
1814 the units ranging from the Middle Triassic Sikhari Formation to Middle Eocene
1815 Kalograia-Ardana Formation (Chen et al., 2019; Glazer et al., 2021) were derived

1
2
3
4
5
6
7
8
9
10
11
12
13
14
15
16
17
18
19
20
21
22
23
24
25
26
27
28
29
30
31
32
33
34
35
36
37
38
39
40
41
42
43
44
45
46
47
48
49
50
51
52
53
54
55
56
57
58
59
60
61
62
63
64
65

1816 directly from the Eurasian active continental margin in the NW Pontides (Meinhold
1817 et al., 2008; Löwen et al., 2017, 2020). An alternative considered by Glazer et al.
1818 (2021) is that the Kyrenia Range originated between the Kırşehir continental block
1819 and the Anatolides/Taurides (Fig. 13c1-c2), still far to the north of its present
1820 location. In both options, Carboniferous zircons became rare in Upper Oligocene
1821 and younger lithologies because they were structurally removed from the dominant
1822 Upper Paleozoic zircon source(s) following southward emplacement of the Kyrenia
1823 Range during the Eocene to near its present position in the eastern Mediterranean
1824 (Glazer et al., 2021).

1825 The combined detrital zircon data also question model 3, especially the
1826 preferred Eurasian (Pontide) origin of the Kyrenia Range. Although there are
1827 similarities in the ages of geological units in the Pontides and Anatolides/Taurides
1828 (e.g., Upper Cretaceous ophiolites and continental margin arc units), there are also
1829 significant differences, as follows. Triassic sandstones of the Tauride autochthon
1830 have Carboniferous zircon populations (ca. 7%) that are comparable to those of
1831 the Middle Triassic to Oligocene sandstones of the Kyrenia Range (7-13%), in
1832 contrast to the Triassic to Jurassic-aged sediments of the Pontides (14-25%)
1833 (Akdoğan et al., 2018). Specially, Jurassic granitoids are widespread in the eastern
1834 and central Pontides (e.g., Genç and Tüysüz, 2010; Ustaömer et al., 2013, 2020;
1835 Okay et al., 2015). Upper Triassic-Lower Jurassic (210-190 Ma) detrital zircons
1836 dominate (40-67%) the Jurassic sandstones of the E Pontides (Akdoğan et al.,
1837 2018), but are very rare in the Kyrenia Range samples (Fig. 11). Post-
1838 Carboniferous clastic sediments in the Pontides are not always greatly enriched in

1
2
3
4
5
6
7
8
9
10
11
12
13
14
15
16
17
18
19
20
21
22
23
24
25
26
27
28
29
30
31
32
33
34
35
36
37
38
39
40
41
42
43
44
45
46
47
48
49
50
51
52
53
54
55
56
57
58
59
60
61
62
63
64
65

1839 Carboniferous zircons (8-25%) (Akdoğan et al., 2018), suggesting that source and
1840 distribution were localised.

1841 The Pontides were located along the northern margin of Tethys as a whole
1842 during the Upper Paleozoic to the Upper Cretaceous or the Paleogene when
1843 collision occurred in different interpretations (e.g., Barrier et al., 2018; Okay et al.,
1844 2018). On the other hand, some authors restore the Upper Paleozoic Sakarya arc
1845 close to, or directly along the northern margin of Gondwana (e.g., Göncüoğlu et
1846 al., 2007; Şengör et al., 2019), which, if correct, could have provided zircons
1847 directly to the north-Gondwana margin (Anatolides) (see Robertson, 2022 for
1848 discussion).

1849 In line with the known regional geology, possible timings of southward
1850 emplacement of the Kyrenia Range over the Taurides would be Late Cretaceous
1851 (Campanian-Maastrichtian) or Eocene, together with ophiolitic and continental
1852 margin units (e.g., Özgül, 1984a; Mackintosh and Robertson, 2009; McPhee and
1853 van Hinsbergen, 2019).

1854 The highest and most southerly travelled of the Tauride thrust sheets is the
1855 Hadim nappe, which reaches the Mediterranean coast (near Silifke) (MTA, 2011).
1856 However, there are no counterparts of the Kyrenia Range tectonostratigraphy
1857 within the Tauride units emplaced during the Late Cretaceous or the Eocene, or
1858 any indications of the former existence of km-thick thrust stack above the Hadim
1859 nappe (e.g., low-grade metamorphism). In addition, structural and facies evidence
1860 indicate that both the Antalya Complex and the Alanya metamorphic massif were
1861 emplaced northwards over the southern margin of the Tauride carbonate platforms

1
2
3
4
5
6
7
8
9
10
11
12
13
14
15
16
17
18
19
20
21
22
23
24
25
26
27
28
29
30
31
32
33
34
35
36
37
38
39
40
41
42
43
44
45
46
47
48
49
50
51
52
53
54
55
56
57
58
59
60
61
62
63
64
65

1862 during the Paleocene to Middle Eocene (Monod, 1977; Özgül, 1984b; Robertson
1863 and Parlak, 2020; Robertson et al., 2020). The Hadim nappe locally overrode the
1864 Antalya Complex and the Alanya Massif due to slightly later Eocene emplacement
1865 (Özgül, 1984b; MTA, 2011). The Eocene emplaced Alanya Massif would have
1866 constituted a barrier to overthrusting by the Kyrenia Range.

1867 Rather than an isolated structural unit (klippen), the Kyrenia Range is
1868 instead part of a pile of thrust sheets that extends eastward through SE Turkey into
1869 Iran. The Kyrenia Range runs under the sea and comes on land as the Misis
1870 Mountains, that in turn links northeastwards with the Andırın Range, then with the
1871 Engizek Mountains and the Bilits suture zone of SE Turkey (e.g., Perinçek and
1872 Kozlu, 1984; Robertson and Woodcock, 1986; Kempler and Garfunkel, 1994;
1873 Robertson et al., 2006). Mesozoic carbonate platform units ('Andırın limestones'),
1874 similar to those of the Kyrenia Range, are located at a low level in the regional
1875 tectonic pile, overlain by Upper Cretaceous ophiolitic, metamorphic and arc-type
1876 magmatic rocks in SE Turkey (Perinçek and Kozlu, 1984; Robertson et al., 2006;
1877 Nurlu et al., 2016). Deriving the Kyrenia Range from far to the north in a high
1878 structural position and then having it emplaced in a low structural position far to
1879 the south would require major, regional out-of-sequence thrusting for which field
1880 evidence is currently lacking (e.g., Robertson et al., 2021b).

1881 In addition, southward emplacement of the Kyrenia Range as a whole (pre-
1882 Late Eocene) would imply the presence of a major foreland basin including
1883 abundant detritus beneath and to the south of the Kyrenia Range. This crust is
1884 unfortunately hidden because of Upper Miocene southward thrusting (accepted in

1
2
3
4
5
6
7
8
9
10
11
12
13
14
15
16
17
18
19
20
21
22
23
24
25
26
27
28
29
30
31
32
33
34
35
36
37
38
39
40
41
42
43
44
45
46
47
48
49
50
51
52
53
54
55
56
57
58
59
60
61
62
63
64
65

1885 all three models). However, it is notable that the ophiolitic and continental margin
1886 detritus occurs within the Middle Eocene Kaolgrai-Ardana Formation (i.e., part of
1887 the range stratigraphy) suggesting that only this material rather than the entire pre-
1888 Late Eocene stratigraphy of Kyrenia Range was derived from the north.

1889

1890 6.7 Zircon texture/recycling and wider implications

1891 We propose that the combined zircon data presented here are more consistent
1892 with model 1 than with the alternative models 2 and 3. A possible objection is that
1893 the Carboniferous zircon grains are relatively angular (Chen et al., 2019; Glazer et
1894 al., 2021; this study) (Fig. 11). However, evidence from elsewhere increasingly
1895 suggests that angular to subangular zircon grains can survive multiple cycles of
1896 erosion. Variable-distance transport by fluvial or gravity-flow processes may not
1897 result in significant rounding, even during multiple sediment cycling (e.g., Mange
1898 and Maurer, 1992; Garzanti et al., 2015; Zoleikhaei et al., 2015). Phanerozoic
1899 zircons throughout Turkey are mainly euhedral/subhedral, with well-rounded
1900 zircons being generally restricted to the older Precambrian (T. Ustaömer, personal
1901 communication, 2021). The degree of rounding is therefore not a reliable indicator
1902 of the proximity of zircon sources.

1903 As summarized above (sections 4 and 6.2), the Middle Triassic, Upper
1904 Cretaceous and Eocene samples from throughout the Kyrenia Range contain
1905 subordinate, but pronounced, fractions of euhedral/subhedral zircons of
1906 Carboniferous and Permian ages (Fig. 11). Similar-aged zircons are also present
1907 in Middle-Upper Triassic Tauride samples in some units (Ustaömer et al., 2020). In

1
2
3
4
5
6
7
8
9
10
11
12
13
14
15
16
17
18
19
20
21
22
23
24
25
26
27
28
29
30
31
32
33
34
35
36
37
38
39
40
41
42
43
44
45
46
47
48
49
50
51
52
53
54
55
56
57
58
59
60
61
62
63
64
65

1908 contrast, Carboniferous and Permian zircons are relatively rare in the Oligocene-
1909 Upper Miocene sediments (Fig. 11). Contemporaneous subsidence of the Cilicia
1910 Basin terminated the input of Upper Paleozoic zircons from the north. Provenance
1911 then switched to the east (Fig. 2), mainly from SE Turkey. Zircons from the Taurides
1912 of SE Turkey are mainly Precambrian, without Carboniferous-Devonian zircons
1913 (Ustaömer et al., 2020), explaining their sparsity in the Oligocene-Miocene
1914 sediments of the Kyrenia Range. Interestingly, where present, Carboniferous-
1915 Permian zircons are mainly rounded/subrounded in the Oligocene-Miocene
1916 sediments (Fig. 11). A possible explanation is that the angular/subangular zircons
1917 were ultimately derived from the north, including the Konya Complex in central
1918 Anatolia, involving relatively rapid transport and redepositional events (Middle-Late
1919 Triassic and Late Cretaceous). In contrast, the rare, but better-rounded
1920 Carboniferous-Permian grains in the Oligocene-Upper Miocene samples were
1921 derived from the E Taurides. Lithologies of these ages in this area (e.g., Malatya
1922 Metamorphics) (Perinçek and Kozlu, 1984; Robertson et al., 2021a, b) were
1923 ultimately sourced from the Precambrian of the Arabian-Nubian Shield rather than
1924 Paleotethys, explaining the textural difference.

1925 Eocene final suturing of the İzmir-Ankara-Erzincan ocean basin (Northern
1926 Neotethys) and the Inner Tauride ocean (controversial for some authors; e.g., van
1927 Hinsbergen et al., 2020), and related regional-scale thrusting (see Section 2) were
1928 followed by uplift, erosion and fluvial reworking, as indicated by the extensive
1929 accumulation of Oligocene red bed-type clastic sediments throughout Anatolia
1930 ('Kastel Formation'); e.g., Aktoprak Formation of the Ulukışla Basin (Fig. 1) (Clark

1
2
3
4
5
6
7
8
9
10
11
12
13
14
15
16
17
18
19
20
21
22
23
24
25
26
27
28
29
30
31
32
33
34
35
36
37
38
39
40
41
42
43
44
45
46
47
48
49
50
51
52
53
54
55
56
57
58
59
60
61
62
63
64
65

1931 and Robertson, 2002; Akgün et al., 2021). Some of the associated detrital zircons
1932 were redeposited into the eastern Mediterranean basin including the Kyrenia
1933 Range via near-coastal Miocene basins (Chen et al., 2021).

1934 Our preferred development of the Kyrenia Range along the northern margin
1935 of the Southern Neotethys (Model 1) has additional implications:

1936 (1) Ideally zircon geochronology allows unique sources to be identified.
1937 However, conjugate rifting places similar aged units on opposite sides of ocean
1938 basins that ultimately suture. A good example is the Triassic rifting of Precambrian
1939 fragments from the NE African/Arabian-Nubian Shield to form microcontinents to
1940 the north of the Southern Neotethys. The source of Precambrian zircons in Cyprus
1941 was Anatolia rather than North Africa-Levant (see section 6.3). If the
1942 Mediterranean basin had already completely closed, comparable with many suture
1943 zones, then the recognition of southerly versus northerly provenances could be
1944 more very difficult;

1945 (2) Additional complications arise where multiple suture zones exist in areas
1946 that could have supplied detrital zircons. In the case of Turkey, there are similarities
1947 in the timing and setting of more than one sutured ocean basin (S vs. N Neotethys)
1948 and it is necessary to identify unique zircon-bearing units that could have supplied
1949 zircons (e.g., Upper Cretaceous and Eocene granitoids of SE Turkey);

1950 (3) Interpretations need to take account of the propensity for zircons to be
1951 recycled multiple times through successive geological units without necessarily
1952 become texturally mature (i.e., well-rounded). During such recycling, zircons may
1953 either be concentrated or dispersed according to local sedimentological conditions.

1
2
3
4
5
6
7
8
9
10
11
12
13
14
15
16
17
18
19
20
21
22
23
24
25
26
27
28
29
30
31
32
33
34
35
36
37
38
39
40
41
42
43
44
45
46
47
48
49
50
51
52
53
54
55
56
57
58
59
60
61
62
63
64
65

1954 Based on this study, recycling is likely to have taken place from Upper Paleozoic
1955 granitoid rocks to, successively upper Carboniferous-earliest Permian, Mid-Upper
1956 Triassic and post-Cretaceous formations;

1957 (4) Interpretations of detrital zircons geochronology are critically dependent
1958 on a knowledge of paleo-drainage, which is commonly eroded in orogenic belts,
1959 together with sub-aqueous paleocurrents. A good example is the present evidence
1960 of Neogene generally westward sediment transport away from the Southern
1961 Neotethyan suture zone into the eastern Mediterranean basin, including the
1962 Kyrenia Range;

1963 (5) Interpretation of detrital zircon data is enhanced when complementary
1964 analytical data are available, including from zircon trace elements and Lu-Hf
1965 isotopes. In the present study, the trace-element data allowed zircon sources
1966 during the latest Cretaceous and Eocene to be related to the availability of supra-
1967 subduction zone-type ophiolitic debris (including boninites) that was derived from
1968 outside the immediate area. Lu-Hf isotopic data particularly aid recognition of
1969 evolved versus juvenile crustal sources, such as the Upper Cretaceous and
1970 Eocene granitoids in SE Turkey.

1971 (6) Finally, interpretation of the detrital zircon geochronology of any particular
1972 region is dependent on the overall geological knowledge, in this case the North
1973 Africa/Arabia-Eastern Mediterranean-Anatolia region.

1974

1975 7. Conclusions

1976 A combination of new and existing detrital zircon geochronology, new and existing

1
2
3
4
5
6
7
8
9
10
11
12
13
14
15
16
17
18
19
20
21
22
23
24
25
26
27
28
29
30
31
32
33
34
35
36
37
38
39
40
41
42
43
44
45
46
47
48
49
50
51
52
53
54
55
56
57
58
59
60
61
62
63
64
65

1977 zircon Hf isotopic evidence and new zircon trace element data, together with
1978 published geological evidence (especially published paleocurrent data), allows
1979 systematic interpretation of the provenance and tectonic setting of the clastic
1980 sediments of Triassic to Neogene age throughout the Kyrenia Range of northern
1981 Cyprus. The new zircon data (24 samples) are mainly from four transects of the
1982 Kyrenia Range (over ca. 150 km laterally) and include previously unsampled time
1983 slices (e.g., Late Eocene-Early Oligocene, Pliocene). The new zircon trace
1984 element data for Carboniferous to Triassic grains also allow tectonic discrimination
1985 of continental margin arc versus intra-plate settings

1986 Two stratigraphic ages are refined according to maximum depositional zircon
1987 age; i.e., the Kiparisso Vouno Member (Santonian-Late Campanian) is ca. 3 Ma
1988 older than previously inferred, and the Lapatza Gypsum is no older than 5.4 Ma.

1989 In nearly all of the sandstones analysed, Precambrian-Cambrian zircons
1990 predominate, with major age peaks at ca. 930 Ma, 630 Ma and 530 Ma. These
1991 dominantly Pan-African and Grenvillian zircon populations were derived from
1992 Cadomian basement units in Anatolia, following Triassic rifting of microcontinents
1993 from North Africa (Gondwana) during opening of the Southern Neotethys.

1994 Carboniferous-Permian zircons form significant age populations (up to 13%)
1995 in some of the samples, peaking at 320 Ma, 305 Ma and 295 Ma. Zircons in the
1996 pre-Oligocene sandstones are mainly euhedral. The Upper Paleozoic zircons were
1997 originally derived from Upper Paleozoic magmatic arc units, possibly following
1998 closure of Paleotethys farther west (Aegean-Balkan region). The provenance of
1999 the Upper Paleozoic zircons in the Kyrenia Range is preferentially explained by

1
2
3
4
5
6
7
8
9
10
11
12
13
14
15
16
17
18
19
20
21
22
23
24
25
26
27
28
29
30
31
32
33
34
35
36
37
38
39
40
41
42
43
44
45
46
47
48
49
50
51
52
53
54
55
56
57
58
59
60
61
62
63
64
65

2000 repeated recycling of siliciclastic sediments; i.e., during Carboniferous-earliest
2001 Permian, Mid-Upper Triassic and Upper Cretaceous-Paleogene. In support, there
2002 is much paleocurrent evidence of Mid-Upper Triassic southward reworking of
2003 Paleotethyan detritus within central Anatolia.

2004 Upper Cretaceous zircons (up to 16%) have age peaks of 99-85 Ma and are
2005 characterised by highly variable U/Yb and Nb/Yb ratios. The clastic sediment
2006 supply included ophiolitic (92-84 Ma) and volcanic arc (ca. 88-70 Ma) units,
2007 together with relatively minor metamorphic rock-derived detritus, potentially from
2008 the Alanya Massif to the north.

2009 Subordinate Paleogene zircons occur in the Upper Miocene sandstones (up
2010 to 14%) were potentially derived from localised Lower-Mid Eocene magmatic rocks
2011 in central or SE Turkey.

2012 Oligocene-Pliocene sandstones contain sparse zircons of Carboniferous and
2013 Permian age (up to 6%), which are relatively well rounded. These zircons were
2014 recycled through non-marine continental environments before being finally
2015 redeposited within turbidites. The Oligocene-Pliocene sandstones also contain
2016 abundant Upper Cretaceous zircons (up to 52%), with age peaks at 84 Ma, 80 Ma,
2017 75 Ma and 70 Ma. The main source of these zircons is likely to have been coeval
2018 continental arc granitoid rocks, as widely exposed in eastern Anatolia.

2019 A significant Miocene zircon fraction (up to 17%), with major age peaks at ca.
2020 20-17 Ma, was probably derived from evolved, calc-alkaline magmatic rocks in SE
2021 Turkey. The more common Messinian zircons in the eastern range samples (up to
2022 55%) compared to the western range ones (<1%) could be explained by derivation

1
2
3
4
5
6
7
8
9
10
11
12
13
14
15
16
17
18
19
20
21
22
23
24
25
26
27
28
29
30
31
32
33
34
35
36
37
38
39
40
41
42
43
44
45
46
47
48
49
50
51
52
53
54
55
56
57
58
59
60
61
62
63
64
65

2023 from Messinian airfall tuffs and ignimbrites in central Turkey.

2024 Paleocene-Lower Miocene zircons are characterised by highly variable $\epsilon\text{Hf}(t)$
2025 values, with derivation from juvenile materials (e.g., remnant Neotethys) and/or
2026 reworked crust (e.g., exposed 'microcontinental' or metamorphic units).

2027 The combined zircon geochronological, isotopic and zircon trace element
2028 evidence indicates a marked change in provenance between pre-Oligocene and
2029 post-Oligocene. The Southern Neotethys sutured in southeast Anatolia during
2030 Oligocene-Miocene, creating a dominant source from the Tauride thrust sheets in
2031 SE Turkey. Collision-related uplift in S and SE Turkey generated sediment that was
2032 transported into the easternmost deep-sea Mediterranean, including the future
2033 Kyrenia Range. Paleogene zircons were supplied continuously from the Middle
2034 Miocene-Pliocene, which is explicable by first, subduction and later, by collision-
2035 related magmatism in southeast Turkey. Upper Miocene grains with near
2036 chondritic to juvenile $\epsilon\text{Hf}(t)$ could have a tuff/ignimbrite origin in central Turkey. Also,
2037 Messinian zircons from post-collisional magmatic rocks were supplied to
2038 Tortonian-Messinian sediments in the eastern Kyrenia Range.

2039 The combined evidence has also been used to test three different tectonic
2040 models: i.e., the Kyrenia Range developed along the northern margin of the
2041 Southern Neotethys; the range originated along the northern margin of North Africa;
2042 or the range represents a far-travelled allochthon emplaced from the southern
2043 margin of Eurasia, or possibly from the Anatolides (Afyon zone). In the light of the
2044 regional geological evidence, the combined zircon and other geochemical data
2045 assembled here, mainly supports the first hypothesis that the Kyrenia Range

1
2
3
4
5
6
7
8
9
10
11
12
13
14
15
16
17
18
19
20
21
22
23
24
25
26
27
28
29
30
31
32
33
34
35
36
37
38
39
40
41
42
43
44
45
46
47
48
49
50
51
52
53
54
55
56
57
58
59
60
61
62
63
64
65

2046 developed along the northern margin of the Southern Neotethys; this was passive
2047 during the Triassic, active during the Late Cretaceous-Paleogene and collision-
2048 related during the Miocene-Recent. The dominant sources during the pre-
2049 Oligocene were generally in southern Anatolia to the north and northeast, whereas
2050 from Oligocene onwards supply was largely from SE Anatolia related to the
2051 development of post-collisional river catchments.

2052

2053 Declaration of Competing Interest

2054 The authors declare that they have no known competing financial interests or
2055 personal relationships that could have appeared to influence the work reported in
2056 this paper.

2057

2058 Acknowledgements

2059 This work was financially supported by the National Natural Science
2060 Foundation of China (41888101, 91755000 and 42002126). Fieldwork by the
2061 second author was aided by the John Dixon Memorial Fund. Osman Parlak and
2062 Zhongyu Meng kindly assisted in the field. Shitou Wu and Shaohua Zhang are
2063 kindly thanked for analytical assistance. We are very grateful to Lin Ding, Xiumian
2064 Hu, Fangyang Hu, Timothy Kinnaird, Chuanzhou Liu, Tong Liu, Gillian McCay,
2065 Qingren Meng, Mehmet Necdet, Romesh Palamakumbura, Osman Parlak,
2066 Hongbing Tan, Timur Ustaömer, Bo Wan and Dicheng Zhu for beneficial discussion.
2067 The manuscript benefitted from comments by Alexandros Konstantinou, an
2068 anonymous reviewer and the editor, Carlo Doglioni.

1
2
3
4
5
6
7
8
9
10
11
12
13
14
15
16
17
18
19
20
21
22
23
24
25
26
27
28
29
30
31
32
33
34
35
36
37
38
39
40
41
42
43
44
45
46
47
48
49
50
51
52
53
54
55
56
57
58
59
60
61
62
63
64
65

2069
2070
2071
2072
2073
2074
2075
2076
2077
2078
2079
2080
2081
2082
2083
2084
2085
2086
2087
2088
2089
2090
2091

References

Abbo, A., Avigad, D., Gerdess, A. and Güngör, T., 2015. Cadomian basement and Paleozoic to Triassic siliciclastics of the Taurides (Karacahisar dome, south-central Turkey): paleogeographic constraints from U–Pb–Hf in zircons. *Lithos* 227, 122-139. <http://doi.org/10.1016/j.lithos.2015.03.023>

Akal, C., Candan, O., Koralay, O.E., Oberhänsli, R., Chen, F. and Prelević, D., 2012. Early Triassic potassic volcanism in the Afyon Zone of the Anatolides/Turkey: implications for the rifting of the Neo-Tethys. *Int. J. Earth Sci.* 101, 177-194. <http://doi.org/10.1007/s00531-011-0654-2>

Akdoğan, R., Okay, A. and Dunkl, I., 2018. Triassic-Jurassic arc magmatism in the Pontides as revealed by the U-Pb detrital zircon ages in the Jurassic sandstones of northeastern Turkey. *Turk. J. Earth Sci.* 27, 89-109. <http://doi.org/10.3906/yer-1706-19>

Akgün, F., Kayseri - Özer, M.S., Tekin, E., Varol, B., Şen, Ş., Herece, E., Gündoğan, İ., Sözeri, K. and Us, M.S., 2021. Late Eocene to Late Miocene palaeoecological and palaeoenvironmental dynamics of the Ereğli - Ulukışla Basin (Southern Central Anatolia). *Geol. J.* 56, 673-703. <http://doi.org/10.1002/gj.4021>

Akin, L., Aydar, E., Schmitt, A.K., Çubukçu, H.E. and Gerdess, A., 2021. Zircon geochronology and O-Hf isotopes of Cappadocian ignimbrites: New insights into continental crustal architecture underneath the Central Anatolian Volcanic Province, Turkey. *Gondwana Res.* 91, 166-187. <http://doi.org/10.1016/j.gr.2020.12.003>

1
2
3
4
5
6
7
8
9
10
11
12
13
14
15
16
17
18
19
20
21
22
23
24
25
26
27
28
29
30
31
32
33
34
35
36
37
38
39
40
41
42
43
44
45
46
47
48
49
50
51
52
53
54
55
56
57
58
59
60
61
62
63
64
65

2092 Aksu, A., Hall, J. and Yaltırak, C., 2021. Miocene–Quaternary tectonic, kinematic and
2093 sedimentary evolution of the eastern Mediterranean Sea: A regional synthesis.
2094 Earth-Sci. Rev. 220, 103719. <http://doi.org/10.1016/j.earscirev.2021.103719>

2095 Aktaş, G. and Robertson, A.H.F., 1984. The Maden Complex, SE Turkey: evolution of a
2096 Neotethyan active margin. In: J.E. Dixon and A.H.F. Robertson (Editors), The
2097 Geological Evolution of the Eastern Mediterranean. Geological Society of London,
2098 Special Publications, pp. 375-402.

2099 Aktaş, G. and Robertson, A.H.F., 1990. Tectonic evolution of the Tethys suture zone in
2100 SE Turkey: evidence from the petrology and geochemistry of Late Cretaceous and
2101 Middle Eocene extrusives. In: J. Malpas, E.M. Moores, A. Panayiotou and C.
2102 Xenophontos (Editors), Ophiolites-Oceanic Crustal Analogues. Proceedings of the
2103 International Symposium 'Troodos 1987'. Cyprus Geological Survey Department,
2104 Nicosia, pp. 311-329.

2105 Al-Riyami, K., Robertson, A., Dixon, J. and Xenophontos, C., 2002. Origin and
2106 emplacement of the Late Cretaceous Baer–Bassit ophiolite and its metamorphic
2107 sole in NW Syria. Lithos 65, 225-260. [http://doi.org/10.1016/S0024-4937\(02\)00167-6](http://doi.org/10.1016/S0024-4937(02)00167-6)

2109 Al-Riyami, K. and Robertson, A.H.F., 2002. Mesozoic sedimentary and magmatic
2110 evolution of the Arabian continental margin, northern Syria: evidence from the
2111 Baer–Bassit Melange. Geol. Mag. 139, 395-420.
2112 <http://doi.org/10.1017/s0016756802006660>

2113 Altıner, D., Koçyiğit, A., Farinacci, A., Nicosia, U. and Conti, M., 1991. Jurassic, Lower
2114 Cretaceous stratigraphy and paleogeographic evolution of the southern part of
2115 north-western Anatolia. Geol. Romana 27, 13-80.

1
2
3
4
5
6
7
8
9
10
11
12
13
14
15
16
17
18
19
20
21
22
23
24
25
26
27
28
29
30
31
32
33
34
35
36
37
38
39
40
41
42
43
44
45
46
47
48
49
50
51
52
53
54
55
56
57
58
59
60
61
62
63
64
65

2116 Altunkaynak, Ş. and Genç, Ş.C., 2008. Petrogenesis and time-progressive evolution of
2117 the Cenozoic continental volcanism in the Biga Peninsula, NW Anatolia (Turkey).
2118 *Lithos* 102, 316-340. <http://doi.org/10.1016/j.lithos.2007.06.003>

2119 Andersen, T., 2002. Correction of common lead in U–Pb analyses that do not report ²⁰⁴Pb.
2120 *Chem. Geol.* 192, 59-79. [http://doi.org/10.1016/S0009-2541\(02\)00195-X](http://doi.org/10.1016/S0009-2541(02)00195-X)

2121 Andrew, T. and Robertson, A.H.F., 2002. The Beyşehir–Hoyran–Hadim Nappes: genesis
2122 and emplacement of Mesozoic marginal and oceanic units of the northern
2123 Neotethys in southern Turkey. *J. Geol. Soc.* 159, 529-543.
2124 <http://doi.org/10.1144/0016-764901-157>

2125 Arenas, R., Martínez, S.S., Gerdes, A., Albert, R., Fernández, R.D. and Andonaegui, P.,
2126 2014. Re-interpreting the Devonian ophiolites involved in the Variscan suture: U–
2127 Pb and Lu–Hf zircon data of the Moeche Ophiolite (Cabo Ortegal Complex, NW
2128 Iberia). *Int. J. Earth Sci.* 103, 1385-1402. <http://doi.org/10.1007/s00531-013-0880->
2129 [x](http://doi.org/10.1007/s00531-013-0880-x)

2130 Arger, J., Mitchell, J., Westaway, R.W.C., Bozkurt, E., Winchester, J.A. and Piper, J.D.A.,
2131 2000. Neogene and Quaternary volcanism of southeastern Turkey. In: E. Bozkurt,
2132 J.A. Winchester and J.D.A. Piper (Editors), *Tectonics and Magmatism in Turkey*
2133 *and the Surrounding Area*. Geological Society, London, Special Publication, pp.
2134 459-487.

2135 Artiaga, D., García-Veigas, J., Cendón, D.I., Atalar, C. and Gibert, L., 2021. The Messinian
2136 evaporites of the Mesaoria basin (North Cyprus): A discrepancy with the current
2137 chronostratigraphic understanding. *Palaeogeogr. Palaeoclimatol. Palaeoecol.* 584.
2138 <http://doi.org/10.1016/j.palaeo.2021.110681>

1
2
3
4
5
6
7
8
9
10
11
12
13
14
15
16
17
18
19
20
21
22
23
24
25
26
27
28
29
30
31
32
33
34
35
36
37
38
39
40
41
42
43
44
45
46
47
48
49
50
51
52
53
54
55
56
57
58
59
60
61
62
63
64
65

2139 Asan, K. and Kurt, H., 2011. Petrology and geochemistry of post - collisional early
2140 miocene volcanism in the Karacadağ Area (Central Anatolia, Turkey). *Acta Geol.*
2141 *Sin. Ed.* 85, 1100-1117. <http://doi.org/10.1111/j.1755-6724.2011.00543.x>

2142 Aydar, E., 1998. Early Miocene to Quaternary evolution of volcanism and the basin
2143 formation in western Anatolia: a review. *J. Volcanol. Geotherm. Res.* 85, 69-82.
2144 [http://doi.org/10.1016/S0377-0273\(98\)00050-X](http://doi.org/10.1016/S0377-0273(98)00050-X)

2145 Aydar, E., Schmitt, A.K., Çubukçu, H.E., Akin, L., Ersoy, O., Sen, E., Duncan, R.A. and
2146 Atici, G., 2012. Correlation of ignimbrites in the central Anatolian volcanic province
2147 using zircon and plagioclase ages and zircon compositions. *J. Volcanol. Geotherm.*
2148 *Res.* 213, 83-97. <http://doi.org/10.1016/j.jvolgeores.2011.11.005>

2149 Balmer, E.M., Robertson, A.H.F., Raffi, I. and Kroon, D., 2019. Pliocene–Pleistocene
2150 sedimentary development of the syntectonic Polis graben, NW Cyprus: evidence
2151 from facies analysis, nannofossil biochronology and strontium isotope dating. *Geol.*
2152 *Mag.* 156, 889-917. <http://doi.org/10.1017/s0016756818000286>

2153 Baroz, F., 1979. Etude géologique dans le Pentadaktylos et la Mesaoria (Chypre
2154 Septentrionale). Doctor of Science Thesis (Published). Université de Nancy,
2155 France, 434 pp.

2156 Baroz, F. and Bizon, G., 1974. Le néogène de la chaîne du Pentadaktylos et de la partie
2157 nord de la Mésaoria (Chypre). Etude stratigraphique et micropaléontologique.
2158 *Revue de l'Institut Français du Pétrole* 29, 327-360.
2159 <http://doi.org/10.2516/ogst:1974015>

2160 Barrier, E., Vrielynck, B., Brouillet, J.F. and Brunet, M.F., 2018. Paleotectonic
2161 Reconstruction of the Central Tethyan Realm. Tectono-Sedimentary-Palinspastic
2162 Maps from Late Permian to Pliocene. Atlas of 20 maps (scale 1/15000000).
2163 CCGM/CGMW, Paris.

1
2
3
4
5
6
7
8
9
10
11
12
13
14
15
16
17
18
19
20
21
22
23
24
25
26
27
28
29
30
31
32
33
34
35
36
37
38
39
40
41
42
43
44
45
46
47
48
49
50
51
52
53
54
55
56
57
58
59
60
61
62
63
64
65

2164 Ben-Avraham, Z., Tibor, G., Limonov, A., Leybov, M., Ivanov, M., Tokarev, M.Y. and
2165 Woodside, J., 1995. Structure and tectonics of the eastern Cyprean Arc. *Mar. Pet.*
2166 *Geol.* 12, 263-271. [http://doi.org/10.1016/0264-8172\(95\)98379-J](http://doi.org/10.1016/0264-8172(95)98379-J)

2167 Beyarslan, M., Lin, Y.-C., Bingöl, A.F. and Chung, S.-L., 2016. Zircon U-Pb age and
2168 geochemical constraints on the origin and tectonic implication of Cadomian
2169 (Ediacaran-Early Cambrian) magmatism in SE Turkey. *J. Asian Earth Sci.* 130,
2170 223-238. <http://doi.org/10.1016/j.jseaes.2016.08.006>

2171 Bingöl, A.F., Beyarslan, M., Lin, Y.-C. and Lee, H.-Y., 2018. Geochronological and
2172 geochemical constraints on the origin of the Southeast Anatolian ophiolites, Turkey.
2173 *Arab. J. Geosci.* 11, 569. <http://doi.org/10.1007/s12517-018-3880-0>

2174 Bingöl, E., 1977. The geology of Muratdagi on the petrology of the main rock units. *Bull.*
2175 *Geol. Soc. Turk.* 20, 13-66.

2176 Booth, M.G., Robertson, A.H.F., Tasli, K. and İnan, N., 2014. Late Cretaceous to Late
2177 Eocene Hekimhan Basin (Central Eastern Turkey) as a supra-ophiolite
2178 sedimentary/magmatic basin related to the later stages of closure of Neotethys.
2179 *Tectonophysics* 635, 6-32. <http://doi.org/10.1016/j.tecto.2014.05.039>

2180 Bortolotti, V., Chiari, M., Göncüoğlu, M.C., Principi, G., Saccani, E., Tekin, U.K. and
2181 Tassinari, R., 2018. The Jurassic–Early Cretaceous basalt–chert association in the
2182 ophiolites of the Ankara Mélange, east of Ankara, Turkey: age and geochemistry.
2183 *Geol. Mag.* 155, 451-478. <http://doi.org/10.1017/s0016756817000401>

2184 Boulton, S.J., 2009. Record of Cenozoic sedimentation from the Amanos Mountains,
2185 Southern Turkey: implications for the inception and evolution of the Arabia–Eurasia
2186 continental collision. *Sediment. Geol.* 216, 29-47.
2187 <http://doi.org/10.1016/j.sedgeo.2009.01.008>

2188 Boulton, S.J. and Robertson, A.H.F., 2008. The Neogene–Recent Hatay Graben, South
2189 Central Turkey: graben formation in a setting of oblique extension (transtension)

1
2
3
4
5
6
7
8
9
10
11
12
13
14
15
16
17
18
19
20
21
22
23
24
25
26
27
28
29
30
31
32
33
34
35
36
37
38
39
40
41
42
43
44
45
46
47
48
49
50
51
52
53
54
55
56
57
58
59
60
61
62
63
64
65

2190 related to post-collisional tectonic escape. *Geol. Mag.* 145, 800-821.
2191 <http://doi.org/10.1017/S0016756808005013>

2192 Bouvier, A., Vervoort, J.D. and Patchett, P.J., 2008. The Lu–Hf and Sm–Nd isotopic
2193 composition of CHUR: Constraints from unequilibrated chondrites and implications
2194 for the bulk composition of terrestrial planets. *Earth Planet. Sci. Lett.* 273, 48-57.
2195 <http://doi.org/10.1016/j.epsl.2008.06.010>

2196 Bretschneider, L., Hathorne, E.C., Huang, H., Lübbers, J., Kochhann, K.G., Holbourn, A.,
2197 Kuhnt, W., Thiede, R., Gebregiorgis, D. and Giosan, L., 2021. Provenance and
2198 weathering of clays delivered to the Bay of Bengal during the middle Miocene:
2199 Linkages to tectonics and monsoonal climate. *Paleoceanogr. Paleoclimatology* 36,
2200 e2020PA003917. <http://doi.org/10.1029/2020PA003917>

2201 Calon, T., Aksu, A. and Hall, J., 2005a. The Neogene evolution of the outer Latakia Basin
2202 and its extension into the eastern Mesaoria Basin (Cyprus), eastern Mediterranean.
2203 *Mar. Geol.* 221, 61-94. <http://doi.org/10.1016/j.margeo.2005.03.013>

2204 Calon, T., Aksu, A. and Hall, J., 2005b. The Oligocene-Recent evolution of the Mesaoria
2205 Basin (Cyprus) and its western marine extension, Eastern Mediterranean. *Mar.*
2206 *Geol.* 221, 95-120. <http://doi.org/10.1016/j.margeo.2005.03.012>

2207 Candan, O., Akal, C., Koralay, O.E., Okay, A.I., Oberhänsli, R., Prelević, D. and Mertz-
2208 Kraus, R., 2016. Carboniferous granites on the northern margin of Gondwana,
2209 Anatolide-Tauride Block, Turkey – Evidence for southward subduction of
2210 Paleotethys. *Tectonophysics* 683, 349-366.
2211 <http://doi.org/10.1016/j.tecto.2016.06.030>

2212 Candan, O., Koralay, O.E., Akal, C., Kaya, O., Oberhänsli, R., Dora, O.Ö., Konak, N. and
2213 Chen, F., 2011. Supra-Pan-African unconformity between core and cover series
2214 of the Menderes Massif/Turkey and its geological implications. *Precambrian Res.*
2215 184, 1-23. <http://doi.org/10.1016/j.precamres.2010.09.010>

1
2
3
4
5
6
7
8
9
10
11
12
13
14
15
16
17
18
19
20
21
22
23
24
25
26
27
28
29
30
31
32
33
34
35
36
37
38
39
40
41
42
43
44
45
46
47
48
49
50
51
52
53
54
55
56
57
58
59
60
61
62
63
64
65

2216 Cavazza, W., Cattò, S., Zattin, M., Okay, A.I. and Reiners, P., 2018. Thermochronology
2217 of the Miocene Arabia-Eurasia collision zone of southeastern Turkey. *Geosphere*
2218 14, 2277-2293. <http://doi.org/10.1130/GES01637.1>

2219 Cawood, P.A., Hawkesworth, C.J. and Dhuime, B., 2012. Detrital zircon record and
2220 tectonic setting. *Geology* 40, 875-878. <http://doi.org/10.1130/g32945.1>

2221 Çelik, Ö.F., Chiaradia, M., Marzoli, A., Billor, Z. and Marschik, R., 2013. The Eldivan
2222 ophiolite and volcanic rocks in the İzmir–Ankara–Erzincan suture zone, Northern
2223 Turkey: Geochronology, whole-rock geochemical and Nd–Sr–Pb isotope
2224 characteristics. *Lithos* 172, 31-46. <http://doi.org/10.1016/j.lithos.2013.03.010>

2225 Çetinkaplan, M., 2018. Anamur (Alanya Masifi, Mersin) Bölgesinde yer alan Prekambriyen
2226 yaşlı kayaçların çok evreli P-T-t evrimi (Multi-Stage P-T-t evolution of Precambrian-
2227 aged rocks in Anamur (Alanya Massif, Mersin) Region). *Geological Bulletin of*
2228 *Turkey* 61, 91-130 (in Turkish with English abstract).
2229 <http://doi.org/10.25288/tjb.358187>

2230 Çetinkaplan, M., Pourteau, A., Candan, O., Koralay, O.E., Oberhänsli, R., Okay, A.I., Chen,
2231 F., Kozlu, H. and Şengün, F., 2016. P–T–t evolution of eclogite/blueschist facies
2232 metamorphism in Alanya Massif: time and space relations with HP event in Bitlis
2233 Massif, Turkey. *Int. J. Earth Sci.* 105, 247-281. [http://doi.org/10.1007/s00531-014-](http://doi.org/10.1007/s00531-014-1092-8)
2234 [1092-8](http://doi.org/10.1007/s00531-014-1092-8)

2235 Chan, G.H.-N., Malpas, J., Xenophontos, C. and Lo, C.-H., 2008. Magmatism associated
2236 with Gondwanaland rifting and Neo-Tethyan oceanic basin development: evidence
2237 from the Mamonia Complex, SW Cyprus. *J. Geol. Soc.* 165, 699-709.
2238 <http://doi.org/10.1144/0016-76492007-050>

2239 Chauvel, C., Lewin, E., Carpentier, M., Arndt, N.T. and Marini, J.-C., 2008. Role of
2240 recycled oceanic basalt and sediment in generating the Hf–Nd mantle array. *Nat.*
2241 *Geosci.* 1, 64-67. <http://doi.org/10.1038/ngeo.2007.51>

1
2
3
4
5
6
7
8
9
10
11
12
13
14
15
16
17
18
19
20
21
22
23
24
25
26
27
28
29
30
31
32
33
34
35
36
37
38
39
40
41
42
43
44
45
46
47
48
49
50
51
52
53
54
55
56
57
58
59
60
61
62
63
64
65

2242 Chen, G. and Robertson, A.H.F., 2021a. Early Miocene calc-alkaline felsic tuffs within
2243 deep-marine turbidites in the Kyrenia Range, north Cyprus, with a possible post-
2244 collisional eruptive centre in western Anatolia. *Geol. Mag.* 1-13.
2245 <http://doi.org/10.1017/S0016756820001399>

2246 Chen, G. and Robertson, A.H.F., 2021b. Evidence from Late Cretaceous-Paleogene
2247 volcanic rocks of the Kyrenia Range, northern Cyprus for the northern, active
2248 continental margin of the Southern Neotethys. *Lithos* 380, 105835.
2249 <http://doi.org/10.1016/j.lithos.2020.105835>

2250 Chen, G., Robertson, A.H.F. and Ustaömer, T., 2019. U–Pb detrital zircon ages used to
2251 infer provenance and tectonic setting of Late Triassic–Miocene sandstones related
2252 to the Tethyan development of Cyprus. *J. Geol. Soc.* 176, 863-884.
2253 <http://doi.org/10.1144/jgs2018-207>

2254 Chen, G., Robertson, A.H.F., Parlak, O. and Wu, F.-Y., 2021. Source to sink in the
2255 easternmost Mediterranean: insights from the provenance of Oligo-Miocene
2256 turbidites in the south Turkish basins, AGU 2021 Fall Meeting, New Orleans, LA
2257 and virtual, pp. 1.

2258 Chen, G., Robertson, A.H.F., Parlak, O. and Wu, F.-Y., 2022. Provenance of sandstones
2259 related to pre, syn and post-rifting of N Gondwana: evidence from detrital zircon
2260 geochronology (Antalya Complex, E Mediterranean), 21st International
2261 Sedimentological Congress, Beijing, China, pp. 1-2.

2262 Clark, M. and Robertson, A., 2002. The role of the Early Tertiary Ulukışla Basin, southern
2263 Turkey, in suturing of the Mesozoic Tethys ocean. *J. Geol. Soc.* 159, 673-690.
2264 <http://doi.org/10.1144/0016-764902-015>

2265 Clift, P., Gaedicke, C., Edwards, R., Il Lee, J., Hildebrand, P., Amjad, S., White, R.S. and
2266 Schlüter, H.-U., 2002. The stratigraphic evolution of the Indus Fan and the history

1
2
3
4
5
6
7
8
9
10
11
12
13
14
15
16
17
18
19
20
21
22
23
24
25
26
27
28
29
30
31
32
33
34
35
36
37
38
39
40
41
42
43
44
45
46
47
48
49
50
51
52
53
54
55
56
57
58
59
60
61
62
63
64
65

2267 of sedimentation in the Arabian Sea. *Mar. Geophys. Res.* 23, 223-245.
2268 <http://doi.org/10.1023/A:1023627123093>

2269 Clift, P.D., 2002. A brief history of the Indus River. In: P.D. Clift, D. Kroon, C. Gaedicke
2270 and J. Craig (Editors), *The Tectonic and Climatic Evolution of the Arabian Sea*
2271 *Region*. Geological Society of London, Special Publications, pp. 237-258.

2272 Cocks, L.R.M. and Torsvik, T.H., 2006. European geography in a global context from the
2273 Vendian to the end of the Palaeozoic. In: D.G. Gee and R.A. Stephenson (Editors),
2274 *European Lithosphere Dynamics*. Geological Society, London, *Memoirs*, pp. 83-
2275 95.

2276 Cohen, K.M., Finney, S.C., Gibbard, P.L. and Fan, J., 2021. The ICS international
2277 Chronostratigraphic Chart. *Episodes* 36, 199-204.

2278 Collins, A.S. and Robertson, A.H.F., 1998. Processes of Late Cretaceous to Late Miocene
2279 episodic thrust-sheet translation in the Lycian Taurides, SW Turkey. *J. Geol. Soc.*
2280 155, 759-772. <http://doi.org/10.1144/gsjgs.155.5.0759>

2281 Corfu, F., Hanchar, J.M., Hoskin, P.W. and Kinny, P., 2003. Atlas of zircon textures. *Rev.*
2282 *Mineral. Geochem.* 53, 469-500. <http://doi.org/10.2113/0530469>

2283 Cosentino, D., Buchwaldt, R., Sampalmieri, G., Iadanza, A., Cipollari, P., Schildgen, T.F.,
2284 Hinnov, L.A., Ramezani, J. and Bowring, S.A., 2013. Refining the Mediterranean
2285 “Messinian gap” with high-precision U-Pb zircon geochronology, central and
2286 northern Italy. *Geology* 41, 323-326. <http://doi.org/10.1130/G33820.1>

2287 Cosentino, D., Schildgen, T.F., Cipollari, P., Faranda, C., Gliozzi, E., Hudáčeková, N.,
2288 Lucifora, S. and Strecker, M.R., 2012. Late Miocene surface uplift of the southern
2289 margin of the Central Anatolian Plateau, Central Taurides, Turkey. *Geol. Soc. Am.*
2290 *Bull.* 124, 133-145. <http://doi.org/10.1130/b30466.1>

1
2
3
4
5
6
7
8
9
10
11
12
13
14
15
16
17
18
19
20
21
22
23
24
25
26
27
28
29
30
31
32
33
34
35
36
37
38
39
40
41
42
43
44
45
46
47
48
49
50
51
52
53
54
55
56
57
58
59
60
61
62
63
64
65

2291 Darin, M.H., Umhoefer, P.J. and Thomson, S.N., 2018. Rapid Late Eocene exhumation
2292 of the Sivas Basin (central Anatolia) driven by initial Arabia - Eurasia collision.
2293 *Tectonics* 37, 3805-3833. <http://doi.org/10.1029/2017tc004954>

2294 Davies, R. and Simmons, M., 2018. Triassic sequence stratigraphy of the Arabian Plate.
2295 In: M. Poppelreiter (Editor), Lower Triassic to Middle Jurassic Sequence of the
2296 Arabian Plate. EAGE, pp. 101-162.

2297 Dempster, T., Hay, D. and Bluck, B., 2004. Zircon growth in slate. *Geology* 32, 221-224.
2298 <http://doi.org/10.1130/G20156.1>

2299 Dilek, Y. and Altunkaynak, Ş., 2010. Geochemistry of Neogene–Quaternary alkaline
2300 volcanism in western Anatolia, Turkey, and implications for the Aegean mantle. *Int.*
2301 *Geol. Rev.* 52, 631-655. <http://doi.org/10.1080/00206810903495020>

2302 Dilek, Y. and Thy, P., 2006. Age and petrogenesis of plagiogranite intrusions in the Ankara
2303 melange, central Turkey. *Isl. Arc* 15, 44-57. [http://doi.org/10.1111/j.1440-](http://doi.org/10.1111/j.1440-1738.2006.00522.x)
2304 [1738.2006.00522.x](http://doi.org/10.1111/j.1440-1738.2006.00522.x)

2305 Ducloz, C., 1972. The geology of the Bellapais-Kythrea area of the Central Kyrenia Range.
2306 *Bulletin of the Geological Survey Department* 6, Nicosia, Cyprus, 75 pp.

2307 Duman, T.Y., Robertson, A.H.F., Elmacı, H. and Kara, M., 2017. Palaeozoic-Recent
2308 geological development and uplift of the Amanos Mountains (S Turkey) in the
2309 critically located northwesternmost corner of the Arabian continent. *Geodin. Acta*
2310 29, 103-138. <http://doi.org/10.1080/09853111.2017.1323428>

2311 Eiler, J.M., 2001. Oxygen isotope variations of basaltic lavas and upper mantle rocks. *Rev.*
2312 *Mineral. Geochem.* 43, 319-364. <http://doi.org/10.2138/gsrmg.43.1.319>

2313 Elmas, A. and Yılmaz, Y., 2003. Development of an oblique subduction zone-tectonic
2314 evolution of the Tethys suture zone in southeast Turkey. *Int. Geol. Rev.* 45, 827-
2315 840. <http://doi.org/10.2747/0020-6814.45.9.827>

1
2
3
4
5
6
7
8
9
10
11
12
13
14
15
16
17
18
19
20
21
22
23
24
25
26
27
28
29
30
31
32
33
34
35
36
37
38
39
40
41
42
43
44
45
46
47
48
49
50
51
52
53
54
55
56
57
58
59
60
61
62
63
64
65

2316 Ersoy, Y.E., Helvacı, C., Uysal, İ., Karaoğlu, Ö., Palmer, M.R. and Dindi, F., 2012.
2317 Petrogenesis of the Miocene volcanism along the İzmir-Balıkesir Transfer Zone in
2318 western Anatolia, Turkey: Implications for origin and evolution of potassic
2319 volcanism in post-collisional areas. *J. Volcanol. Geotherm. Res.* 241, 21-38.
2320 <http://doi.org/10.1016/j.jvolgeores.2012.05.022>

2321 Erturk, M.A., Beyarslan, M., Chung, S.-L. and Lin, T.-H., 2018. Eocene magmatism
2322 (Maden Complex) in the Southeast Anatolian Orogenic Belt: Magma genesis and
2323 tectonic implications. *Geosci. Front.* 9, 1829-1847.
2324 <http://doi.org/10.1016/j.gsf.2017.09.008>

2325 Eyüboğlu, Y., 2010. Late Cretaceous high - K volcanism in the eastern Pontide orogenic
2326 belt: Implications for the geodynamic evolution of NE Turkey. *Int. Geol. Rev.* 52,
2327 142-186. <http://doi.org/10.1080/00206810902757164>

2328 Feld, C., Mechie, J., Hübscher, C., Hall, J., Nicolaidis, S., Gurbuz, C., Bauer, K., Loudon,
2329 K. and Weber, M., 2017. Crustal structure of the Eratosthenes Seamount, Cyprus
2330 and S. Turkey from an amphibian wide-angle seismic profile. *Tectonophysics* 700,
2331 32-59. <http://doi.org/10.1016/j.tecto.2017.02.003>

2332 Fu, B., Bröcker, M., Ireland, T., Holden, P. and Kinsley, L.P.J., 2015. Zircon U–Pb, O, and
2333 Hf isotopic constraints on Mesozoic magmatism in the Cyclades, Aegean Sea,
2334 Greece. *Int. J. Earth Sci.* 104, 75-87. <http://doi.org/10.1007/s00531-014-1064-z>

2335 Gardosh, M.A., Garfunkel, Z., Druckman, Y. and Buchbinder, B., 2010. Tethyan rifting in
2336 the Levant Region and its role in Early Mesozoic crustal evolution. In: C. Homberg
2337 and M. Bachmann (Editors), *Evolution of the Levant Margin and Western Arabia*
2338 *Platform since the Mesozoic*. Geological Society, London, Special Publications, pp.
2339 9-36.

1
2
3
4
5
6
7
8
9
10
11
12
13
14
15
16
17
18
19
20
21
22
23
24
25
26
27
28
29
30
31
32
33
34
35
36
37
38
39
40
41
42
43
44
45
46
47
48
49
50
51
52
53
54
55
56
57
58
59
60
61
62
63
64
65

2340 Garfunkel, Z., 1998. Constrains on the origin and history of the Eastern Mediterranean
2341 basin. *Tectonophysics* 298, 5-35. [http://doi.org/10.1016/S0040-1951\(98\)00176-0](http://doi.org/10.1016/S0040-1951(98)00176-0)
2342 Garzanti, E., Resentini, A., Andò, S., Vezzoli, G., Pereira, A. and Vermeesch, P., 2015.
2343 Physical controls on sand composition and relative durability of detrital minerals
2344 during ultra - long distance littoral and aeolian transport (N amibia and southern A
2345 ngola). *Sedimentology* 62, 971-996. <http://doi.org/10.1111/sed.12169>
2346 Gehrels, G., 2014. Detrital zircon U-Pb geochronology applied to tectonics. *Annu. Rev.*
2347 *Earth Planet. Sci.* 42, 127-149. <http://doi.org/10.1146/annurev-earth-050212->
2348 [124012](http://doi.org/10.1146/annurev-earth-050212-124012)
2349 Genç, Ş.C. and Tüysüz, O., 2010. Tectonic setting of the Jurassic bimodal magmatism in
2350 the Sakarya Zone (Central and Western Pontides), Northern Turkey: a
2351 geochemical and isotopic approach. *Lithos* 118, 95-111.
2352 <http://doi.org/10.1016/j.lithos.2010.03.017>
2353 Glazer, A., Avigad, D., Morag, N., Güngör, T. and Gerdes, A., 2021. The Kyrenia Terrane
2354 (Northern Cyprus): Detrital Zircon Evidence for Exotic Elements in the Southern
2355 Neotethys. *Tectonics* 40, e2021TC006763. <http://doi.org/10.1029/2021TC006763>
2356 Golan, T., Katzir, Y. and Coble, M.A., 2018. Early Carboniferous anorogenic magmatism
2357 in the Levant: implications for rifting in northern Gondwana. *Int. Geol. Rev.* 60, 101-
2358 108. <http://doi.org/10.1080/00206814.2017.1326089>
2359 Göncüoğlu, M.C., Çapkinoğlu, S., Gursu, S., Noble, P., Turhan, N., Tekin, U.K., Okuyucu,
2360 C. and Göncüoğlu, Y., 2007. The Mississippian in the Central and Eastern
2361 Taurides (Turkey): constraints on the tectonic setting of the Tauride-Anatolide
2362 Platform. *Geol. Carpathica* 58, 427.

1
2
3
4
5
6
7
8
9
10
11
12
13
14
15
16
17
18
19
20
21
22
23
24
25
26
27
28
29
30
31
32
33
34
35
36
37
38
39
40
41
42
43
44
45
46
47
48
49
50
51
52
53
54
55
56
57
58
59
60
61
62
63
64
65

2363 Göncüoğlu, M.C., Göncüoğlu, Y., Kozur, H.W. and Kozlu, H., 2004. Paleozoic stratigraphy
2364 of the Geyikdag Unit in the Eastern Taurides (Turkey): New age data and
2365 implications for Gondwanan evolution. *Geol. Carpath.* 55, 433-447.

2366 Göncüoğlu, M.C. and Kozlu, H., 2000. Early Paleozoic evolution of the NW Gondwanaland:
2367 data from southern Turkey and surrounding regions. *Gondwana Res.* 3, 315-324.
2368 [http://doi.org/10.1016/S1342-937X\(05\)70290-2](http://doi.org/10.1016/S1342-937X(05)70290-2)

2369 Göncüoğlu, M.C., Turhan, N. and Tekin, U.K., 2003. Evidence for the Triassic rifting and
2370 opening of the Neotethyan Izmir-Ankara Ocean and discussion on the presence of
2371 Cimmerian events at the northern edge of the Tauride-Anatolide Platform, Turkey.
2372 *Bolletino Soc. Geol. Ital. Spec. Vol.* 2, 203-212.

2373 Granot, R., 2016. Palaeozoic oceanic crust preserved beneath the eastern Mediterranean.
2374 *Nat. Geosci.* 9, 701-705. <http://doi.org/10.1038/ngeo2784>

2375 Gregory, R.T. and Taylor Jr, H.P., 1981. An oxygen isotope profile in a section of
2376 Cretaceous oceanic crust, Samail Ophiolite, Oman: Evidence for $\delta^{18}\text{O}$ buffering
2377 of the oceans by deep (> 5 km) seawater - hydrothermal circulation at mid - ocean
2378 ridges. *J. Geophys. Res.: Solid Earth* 86, 2737-2755.
2379 <http://doi.org/10.1029/JB086iB04p02737>

2380 Griffin, W., 2008. GLITTER: data reduction software for laser ablation ICP-MS. *Laser
2381 Ablation ICP-MS in the Earth Sciences: Current practices outstanding issues* 40,
2382 308-311.

2383 Grimes, C.B., Wooden, J.L., Cheadle, M.J. and John, B.E., 2015. "Fingerprinting" tectono-
2384 magmatic provenance using trace elements in igneous zircon. *Contrib. Mineral.
2385 Petrol.* 170, 46. <http://doi.org/10.1007/s00410-015-1199-3>

2386 Gürsoy, H., Tatar, O., Piper, J., Koçbulut, F., Akpınar, Z., Huang, B., Roberts, A. and Mesci,
2387 B., 2011. Palaeomagnetic study of the Kepezdağ and Yamadağ volcanic

1
2
3
4
5
6
7
8
9
10
11
12
13
14
15
16
17
18
19
20
21
22
23
24
25
26
27
28
29
30
31
32
33
34
35
36
37
38
39
40
41
42
43
44
45
46
47
48
49
50
51
52
53
54
55
56
57
58
59
60
61
62
63
64
65

2388 complexes, central Turkey: Neogene tectonic escape and block definition in the
2389 central-east Anatolides. *J. Geodyn.* 51, 308-326.
2390 <http://doi.org/10.1016/j.jog.2010.07.004>

2391 Gürsu, S. and Göncüoğlu, M.C., 2005. Early Cambrian back-arc volcanism in the western
2392 Taurides, Turkey: implications for rifting along the northern Gondwanan margin.
2393 *Geol. Mag.* 142, 617-631. <http://doi.org/10.1017/s0016756805000919>

2394 Gürsu, S. and Göncüoğlu, M.C., 2008. Petrogenesis and geodynamic evolution of the Late
2395 Neoproterozoic post-collisional felsic magmatism in NE Afyon area, western
2396 central Turkey. In: N. Ennih and J.-P. Liégeois (Editors), *The Boundaries of the*
2397 *West African Craton. Geological Society of London, Special Publications*, pp. 409-
2398 431.

2399 Gürsu, S., Möller, A., Göncüoğlu, M.C., Köksal, S., Demircan, H., Köksal, F.T., Kozlu, H.
2400 and Sunal, G., 2015. Neoproterozoic continental arc volcanism at the northern
2401 edge of the Arabian Plate, SE Turkey. *Precambrian Res.* 258, 208-233.
2402 <http://doi.org/10.1016/j.precamres.2014.12.017>

2403 Gürsu, S., Möller, A., Usta, D., Köksal, S., Ateş, Ş., Sunkari, E.D. and Göncüoğlu, M.C.,
2404 2017. Laser Ablation Inductively Coupled Plasma Mass Spectrometry U-Pb Dating
2405 of Detrital and Magmatic Zircons of Glacial Diamictites and Pebbles in Late
2406 Ordovician Sediments of the Taurides and Southeast Anatolian Autochthon Belt,
2407 Turkey: Indications for Their Arabian-Nubian Provenance. *J. Geol.* 125, 165-202.
2408 <http://doi.org/10.1086/690199>

2409 Gutnic, M.F., Monod, O., Poisson, A. and Dumont, J., 1979. *Geologie des Taurides*
2410 *Occidentales (Turquie)*, 137. Société Géologique de France, Mémoire, 112 pp.

2411 Hakyemez, A. and Özkan-Altiner, S., 2007. Beşparmak Dağları'ndaki (Kuzey Kıbrıs) Üst
2412 Maastrichtiyen-Eosen İstifinin Planktonik Foraminifer Biyostratigrafisi (Planktonic

1
2
3
4
5
6
7
8
9
10
11
12
13
14
15
16
17
18
19
20
21
22
23
24
25
26
27
28
29
30
31
32
33
34
35
36
37
38
39
40
41
42
43
44
45
46
47
48
49
50
51
52
53
54
55
56
57
58
59
60
61
62
63
64
65

2413 Foraminiferal Biostratigraphy of the Upper Maastrichtian – Eocene Sequence in
2414 the Beşparmak Range, Northern Cyprus), 60th Geological Congress of Turkey.
2415 Abstract Book, Ankara, pp. 416-419.

2416 Hakyemez, Y., Turhan, N., Sönmez, I. and Sümengen, M., 2000. Kuzey Kıbrıs Türk
2417 Cumhuriyeti'nin Jeolojisi (Geology of the Turkish Republic of Northern Cyprus).
2418 Genel Müdürlüğü Jeoloji Etütleri Dairesi, Maden Tektik ve Arama, Ankara, 44 pp.

2419 Hardenberg, M.F. and Robertson, A.H.F., 2007. Sedimentology of the NW margin of the
2420 Arabian plate and the SW–NE trending Nahr El-Kabir half-graben in northern Syria
2421 during the latest Cretaceous and Cenozoic. *Sediment. Geol.* 201, 231-266.
2422 <http://doi.org/10.1016/j.sedgeo.2007.02.009>

2423 Harris, S.E. and Mix, A.C., 2002. Climate and tectonic influences on continental erosion
2424 of tropical South America, 0–13 Ma. *Geology* 30, 447-450.
2425 [http://doi.org/10.1130/0091-7613\(2002\)030<0447:CATIOC>2.0.CO;2](http://doi.org/10.1130/0091-7613(2002)030<0447:CATIOC>2.0.CO;2)

2426 Harrison, R., Newell, W., Batıhanlı, H., Panayides, I., McGeehin, J., Mahan, S., Özhür, A.,
2427 Tsiolakis, E. and Necdet, M., 2004. Tectonic framework and Late Cenozoic
2428 tectonic history of the northern part of Cyprus: implications for earthquake hazards
2429 and regional tectonics. *J. Asian Earth Sci.* 23, 191-210.

2430 Hawkesworth, C. and Kemp, A., 2006. Using hafnium and oxygen isotopes in zircons to
2431 unravel the record of crustal evolution. *Chem. Geol.* 226, 144-162.
2432 <http://doi.org/10.1016/j.chemgeo.2005.09.018>

2433 Hay, D. and Dempster, T., 2009. Zircon behaviour during low-temperature metamorphism.
2434 *J. Petrol.* 50, 571-589. <http://doi.org/10.1093/petrology/egp011>

2435 Hayward, A. and Robertson, A., 1982. Direction of ophiolite emplacement inferred from
2436 Cretaceous and Tertiary sediments of an adjacent autochthon, the Bey Daglari,
2437 southwest Turkey. *Geol. Soc. Am. Bull.* 93, 68-75. [http://doi.org/10.1130/0016-7606\(1982\)93<68:DOOEIF>2.0.CO;2](http://doi.org/10.1130/0016-7606(1982)93<68:DOOEIF>2.0.CO;2)

2438

1
2
3
4
5
6
7
8
9
10
11
12
13
14
15
16
17
18
19
20
21
22
23
24
25
26
27
28
29
30
31
32
33
34
35
36
37
38
39
40
41
42
43
44
45
46
47
48
49
50
51
52
53
54
55
56
57
58
59
60
61
62
63
64
65

2439 Henson, F.R.S., Browne, R.V. and McGinty, J., 1949. A synopsis of the stratigraphy and
2440 geological history of Cyprus. *Quarterly Journal of the Geological Society*, 105, 41
2441 pp.

2442 Hoskin, P.W. and Schaltegger, U., 2003. The composition of zircon and igneous and
2443 metamorphic petrogenesis. *Rev. Mineral. Geochem.* 53, 27-62.
2444 <http://doi.org/10.2113/0530027>

2445 Hu, Z., Liu, Y., Gao, S., Liu, W., Zhang, W., Tong, X., Lin, L., Zong, K., Li, M. and Chen,
2446 H., 2012. Improved in situ Hf isotope ratio analysis of zircon using newly designed
2447 X skimmer cone and jet sample cone in combination with the addition of nitrogen
2448 by laser ablation multiple collector ICP-MS. *J. Anal. At. Spectrom.* 27, 1391-1399.
2449 <http://doi.org/10.1039/C2JA30078H>

2450 Huang, K., Malpas, J. and Xenophontos, C., 2007. Geological studies of igneous rocks
2451 and their relationships along the Kyrenia Range. In: K. Moumani, K. Shawabkeh,
2452 A. Al-Malabeh and M. Abdelghafoor (Editors), 6th International Congress of
2453 Eastern Mediterranean Geology, Amman, Jordan, pp. 53.

2454 Huang, S., Meijers, M.J.M., Eyres, A., Mulch, A. and Fritz, S.A., 2019. Unravelling the
2455 history of biodiversity in mountain ranges through integrating geology and
2456 biogeography. *J. Biogeogr.* 46, 1777-1791. <http://doi.org/10.1111/jbi.13622>

2457 Innocenti, F., Mazzuoli, R., Pasquare, G., Di Brozolo, F.R. and Villari, L., 1975. The
2458 Neogene calcalkaline volcanism of Central Anatolia: geochronological data on
2459 Kayseri-Nigde area. *Geol. Mag.* 112, 349-360.
2460 <http://doi.org/10.1017/S0016756800046744>

2461 Jaffey, N. and Robertson, A., 2005. Non-marine sedimentation associated with Oligocene-
2462 Recent exhumation and uplift of the Central Taurus Mountains, S Turkey.
2463 *Sediment. Geol.* 173, 53-89. <http://doi.org/10.1016/j.sedgeo.2003.11.025>

1
2
3
4
5
6
7
8
9
10
11
12
13
14
15
16
17
18
19
20
21
22
23
24
25
26
27
28
29
30
31
32
33
34
35
36
37
38
39
40
41
42
43
44
45
46
47
48
49
50
51
52
53
54
55
56
57
58
59
60
61
62
63
64
65

2464 Jaffey, N., Robertson, A. and Pringle, M., 2004. Latest Miocene and Pleistocene ages of
2465 faulting, determined by $^{40}\text{Ar}/^{39}\text{Ar}$ single-crystal dating of airfall tuff and silicic
2466 extrusives of the Erciyes Basin, central Turkey: evidence for intraplate deformation
2467 related to the tectonic escape of Anatolia. *Terra Nova* 16, 45-53.
2468 <http://doi.org/10.1111/j.1365-3121.2003.00526.x>

2469 Karaođlan, F., Parlak, O., Hejl, E., Neubauer, F. and Kloetzli, U., 2016. The temporal
2470 evolution of the active margin along the Southeast Anatolian Orogenic Belt (SE
2471 Turkey): Evidence from U–Pb, Ar–Ar and fission track chronology. *Gondwana Res.*
2472 33, 190-208. <http://doi.org/10.1016/j.gr.2015.12.011>

2473 Karaođlan, F., Parlak, O., Klötzli, U., Thöni, M. and Koller, F., 2012. U–Pb and Sm–Nd
2474 geochronology of the ophiolites from the SE Turkey: implications for the
2475 Neotethyan evolution. *Geodin. Acta* 25, 146-161.
2476 <http://doi.org/10.1080/09853111.2013.858948>

2477 Karaođlan, F., Parlak, O., Klötzli, U.R.S., Thöni, M. and Koller, F., 2013. U–Pb and Sm–
2478 Nd geochronology of the Kızıldağ (Hatay, Turkey) ophiolite: implications for the
2479 timing and duration of suprasubduction zone type oceanic crust formation in the
2480 southern Neotethys. *Geol. Mag.* 150, 283-299.
2481 <http://doi.org/10.1017/s0016756812000477>

2482 Karşli, O., Dokuz, A. and Kandemir, R., 2016. Subduction-related Late Carboniferous to
2483 Early Permian Magmatism in the Eastern Pontides, the Camlik and Casurluk
2484 plutons: Insights from geochemistry, whole-rock Sr–Nd and in situ zircon Lu–Hf
2485 isotopes, and U–Pb geochronology. *Lithos* 266-267, 98-114.
2486 <http://doi.org/10.1016/j.lithos.2016.10.007>

2487 Keller, C.B., Boehnke, P. and Schoene, B., 2017. Temporal variation in relative zircon
2488 abundance throughout Earth history. *Geochem. Perspect. Lett.* 3, 179-189.
2489 <http://doi.org/10.7185/geochemlet.1721>

1
2
3
4
5
6
7
8
9
10
11
12
13
14
15
16
17
18
19
20
21
22
23
24
25
26
27
28
29
30
31
32
33
34
35
36
37
38
39
40
41
42
43
44
45
46
47
48
49
50
51
52
53
54
55
56
57
58
59
60
61
62
63
64
65

2490 Kelling, G., Gökçen, S.L., Floyd, P.A. and Gökçen, N., 1987. Neogene tectonics and plate
2491 convergence in the eastern Mediterranean: new data from southern Turkey.
2492 *Geology* 15, 425-429. [http://doi.org/10.1130/0091-7613\(1987\)15<425:NTAPCI>2.0.CO;2](http://doi.org/10.1130/0091-7613(1987)15<425:NTAPCI>2.0.CO;2)
2493
2494 Kempler, D. and Garfunkel, Z., 1994. Structures and kinematics in the northeastern
2495 Mediterranean: a study of an irregular plate boundary. *Tectonophysics* 234, 19-32.
2496 [http://doi.org/10.1016/0040-1951\(94\)90202-X](http://doi.org/10.1016/0040-1951(94)90202-X)
2497 Kempler, D., 1998. Eratosthenes Seamount: The possible spearhead of incipient
2498 continental collision in the Eastern Mediterranean. In: A.H.F. Robertson, K.-C.
2499 Emeis, C. Richter and A. Camerlenghi (Editors), *Proceedings of the Ocean Drilling
2500 Program, Scientific Results. Ocean Drilling Program, College Station, TX*, pp. 709-
2501 721.
2502 Keskin, M., Pearce, J.A. and Mitchell, J., 1998. Volcano-stratigraphy and geochemistry of
2503 collision-related volcanism on the Erzurum–Kars Plateau, northeastern Turkey. *J.
2504 Volcanol. Geotherm. Res.* 85, 355-404. [http://doi.org/10.1016/S0377-0273\(98\)00063-8](http://doi.org/10.1016/S0377-0273(98)00063-8)
2505
2506 Kinnaird, T. and Robertson, A., 2013. Tectonic and sedimentary response to subduction
2507 and incipient continental collision in southern Cyprus, easternmost Mediterranean
2508 region. In: A.H.F. Robertson, O. Parlak and U.C. Ünlügenç (Editors), *Geological
2509 Development of Anatolia and the Easternmost Mediterranean Region. Geological
2510 Society of London, Special Publications*, pp. 585-614.
2511 Kumar, A., Dutt, S., Saraswat, R., Gupta, A.K., Clift, P.D., Pandey, D.K., Yu, Z. and
2512 Kulhanek, D.K., 2020. A late pleistocene sedimentation in the Indus fan, Arabian
2513 Sea, IODP site U1457. *Geol. Mag.* 157, 920-928.
2514 <http://doi.org/10.1017/S0016756819000396>

1
2
3
4
5
6
7
8
9
10
11
12
13
14
15
16
17
18
19
20
21
22
23
24
25
26
27
28
29
30
31
32
33
34
35
36
37
38
39
40
41
42
43
44
45
46
47
48
49
50
51
52
53
54
55
56
57
58
59
60
61
62
63
64
65

2515 Lin, Y.-C., Chung, S.-L., Bingöl, A., Beyarslan, M., Lee, H. and Yang, J.-H., 2015.
2516 Petrogenesis of late Cretaceous Elazığ magmatic rocks from SE Turkey: New age
2517 and geochemical and Sr-Nd-Hf isotopic constraints, Goldschmidt 2015 Abstracts,
2518 Prague, pp. 1869.

2519 Linnemann, U., Ouzegane, K., Drareni, A., Hofmann, M., Becker, S., Gärtner, A. and
2520 Sagawe, A., 2011. Sands of West Gondwana: An archive of secular magmatism
2521 and plate interactions — A case study from the Cambro-Ordovician section of the
2522 Tassili Ouan Ahaggar (Algerian Sahara) using U–Pb–LA-ICP-MS detrital zircon
2523 ages. *Lithos* 123, 188-203. <http://doi.org/10.1016/j.lithos.2011.01.010>

2524 Lord, A.R., Panayides, I., Urquhart, E. and Xenophontos, C., 2000. A
2525 biochronostratigraphical framework for the Late Cretaceous-Recent circum-
2526 Troodos sedimentary sequence, Cyprus. In: I. Panayides, C. Xenophontos and J.
2527 Malpas (Editors), *Proceedings of the Third International Conference on the
2528 Geology of the Eastern Mediterranean*. Cyprus Geological Survey Department,
2529 Nicosia, Cyprus, pp. 289-298.

2530 Löwen, K., Meinhold, G., Arslan, A., Güngör, T. and Berndt, J., 2020. Evolution of the
2531 Palaeotethys in the Eastern Mediterranean: a multi-method approach to unravel
2532 the age, provenance and tectonic setting of the Upper Palaeozoic Konya Complex
2533 and its Mesozoic cover sequence (south-central Turkey). *Int. Geol. Rev.* 62, 389-
2534 414. <http://doi.org/10.1080/00206814.2019.1616619>

2535 Löwen, K., Meinhold, G., Güngör, T. and Berndt, J., 2017. Palaeotethys-related sediments
2536 of the Karaburun Peninsula, western Turkey: constraints on provenance and
2537 stratigraphy from detrital zircon geochronology. *Int. J. Earth Sci.* 106, 2771-2796.
2538 <http://doi.org/10.1007/s00531-017-1458-9>

2539 Mackintosh, P.W. and Robertson, A.H.F., 2009. Structural and sedimentary evidence from
2540 the northern margin of the Tauride platform: Testing models of Late Triassic

1
2
3
4
5
6
7
8
9
10
11
12
13
14
15
16
17
18
19
20
21
22
23
24
25
26
27
28
29
30
31
32
33
34
35
36
37
38
39
40
41
42
43
44
45
46
47
48
49
50
51
52
53
54
55
56
57
58
59
60
61
62
63
64
65

2541 'Cimmerian'uplift and deformation in southern Turkey. *Tectonophysics* 473, 203-
2542 215. <http://doi.org/10.1016/j.tecto.2008.10.031>

2543 Mackintosh, P.W. and Robertson, A.H.F., 2012. Late Devonian–Late Triassic sedimentary
2544 development of the central Taurides, S Turkey: Implications for the northern
2545 margin of Gondwana. *Gondwana Res.* 21, 1089-1114.
2546 <http://doi.org/10.1016/j.gr.2011.07.016>

2547 Mackintosh, P.W. and Robertson, A.H.F., 2013. Sedimentary and structural evidence for
2548 two-phase Upper Cretaceous and Eocene emplacement of the Tauride thrust
2549 sheets in central southern Turkey. In: A.H.F. Robertson, O. Parlak and Ü.C.
2550 Ünlügenç (Editors), *Geological Development of Anatolia and the Easternmost*
2551 *Mediterranean Region*. Geological Society of London, Special Publications, pp.
2552 299-322.

2553 Maffione, M., van Hinsbergen, D.J., de Gelder, G.I., van der Goes, F.C. and Morris, A.,
2554 2017. Kinematics of Late Cretaceous subduction initiation in the Neo - Tethys
2555 Ocean reconstructed from ophiolites of Turkey, Cyprus, and Syria. *J. Geophys.*
2556 *Res.: Solid Earth* 122, 3953-3976. <http://doi.org/10.1002/2016JB013821>

2557 Mange, M.A. and Maurer, H., 2012. *Heavy minerals in colour*. Chapman and Hall, London,
2558 147 pp.

2559 Marcoux, J., Ricou, L., Burg, J. and Brun, J., 1989. Shear-sense criteria in the Antalya and
2560 Alanya thrust system (southwestern Turkey): evidence for a southward
2561 emplacement. *Tectonophysics* 161, 81-91. [http://doi.org/10.1016/0040-](http://doi.org/10.1016/0040-1951(89)90304-1)
2562 [1951\(89\)90304-1](http://doi.org/10.1016/0040-1951(89)90304-1)

2563 Marroni, M., Göncüoğlu, M.C., Frassi, C., Sayit, K., Pandolfi, L., Ellero, A. and Ottria, G.,
2564 2020. The Intra-Pontide ophiolites in Northern Turkey revisited: From birth to death

1
2
3
4
5
6
7
8
9
10
11
12
13
14
15
16
17
18
19
20
21
22
23
24
25
26
27
28
29
30
31
32
33
34
35
36
37
38
39
40
41
42
43
44
45
46
47
48
49
50
51
52
53
54
55
56
57
58
59
60
61
62
63
64
65

2565 of a Neotethyan oceanic domain. *Geosci. Front.* 11, 129-149.
2566 <http://doi.org/10.1016/j.gsf.2019.05.010>

2567 Maury, R.C., Lapierre, H., Bosch, D., Marcoux, J., Krystyn, L., Cotten, J., Bussy, F., Brunet,
2568 P. and Senebier, F., 2008. The alkaline intraplate volcanism of the Antalya nappes
2569 (Turkey): a Late Triassic remnant of the Neotethys. *Bull. Soc. Géol. Fr.* 179, 397-
2570 410. <http://doi.org/10.2113/gssgfbull.179.4.397>

2571 McCay, G.A., 2010. Tectonic-sedimentary evolution of the Girne (Kyrenia) Range and the
2572 Mesarya (Mesaoria) Basin, North Cyprus. Unpublished PhD thesis Thesis,
2573 University of Edinburgh, 586 pp.

2574 McCay, G.A. and Robertson, A.H.F., 2012. Late Eocene–Neogene sedimentary geology
2575 of the Girne (Kyrenia) Range, northern Cyprus: A case history of sedimentation
2576 related to progressive and diachronous continental collision. *Sediment. Geol.* 265,
2577 30-55. <http://doi.org/10.1016/j.sedgeo.2012.03.001>

2578 McCay, G.A. and Robertson, A.H.F., 2013. Upper Miocene–Pleistocene deformation of
2579 the Girne (Kyrenia) Range and Dar Dere (Ovgos) lineaments, northern Cyprus:
2580 role in collision and tectonic escape in the easternmost Mediterranean region. In:
2581 A.H.F. Robertson, O. Parlak and U.C. Ünlügenç (Editors), *Geological*
2582 *Development of Anatolia and the Easternmost Mediterranean Region.* Geological
2583 Society of London, Special Publications, pp. 421-445.

2584 McCay, G.A., Robertson, A.H.F., Kroon, D., Raffi, I., Ellam, R.M. and Necdet, M., 2013.
2585 Stratigraphy of Cretaceous to Lower Pliocene sediments in the northern part of
2586 Cyprus based on comparative $^{87}\text{Sr}/^{86}\text{Sr}$ isotopic, nannofossil and planktonic
2587 foraminiferal dating. *Geol. Mag.* 150, 333-359.
2588 <http://doi.org/10.1017/s0016756812000465>

1
2
3
4
5
6
7
8
9
10
11
12
13
14
15
16
17
18
19
20
21
22
23
24
25
26
27
28
29
30
31
32
33
34
35
36
37
38
39
40
41
42
43
44
45
46
47
48
49
50
51
52
53
54
55
56
57
58
59
60
61
62
63
64
65

2589 McPhee, P.J. and van Hinsbergen, D.J., 2019. Tectonic reconstruction of Cyprus reveals
2590 Late Miocene continental collision of Africa and Anatolia. *Gondwana Res.* 68, 158-
2591 173. <http://doi.org/10.1016/j.gr.2018.10.015>

2592 McPhee, P.J., Altiner, D. and Van Hinsbergen, D.J., 2018. First balanced cross section
2593 across the Taurides fold - thrust belt: geological constraints on the subduction
2594 history of the Antalya slab in southern Anatolia. *Tectonics* 37, 3738-3759.
2595 <http://doi.org/10.1029/2017TC004893>

2596 Meijers, M.J.M., Brocard, G.Y., Whitney, D.L. and Mulch, A., 2020. Paleoenvironmental
2597 conditions and drainage evolution of the central Anatolian lake system (Turkey)
2598 during late Miocene to Pliocene surface uplift. *Geosphere* 16, 490-509.
2599 <http://doi.org/10.1130/ges02135.1>

2600 Meinhold, G. and Frei, D., 2008. Detrital zircon ages from the islands of Inousses and
2601 Psara, Aegean Sea, Greece: constraints on depositional age and provenance.
2602 *Geol. Mag.* 145, 886-891. <http://doi.org/10.1017/S0016756808005505>

2603 Molnar, P., 2004. Late Cenozoic increase in accumulation rates of terrestrial sediment:
2604 How might climate change have affected erosion rates? *Annu. Rev. Earth Planet.*
2605 *Sci.* 32, 67-89. <http://doi.org/10.1146/annurev.earth.32.091003.143456>

2606 Monod, O., 1977. *Récherches Géologique dans les Taurus occidental au sud de Beyşehir*
2607 (Turquie), Université de Paris-Sud, Orsay, France.

2608 Moore, T.A., 1960. The geology and mineral resources of the Astromeritis-Kormakiti area.
2609 Geological Survey Department, Memoir 6, Nicosia, Cyprus, 96 pp.

2610 Morag, N., Haviv, I. and Katzir, Y., 2016. From ocean depths to mountain tops: uplift of
2611 the Troodos ophiolite (Cyprus) constrained by low-temperature thermochronology
2612 and geomorphic analysis. *Tectonics* 35, 622-637.
2613 <http://doi.org/10.1002/2015tc004069>

1
2
3
4
5
6
7
8
9
10
11
12
13
14
15
16
17
18
19
20
21
22
23
24
25
26
27
28
29
30
31
32
33
34
35
36
37
38
39
40
41
42
43
44
45
46
47
48
49
50
51
52
53
54
55
56
57
58
59
60
61
62
63
64
65

2614 MTA, 2011. Geological map of Turkey 1:250,000 (General Directorate of Mineral
2615 Research and Exploration). Maden Tektik ve Arama Genel Müdürlüğü (MTA),
2616 Ankara.

2617 Mukasa, S.B. and Ludden, J.N., 1987. Uranium-lead isotopic ages of plagiogranites from
2618 the Troodos ophiolite, Cyprus, and their tectonic significance. *Geology* 15, 825-
2619 828. [http://doi.org/10.1130/0091-7613\(1987\)15<825:UUAOPF>2.0.CO;2](http://doi.org/10.1130/0091-7613(1987)15<825:UUAOPF>2.0.CO;2)

2620 Necdet, M. and Anıl, M., 2006. The Geology and Geochemistry of the Gypsum Deposits
2621 in Northern Cyprus. *Geosound* 48, 11-50.

2622 Nurlu, N., Parlak, O., Robertson, A.H.F. and von Quadt, A., 2016. Implications of Late
2623 Cretaceous U–Pb zircon ages of granitic intrusions cutting ophiolitic and
2624 volcanogenic rocks for the assembly of the Tauride allochthon in SE Anatolia
2625 (Helete area, Kahramanmaraş Region, SE Turkey). *Int. J. Earth Sci.* 105, 283-314.
2626 <http://doi.org/10.1007/s00531-015-1211-1>

2627 Okay, A.I. and Topuz, G., 2017. Variscan orogeny in the Black Sea region. *Int. J. Earth*
2628 *Sci.* 106, 569-592. <http://doi.org/10.1007/s00531-016-1395-z>

2629 Okay, A.I., 2001. Stratigraphic and metamorphic inversions in the central Menderes Massif:
2630 a new structural model. *Int. J. Earth Sci.* 89, 709-727.
2631 <http://doi.org/10.1007/s005310000098>

2632 Okay, A.I., 2002. Jadeite–chloritoid–glaucophane–lawsonite blueschists in north - west
2633 Turkey: unusually high P/T ratios in continental crust. *J. Metamorph. Geol.* 20, 757-
2634 768. <http://doi.org/10.1046/j.1525-1314.2002.00402.x>

2635 Okay, A.I., Altiner, D. and Kilic, A.M., 2015. Triassic limestone, turbidites and serpentinite–
2636 the Cimmeride orogeny in the Central Pontides. *Geol. Mag.* 152, 460-479.
2637 <http://doi.org/10.1017/S0016756814000429>

1
2
3
4
5
6
7
8
9
10
11
12
13
14
15
16
17
18
19
20
21
22
23
24
25
26
27
28
29
30
31
32
33
34
35
36
37
38
39
40
41
42
43
44
45
46
47
48
49
50
51
52
53
54
55
56
57
58
59
60
61
62
63
64
65

2638 Okay, A.I., Bozkurt, E., Satır, M., Yiğitbaş, E., Crowley, Q.G. and Shang, C.K., 2008a.
2639 Defining the southern margin of Avalonia in the Pontides: geochronological data
2640 from the Late Proterozoic and Ordovician granitoids from NW Turkey.
2641 Tectonophysics 461, 252-264. <http://doi.org/10.1016/j.tecto.2008.02.004>
2642 Okay, A.I., Harris, N.B. and Kelley, S.P., 1998. Exhumation of blueschists along a Tethyan
2643 suture in northwest Turkey. Tectonophysics 285, 275-299.
2644 [http://doi.org/10.1016/S0040-1951\(97\)00275-8](http://doi.org/10.1016/S0040-1951(97)00275-8)
2645 Okay, A.I., Satır, M. and Shang, C.K., 2008b. Ordovician metagranitoid from the
2646 Anatolide - Tauride Block, northwest Turkey: geodynamic implications. Terra
2647 Nova 20, 280-288. <http://doi.org/10.1111/j.1365-3121.2008.00818.x>
2648 Okay, A.I., Sunal, G., Sherlock, S., Kylander - Clark, A.R.C. and Özcan, E., 2020. İzmir -
2649 Ankara Suture as a Triassic to Cretaceous Plate Boundary—Data From Central
2650 Anatolia. Tectonics 39. <http://doi.org/10.1029/2019tc005849>
2651 Okay, A.I., Zattin, M. and Cavazza, W., 2010. Apatite fission-track data for the Miocene
2652 Arabia-Eurasia collision. Geology 38, 35-38. <http://doi.org/10.1130/G30234.1>
2653 Önal, A., Boztuğ, D., Arslan, M., Spell, T.L. and Kueruem, S., 2008. Petrology and ⁴⁰Ar-
2654 ³⁹Ar Age of the Bimodal Orduzu Volcanics (Malatya) from the Western end of the
2655 Eastern Anatolian Neogene Volcanism, Turkey. Turk. J. Earth Sci. 17, 85-109.
2656 Oyan, V., 2018. Ar-Ar dating and petrogenesis of the Early Miocene Taşkapı-Mecitli (Erciş-
2657 Van) granitoid, Eastern Anatolia Collisional Zone, Turkey. J. Asian Earth Sci. 158,
2658 210-226. <http://doi.org/10.1016/j.jseaes.2018.03.002>
2659 Özbey, Z., Ustaömer, T., Robertson, A.H.F. and Ustaömer, P.A., 2013. Tectonic
2660 significance of Late Ordovician granitic magmatism and clastic sedimentation on
2661 the northern margin of Gondwana (Tavşanlı Zone, NW Turkey). J. Geol. Soc. 170,
2662 159-173. <http://doi.org/10.1144/jgs2011-091>

1
2
3
4
5
6
7
8
9
10
11
12
13
14
15
16
17
18
19
20
21
22
23
24
25
26
27
28
29
30
31
32
33
34
35
36
37
38
39
40
41
42
43
44
45
46
47
48
49
50
51
52
53
54
55
56
57
58
59
60
61
62
63
64
65

2663 Özer, S., Sözbilir, H., Özkar, İ., Toker, V. and Sari, B., 2001. Stratigraphy of Upper
2664 Cretaceous–Palaeogene sequences in the southern and eastern Menderes Massif
2665 (western Turkey). *Int. J. Earth Sci.* 89, 852-866.
2666 <http://doi.org/10.1007/s005310000142>

2667 Özgül, N., 1984a. Stratigraphy and tectonic evolution of the central Taurides. In: O. Tekeli
2668 and M.C. Göncüoğlu (Editors), *Proceedings of the International Symposium on the*
2669 *Geology of the Taurus Belt*. MTA, Ankara, pp. 77-90.

2670 Özgül, N., 1984b. Alanya Tektonik Penceresi ve Bati Kesiminin Jeolojisi (Alanya tectonic
2671 window and geology of its western part). *Geological Society of Turkey, Ketin*
2672 *Symposium*, Ankara, pp. 97–120.

2673 Özgül, N., 1997. Stratigraphy of the tectonostratigraphical units around Hadım–Bozkır–
2674 Taşkent region, northern part of the Central Taurides. *Bull. Miner. Resour.*
2675 *Exploration (Turk.)* 119, 113-174.

2676 Palamakumbura, R., 2016. Sedimentary response to the tectonic uplift of the Kyrenia
2677 Range, northern Cyprus, in its Eastern Mediterranean tectonic setting.
2678 Unpublished PhD Thesis Thesis, University of Edinburgh, UK, 417 pp.

2679 Palamakumbura, R.N. and Robertson, A.H.F., 2016. Pleistocene terrace deposition
2680 related to tectonically controlled surface uplift: An example of the Kyrenia Range
2681 lineament in the northern part of Cyprus. *Sediment. Geol.* 339, 46-67.
2682 <http://doi.org/10.1016/j.sedgeo.2016.03.022>

2683 Palamakumbura, R.N. and Robertson, A.H.F., 2018. Pliocene–Pleistocene sedimentary–
2684 tectonic development of the Mesaoria (Mesarya) Basin in an incipient, diachronous
2685 collisional setting: facies evidence from the north of Cyprus. *Geol. Mag.* 155, 997-
2686 1022. <http://doi.org/10.1017/S0016756816001072>

2687 Palamakumbura, R.N., Robertson, A.H.F., Kinnaird, T.C., van Calsteren, P., Kroon, D.
2688 and Tait, J.A., 2016. Quantitative dating of Pleistocene deposits of the Kyrenia

1
2
3
4
5
6
7
8
9
10
11
12
13
14
15
16
17
18
19
20
21
22
23
24
25
26
27
28
29
30
31
32
33
34
35
36
37
38
39
40
41
42
43
44
45
46
47
48
49
50
51
52
53
54
55
56
57
58
59
60
61
62
63
64
65

2689 Range, northern Cyprus: implications for timing, rates of uplift and driving
2690 mechanisms. *J. Geol. Soc.* 173, 933-948. <http://doi.org/10.1144/jgs2015-130>

2691 Parlak, O., 2006. Geodynamic significance of granitoid magmatism in the southeast
2692 Anatolian orogen: geochemical and geochronological evidence from Göksun–Afşin
2693 (Kahramanmaraş, Turkey) region. *Int. J. Earth Sci.* 95, 609-627.

2694 Parlak, O., Karaoğlan, F., Rızaoğlu, T., Klötzli, U., Koller, F. and Billor, Z., 2013. U–Pb
2695 and ⁴⁰Ar–³⁹Ar geochronology of the ophiolites and granitoids from the Tauride belt:
2696 implications for the evolution of the Inner Tauride suture. *J. Geodyn.* 65, 22-37.

2697 Parlak, O. and Robertson, A.H.F., 2004. The ophiolite-related Mersin Melange, southern
2698 Turkey: its role in the tectonic–sedimentary setting of Tethys in the Eastern
2699 Mediterranean region. *Geol. Mag.* 141, 257-286.
2700 <http://doi.org/10.1017/S0016756804009094>

2701 Pearce, J.A., Bender, J., De Long, S., Kidd, W., Low, P., Güner, Y., Saroglu, F., Yilmaz,
2702 Y., Moorbath, S. and Mitchell, J., 1990. Genesis of collision volcanism in Eastern
2703 Anatolia, Turkey. *J. Volcanol. Geotherm. Res.* 44, 189-229.
2704 [http://doi.org/10.1016/0377-0273\(90\)90018-B](http://doi.org/10.1016/0377-0273(90)90018-B)

2705 Perinçek, D. and Kozlu, H., 1984. Stratigraphy and structural relations of the units in the
2706 Afşin-Elbistan-Doğanşehir region (Eastern Taurus). In: O. Tekeli and M.C.
2707 Göncüoğlu (Editors), *Geology of the Taurus Belt: Proceedings of the International*
2708 *Symposium. Maden Tetkik ve Arama Enstitüsü, Ankara*, pp. 181-198.

2709 Pickering, K.T., Poudoux, H., McNeill, L.C., Backman, J., Chemale, F., Kutterolf, S.,
2710 Milliken, K.L., Mukoyoshi, H., Henstock, T.J., Stevens, D.E., Parnell, C. and Dugan,
2711 B., 2020. Sedimentology, stratigraphy and architecture of the Nicobar Fan
2712 (Bengal–Nicobar Fan System), Indian Ocean: Results from International Ocean
2713 Discovery Program Expedition 362. *Sedimentology* 67, 2248-2281.
2714 <http://doi.org/10.1111/sed.12701>

1
2
3
4
5
6
7
8
9
10
11
12
13
14
15
16
17
18
19
20
21
22
23
24
25
26
27
28
29
30
31
32
33
34
35
36
37
38
39
40
41
42
43
44
45
46
47
48
49
50
51
52
53
54
55
56
57
58
59
60
61
62
63
64
65

2715 Platzman, E., Tapirdamaz, C. and Sanver, M., 1998. Neogene anticlockwise rotation of
2716 central Anatolia (Turkey): preliminary palaeomagnetic and geochronological
2717 results. *Tectonophysics* 299, 175-189. <http://doi.org/10.1016/S0040->
2718 1951(98)00204-2

2719 Poisson, A., 1977. Recherches géologiques dans les Taurides occidentales (Turquie).
2720 Unpublished PhD thesis Thesis, Université de Paris-Sud Orsayde, 795 pp.

2721 Poole, A. and Robertson, A., 1991. Quaternary uplift and sea-level change at an active
2722 plate boundary, Cyprus. *J. Geol. Soc.* 148, 909-921.
2723 <http://doi.org/10.1144/gsjgs.148.5.0909>

2724 Pourteau, A., Candan, O. and Oberhänsli, R., 2010. High - pressure metasediments in
2725 central Turkey: Constraints on the Neotethyan closure history. *Tectonics* 29.
2726 <http://doi.org/10.1029/2009TC002650>

2727 Pourteau, A., Oberhänsli, R., Candan, O., Barrier, E. and Vrielynck, B., 2016. Neotethyan
2728 closure history of western Anatolia: a geodynamic discussion. *Int. J. Earth Sci.* 105,
2729 203-224. <http://doi.org/10.1007/s00531-015-1226-7>

2730 Racano, S., Jara - Muñoz, J., Cosentino, D. and Melnick, D., 2020. Variable Quaternary
2731 Uplift Along the Southern Margin of the Central Anatolian Plateau Inferred From
2732 Modeling Marine Terrace Sequences. *Tectonics* 39.
2733 <http://doi.org/10.1029/2019tc005921>

2734 Reiche, S. and Hübscher, C., 2015. The Hecataeus Rise, easternmost Mediterranean: A
2735 structural record of Miocene-Quaternary convergence and incipient continent-
2736 continent-collision at the African-Anatolian plate boundary. *Mar. Pet. Geol.* 67,
2737 368-388. <http://doi.org/10.1016/j.marpetgeo.2015.04.021>

2738 Ring, U. and Pantazides, H., 2019. The uplift of the Troodos massif, Cyprus. *Tectonics* 38,
2739 3124-3139. <http://doi.org/10.1029/2019TC005514>

1
2
3
4
5
6
7
8
9
10
11
12
13
14
15
16
17
18
19
20
21
22
23
24
25
26
27
28
29
30
31
32
33
34
35
36
37
38
39
40
41
42
43
44
45
46
47
48
49
50
51
52
53
54
55
56
57
58
59
60
61
62
63
64
65

2740 Robertson, A.H.F. and Dixon, J.E., 1984. Introduction: aspects of the geological evolution
2741 of the Eastern Mediterranean. In: J.E. Dixon and A.H.F. Robertson (Editors), The
2742 Geological Evolution of the Eastern Mediterranean. Geological Society of London,
2743 Special Publications, pp. 1-74.

2744 Robertson, A.H.F. and Kinnaird, T.C., 2016. Structural development of the central Kyrenia
2745 Range (north Cyprus) in its regional setting in the eastern Mediterranean region.
2746 Int. J. Earth Sci. 105, 417-437. <http://doi.org/10.1007/s00531-015-1215-x>

2747 Robertson, A.H.F. and Parlak, O., 2020. Late Cretaceous-Palaeocene subduction-
2748 collision-exhumation of a microcontinent along the northern, active margin of South
2749 Neotethys: evidence from the Alanya Massif and the adjacent Antalya Complex (S
2750 Turkey). J. Asian Earth Sci. 104467. <http://doi.org/10.1016/j.jseaes.2020.104467>

2751 Robertson, A.H.F. and Ustaömer, T., 2009a. Formation of the Late Palaeozoic Konya
2752 Complex and comparable units in southern Turkey by subduction–accretion
2753 processes: Implications for the tectonic development of Tethys in the Eastern
2754 Mediterranean region. Tectonophysics 473, 113-148.
2755 <http://doi.org/10.1016/j.tecto.2008.10.027>

2756 Robertson, A.H.F. and Ustaömer, T., 2009b. Upper Palaeozoic subduction/accretion
2757 processes in the closure of Palaeotethys: Evidence from the Chios Melange (E
2758 Greece), the Karaburun Melange (W Turkey) and the Teke Dere Unit (SW Turkey).
2759 Sediment. Geol. 220, 29-59. <http://doi.org/10.1016/j.sedgeo.2009.06.005>

2760 Robertson, A.H.F. and Waldron, J., 1990. Geochemistry and tectonic setting of Late
2761 Triassic and late Jurassic–Early Cretaceous basaltic extrusives from the Antalya
2762 Complex, SW Turkey. In: M.Y. Savaşçin and A.H. Eronat (Editors), Proceedings
2763 of the International Earth Sciences Congress on Aegean Regions, Izmir, Turkey,
2764 pp. 279-299.

1
2
3
4
5
6
7
8
9
10
11
12
13
14
15
16
17
18
19
20
21
22
23
24
25
26
27
28
29
30
31
32
33
34
35
36
37
38
39
40
41
42
43
44
45
46
47
48
49
50
51
52
53
54
55
56
57
58
59
60
61
62
63
64
65

2765 Robertson, A.H.F. and Woodcock, N.H., 1979. Mamonia Complex, southwest Cyprus:
2766 Evolution and emplacement of a Mesozoic continental margin. *Geol. Soc. Am. Bull.*
2767 90, 651-665. [http://doi.org/10.1130/0016-7606\(1979\)90<651:mcscea>2.0.co;2](http://doi.org/10.1130/0016-7606(1979)90<651:mcscea>2.0.co;2)

2768 Robertson, A.H.F. and Woodcock, N.H., 1984. The SW segment of the Antalya Complex,
2769 Turkey as a Mesozoic-Tertiary Tethyan continental margin. In: J.E. Dixon and
2770 A.H.F. Robertson (Editors), *The Geological Evolution of the Eastern*
2771 *Mediterranean*. Geological Society of London, Special Publications, pp. 251-271.

2772 Robertson, A.H.F. and Woodcock, N.H., 1986. The role of the Kyrenia Range Lineament,
2773 Cyprus, in the geological evolution of the eastern Mediterranean area. *Philos.*
2774 *Trans. R. Soc. Lond., Math. Phys. Sci.* 317, 141-177.
2775 <http://doi.org/10.1098/rsta.1986.0030>

2776 Robertson, A.H.F., 1990. Tectonic evolution of Cyprus. In: J. Malpas, E.M. Moores, A.
2777 Panayiotou and C. Xenophontos (Editors), *Ophiolites-Oceanic Crustal Analogues:*
2778 *Proceedings of the International Symposium 'Troodos 1987'*. Cyprus Geological
2779 Survey Department, Nicosia, pp. 235-250.

2780 Robertson, A.H.F., 1998. Mesozoic-Tertiary tectonic evolution of the easternmost
2781 Mediterranean area: integration of marine and land evidence. In: A.H.F. Robertson,
2782 K.-C. Emeis, C. Richter and A. Camerlenghi (Editors), *Proceedings of the Ocean*
2783 *Drilling Program, Scientific Results*. Ocean Drilling Program, College Station, TX,
2784 pp. 723-782.

2785 Robertson, A.H.F., 2022. Palaeozoic-Early Mesozoic transition from Palaeotethys to
2786 Neotethys: Synthesis of data and interpretations from the northern periphery of
2787 Gondwana (central and western Anatolia, Aegean, Balkans and Sicily). *Earth-Sci.*
2788 *Rev.* 230, 104000. <http://doi.org/10.1016/j.earscirev.2022.104000>

2789 Robertson, A.H.F., Boulton, S.J., Taslı, K., Yıldırım, N., İnan, N., Yıldız, A. and Parlak, O.,
2790 2016. Late Cretaceous-Miocene sedimentary development of the Arabian

1
2
3
4
5
6
7
8
9
10
11
12
13
14
15
16
17
18
19
20
21
22
23
24
25
26
27
28
29
30
31
32
33
34
35
36
37
38
39
40
41
42
43
44
45
46
47
48
49
50
51
52
53
54
55
56
57
58
59
60
61
62
63
64
65

2791 continental margin in SE Turkey (Adiyaman region): Implications for regional
2792 palaeogeography and the closure history of Southern Neotethys. *J. Asian Earth*
2793 *Sci.* 115, 571-616. <http://doi.org/10.1016/j.jseaes.2015.01.025>

2794 Robertson, A.H.F., McCay, G.A., Tasli, K. and Yıldız, A., 2014. Eocene development of
2795 the northerly active continental margin of the Southern Neotethys in the Kyrenia
2796 Range, north Cyprus. *Geol. Mag.* 151, 692-731.
2797 <http://doi.org/10.1017/s0016756813000563>

2798 Robertson, A.H.F., Necdet, M., Raffi, I. and Chen, G., 2019. Early Messinian manganese
2799 deposition in NE Cyprus related to cyclical redox changes in a silled hemipelagic
2800 basin prior to the Mediterranean salinity Crisis. *Sediment. Geol.* 385, 126-148.
2801 <http://doi.org/10.1016/j.sedgeo.2019.03.009>

2802 Robertson, A.H.F., Parlak, O. and Ustaömer, T., 2012a. Overview of the Palaeozoic-
2803 Neogene evolution of Neotethys in the Eastern Mediterranean region (southern
2804 Turkey, Cyprus, Syria). *Pet. Geosci.* 18, 381-404.
2805 <http://doi.org/10.1144/petgeo2011-091>

2806 Robertson, A.H.F., Parlak, O. and Ustaömer, T., 2021a. Late Palaeozoic extensional
2807 volcanism along the northern margin of Gondwana in southern Turkey:
2808 implications for Palaeotethyan development. *Int. J. Earth Sci.* 110, 1961-1994.
2809 <http://doi.org/10.1007/s00531-021-02051-7>

2810 Robertson, A.H.F., Parlak, O., Kinnaird, T.C., Taslı, K. and Dumitrica, P., 2020. Cambrian-
2811 Eocene pre-rift, pulsed rift, passive margin and emplacement processes along the
2812 northern margin of the Southern Neotethys: evidence from the Antalya Complex in
2813 the Alanya Window (S Turkey). *J. Asian Earth Sci.*: X 3, 100026.
2814 <http://doi.org/10.1016/j.jaesx.2020.100026>

2815 Robertson, A.H.F., Parlak, O., Ustaömer, T., Taslı, K. and Dumitrica, P., 2021b. Late
2816 Palaeozoic-Neogene sedimentary and tectonic development of the Tauride

1
2
3
4
5
6
7
8
9
10
11
12
13
14
15
16
17
18
19
20
21
22
23
24
25
26
27
28
29
30
31
32
33
34
35
36
37
38
39
40
41
42
43
44
45
46
47
48
49
50
51
52
53
54
55
56
57
58
59
60
61
62
63
64
65

2817 continent and adjacent Tethyan ocean basins in eastern Turkey: new data and
2818 integrated interpretation. *J. Asian Earth Sci.* 104859.
2819 <http://doi.org/10.1016/j.jseaes.2021.104859>

2820 Robertson, A.H.F., Parlak, O., Ustaömer, T., Taslı, K., İnan, N., Dumitrica, P. and
2821 Karaoğlan, F., 2013. Subduction, ophiolite genesis and collision history of Tethys
2822 adjacent to the Eurasian continental margin: new evidence from the Eastern
2823 Pontides, Turkey. *Geodin. Acta* 26, 230-293.
2824 <http://doi.org/10.1080/09853111.2013.877240>

2825 Robertson, A.H.F., Tasli, K. and İnan, N., 2012b. Evidence from the Kyrenia Range,
2826 Cyprus, of the northerly active margin of the Southern Neotethys during Late
2827 Cretaceous–Early Cenozoic time. *Geol. Mag.* 149, 264-290.
2828 <http://doi.org/10.1017/s0016756811000677>

2829 Robertson, A.H.F., Unlüğenç, Ü.C., İnan, N. and Tasli, K., 2004. The Misis–Andırın
2830 Complex: a Mid-Tertiary melange related to late-stage subduction of the Southern
2831 Neotethys in S Turkey. *J. Asian Earth Sci.* 22, 413-453.
2832 [http://doi.org/10.1016/s1367-9120\(03\)00062-2](http://doi.org/10.1016/s1367-9120(03)00062-2)

2833 Robertson, A.H.F., Ustaömer, T., Parlak, O., Ünlüğenç, U.C., Taşlı, K. and İnan, N., 2006.
2834 The Berit transect of the Tauride thrust belt, S Turkey: Late Cretaceous-Early
2835 Cenozoic accretionary/collisional processes related to closure of the Southern
2836 Neotethys. *J. Asian Earth Sci.* 27, 108-145.
2837 <http://doi.org/10.1016/j.jseaes.2005.02.004>

2838 Rojay, B., Altiner, D., Altiner, S.Ö., Pırlı Önen, A., James, S. and Thirlwall, M.F., 2004.
2839 Geodynamic significance of the Cretaceous pillow basalts from North Anatolian
2840 Ophiolitic Mélange Belt (Central Anatolia, Turkey): geochemical and
2841 paleontological constraints. *Geodin. Acta* 17, 349-361.
2842 <http://doi.org/10.3166/ga.17.349-361>

1
2
3
4
5
6
7
8
9
10
11
12
13
14
15
16
17
18
19
20
21
22
23
24
25
26
27
28
29
30
31
32
33
34
35
36
37
38
39
40
41
42
43
44
45
46
47
48
49
50
51
52
53
54
55
56
57
58
59
60
61
62
63
64
65

2843 Rolland, Y., Sosson, M., Adamia, S. and Sadradze, N., 2011. Prolonged Variscan to
2844 Alpine history of an active Eurasian margin (Georgia, Armenia) revealed by
2845 $^{40}\text{Ar}/^{39}\text{Ar}$ dating. *Gondwana Res.* 20, 798-815.
2846 <http://doi.org/10.1016/j.gr.2011.05.007>

2847 Roveri, M., Flecker, R., Krijgsman, W., Lofi, J., Lugli, S., Manzi, V., Sierro, F.J., Bertini, A.,
2848 Camerlenghi, A., De Lange, G., Govers, R., Hilgen, F.J., Hübscher, C., Meijer, P.T.
2849 and Stoica, M., 2014. The Messinian Salinity Crisis: Past and future of a great
2850 challenge for marine sciences. *Mar. Geol.* 352, 25-58.
2851 <http://doi.org/10.1016/j.margeo.2014.02.002>

2852 Rubatto, D., 2002. Zircon trace element geochemistry: partitioning with garnet and the link
2853 between U–Pb ages and metamorphism. *Chem. Geol.* 184, 123-138.
2854 [http://doi.org/10.1016/S0009-2541\(01\)00355-2](http://doi.org/10.1016/S0009-2541(01)00355-2)

2855 Şahin, N., Altiner, D. and Bülent Ercengiz, M., 2012. Discovery of Middle Permian
2856 volcanism in the Antalya Nappes, southern Turkey: tectonic significance and global
2857 meaning. *Geodin. Acta* 25, 286-304.
2858 <http://doi.org/10.1080/09853111.2013.858949>

2859 Sarıfakıoğlu, E., Dilek, Y., Sevin, M. and Sorkhabi, R., 2017. New synthesis of the Izmir-
2860 Ankara-Erzincan suture zone and the Ankara mélangé in northern Anatolia based
2861 on new geochemical and geochronological constraints. In: R. Sorkhabi (Editor),
2862 *Tectonic Evolution, Collision, and Seismicity of Southwest Asia: In Honor of*
2863 *Manuel Berberian's Forty-Five Years of Research Contributions. Geological*
2864 *Society of America, Special Papers*, pp. 1-63.

2865 Sayit, K., Bedi, Y., Tekin, U.K., Göncüoğlu, M.C. and Okuyucu, C., 2017. Middle Triassic
2866 back-arc basalts from the blocks in the Mersin Melange, southern Turkey:
2867 Implications for the geodynamic evolution of the Northern Neotethys. *Lithos* 268,
2868 102-113. <http://doi.org/10.1016/j.lithos.2016.10.032>

1
2
3
4
5
6
7
8
9
10
11
12
13
14
15
16
17
18
19
20
21
22
23
24
25
26
27
28
29
30
31
32
33
34
35
36
37
38
39
40
41
42
43
44
45
46
47
48
49
50
51
52
53
54
55
56
57
58
59
60
61
62
63
64
65

2869 Sayit, K., Bedi, Y., Tekin, U.K. and Okuyucu, C., 2020. Carnian (Upper Triassic) Lavas
2870 and Tuffites from the Mersin Mélange: Evidence for Intraoceanic Arc Rifting in the
2871 Northern Neotethys. *J. Geol.* 128, 445-464. <http://doi.org/10.1086/711000>

2872 Sayit, K., Göncüoğlu, M.C. and Tekin, U.K., 2015. Middle Carnian arc-type basalts from
2873 the Lycian nappes, southwestern Anatolia: Early Late Triassic subduction in the
2874 northern branch of Neotethys. *J. Geol.* 123, 561-579.
2875 <http://doi.org/10.1086/683664>

2876 Schildgen, T.F., Cosentino, D., Bookhagen, B., Niedermann, S., Yıldırım, C., Echtler, H.,
2877 Wittmann, H. and Strecker, M.R., 2012. Multi-phased uplift of the southern margin
2878 of the Central Anatolian plateau, Turkey: A record of tectonic and upper mantle
2879 processes. *Earth Planet. Sci. Lett.* 317-318, 85-95.
2880 <http://doi.org/10.1016/j.epsl.2011.12.003>

2881 Schleiffarth, W.K., Darin, M.H., Reid, M.R. and Umhoefer, P.J., 2018. Dynamics of
2882 episodic Late Cretaceous–Cenozoic magmatism across Central to Eastern
2883 Anatolia: New insights from an extensive geochronology compilation. *Geosphere*
2884 14, 1990-2008. <http://doi.org/10.1130/ges01647.1>

2885 Şengör, A.M.C. and Yılmaz, Y., 1981. Tethyan evolution of Turkey: a plate tectonic
2886 approach. *Tectonophysics* 75, 181-241. [http://doi.org/10.1016/0040-1951\(81\)90275-4](http://doi.org/10.1016/0040-1951(81)90275-4)

2887

2888 Şengör, A.M.C., Lom, N., Sunal, G., Zabcı, C. and Sancar, T., 2019. The phanerozoic
2889 palaeotectonics of Turkey. Part I: an inventory. *Mediterr. Geosci. Rev.* 1, 91-161.
2890 <http://doi.org/10.1007/s42990-019-00007-3>

2891 Şengün, F., Zack, T. and Dunkl, I., 2020. Provenance of detrital rutiles from the Jurassic
2892 sandstones in the Central Sakarya Zone, NW Turkey: U-Pb ages and trace

1
2
3
4
5
6
7
8
9
10
11
12
13
14
15
16
17
18
19
20
21
22
23
24
25
26
27
28
29
30
31
32
33
34
35
36
37
38
39
40
41
42
43
44
45
46
47
48
49
50
51
52
53
54
55
56
57
58
59
60
61
62
63
64
65

2893 element geochemistry. *Geochemistry* 80, 125667.
2894 <http://doi.org/10.1016/j.chemer.2020.125667>

2895 Shaanan, U., Avigad, D., Morag, N., GÜngör, T. and Gerdes, A., 2021. Drainage response
2896 to Arabia–Eurasia collision: Insights from provenance examination of the Cyprian
2897 Kythrea flysch (Eastern Mediterranean Basin). *Basin Res.* 33, 26-47.
2898 <http://doi.org/10.1111/bre.12452>

2899 Sharief, F.A., 1986. Depositional environments of the Triassic system in central Saudi
2900 Arabia. *Geol. J.* 21, 403-420. <http://doi.org/10.1002/gj.3350210406>

2901 Sharkov, E., Chernyshev, I., Devyatkin, E., Dodonov, A., Ivanenko, V., Karpenko, M.,
2902 Lebedev, V., Novikov, V., Hanna, S. and Khatib, K., 1998. New data on the
2903 geochronology of upper Cenozoic plateau basalts from the northeastern periphery
2904 of the Red Sea Rift area (northern Syria). *Trans. Russ. Acad. Sci.-Earth Sci. Sect.*
2905 358, 19-22.

2906 Sharkov, E., Chernyshev, I., Devyatkin, E., Dodonov, A., Ivanenko, V., Karpenko, M.,
2907 Leonov, Y.G., Novikov, V., Hanna, S. and Khatib, K., 1994. Geochronology of Late
2908 Cenozoic basalts in western Syria. *Petrology* 2, 385-394.

2909 Sherlock, S., Kelley, S., Inger, S., Harris, N. and Okay, A., 1999. ⁴⁰Ar-³⁹Ar and Rb-Sr
2910 geochronology of high-pressure metamorphism and exhumation history of the
2911 Tavsanlı Zone, NW Turkey. *Contrib. Mineral. Petrol.* 137, 46-58.
2912 <http://doi.org/10.1007/PL00013777>

2913 Stampfli, G.M. and Borel, G., 2002. A plate tectonic model for the Paleozoic and Mesozoic
2914 constrained by dynamic plate boundaries and restored synthetic oceanic isochrons.
2915 *Earth Planet. Sci. Lett.* 196, 17-33. [http://doi.org/10.1016/S0012-821X\(01\)00588-](http://doi.org/10.1016/S0012-821X(01)00588-)
2916 X

2917 Teipel, U., Eichhorn, R., Loth, G., Rohrmüller, J., Höll, R. and Kennedy, A., 2004. U-Pb
2918 SHRIMP and Nd isotopic data from the western Bohemian Massif (Bayerischer

1
2
3
4
5
6
7
8
9
10
11
12
13
14
15
16
17
18
19
20
21
22
23
24
25
26
27
28
29
30
31
32
33
34
35
36
37
38
39
40
41
42
43
44
45
46
47
48
49
50
51
52
53
54
55
56
57
58
59
60
61
62
63
64
65

2919 Wald, Germany): implications for upper Vendian and lower Ordovician magmatism.
2920 Int. J. Earth Sci. 93, 782-801. <http://doi.org/10.1007/s00531-004-0419-2>

2921 Tekin, U.K., Okuyucu, C., Sayit, K., Bedi, Y., Noble, P.J., Krystyn, L. and Göncüoğlu, M.C.,
2922 2019. Integrated Radiolaria, benthic foraminifera and conodont biochronology of
2923 the pelagic Permian blocks/tectonic slices and geochemistry of associated
2924 volcanic rocks from the Mersin Mélange, southern Turkey: Implications for the
2925 Permian evolution of the northern Neotethys. *Isl. Arc* 28, e12286.
2926 <http://doi.org/10.1111/iar.12286>

2927 Tien, C.-Y., Lin, Y.-C., Chu, M.-F., Chung, S.-L. and Bingöl, A.F., 2017. A hidden Late
2928 Cretaceous arc and subsequent magmatic events in the Caucasus-Iran-Anatolia
2929 (CIA) orogenic belt: Detrital zircon U-Pb and Hf isotopic constraints, AGU Fall
2930 Meeting Abstracts, pp. T41A-0608.

2931 Torley, J.M. and Robertson, A.H.F., 2018. New evidence and interpretation of facies,
2932 provenance and geochemistry of late Triassic-early Cretaceous Tethyan deep-
2933 water passive margin-related sedimentary rocks (Ayios Photios Group), SW
2934 Cyprus in the context of eastern Mediterranean geodynamics. *Sediment. Geol.* 377,
2935 82-110. <http://doi.org/10.1016/j.sedgeo.2018.09.001>

2936 Trifonov, V., Dodonov, A., Sharkov, E., Golovin, D., Chernyshev, I., Lebedev, V., Ivanova,
2937 T., Bachmanov, D., Rukieh, M. and Ammar, O., 2011. New data on the Late
2938 Cenozoic basaltic volcanism in Syria, applied to its origin. *J. Volcanol. Geotherm.*
2939 *Res.* 199, 177-192. <http://doi.org/10.1016/j.jvolgeores.2010.01.013>

2940 Tripathy, G.R., Singh, S.K. and Ramaswamy, V., 2014. Major and trace element
2941 geochemistry of Bay of Bengal sediments: Implications to provenances and their
2942 controlling factors. *Palaeogeogr. Palaeoclimatol. Palaeoecol.* 397, 20-30.
2943 <http://doi.org/10.1016/j.palaeo.2013.04.012>

1
2
3
4
5
6
7
8
9
10
11
12
13
14
15
16
17
18
19
20
21
22
23
24
25
26
27
28
29
30
31
32
33
34
35
36
37
38
39
40
41
42
43
44
45
46
47
48
49
50
51
52
53
54
55
56
57
58
59
60
61
62
63
64
65

2944 Tsikouras, B., Lai, C.-K., Ifandi, E., Norazme, N.A., Teo, C.-H. and Xia, X.-P., 2021. New
2945 zircon radiometric U-Pb ages and Lu-Hf isotopic data from the ultramafic-mafic
2946 sequences of Ranau and Telupid (Sabah, eastern Malaysia): Time to reconsider
2947 the geological evolution of Southeast Asia? *Geology* 49, 789-793.
2948 <http://doi.org/10.1130/G48126.1>

2949 Ustaömer, P.A., Ustaömer, T., Collins, A.S. and Robertson, A.H.F., 2009. Cadomian
2950 (Ediacaran–Cambrian) arc magmatism in the Bitlis Massif, SE Turkey: Magmatism
2951 along the developing northern margin of Gondwana. *Tectonophysics* 473, 99-112.
2952 <http://doi.org/10.1016/j.tecto.2008.06.010>

2953 Ustaömer, P.A., Ustaömer, T., Gerdes, A., Robertson, A.H.F. and Collins, A.S., 2012.
2954 Evidence of Precambrian sedimentation/magmatism and Cambrian
2955 metamorphism in the Bitlis Massif, SE Turkey utilising whole-rock geochemistry
2956 and U–Pb LA-ICP-MS zircon dating. *Gondwana Res.* 21, 1001-1018.
2957 <http://doi.org/10.1016/j.gr.2011.07.012>

2958 Ustaömer, T., Robertson, A.H.F., Ustaömer, P.A., Gerdes, A. and Peytcheva, I., 2013.
2959 Constraints on Variscan and Cimmerian magmatism and metamorphism in the
2960 Pontides (Yusufeli–Artvin area), NE Turkey from U–Pb dating and granite
2961 geochemistry. In: A.H.F. Robertson, O. Parlak and U.C. Ünlügenç (Editors),
2962 Geological Development of Anatolia and the Easternmost Mediterranean Region.
2963 Geological Society of London, Special Publications, pp. 49-74.

2964 Ustaömer, T., Ustaömer, P.A., Robertson, A.H.F. and Gerdes, A., 2016. Implications of
2965 U–Pb and Lu–Hf isotopic analysis of detrital zircons for the depositional age,
2966 provenance and tectonic setting of the Permian–Triassic Palaeotethyan Karakaya
2967 Complex, NW Turkey. *Int. J. Earth Sci.* 105, 7-38. [http://doi.org/10.1007/s00531-](http://doi.org/10.1007/s00531-015-1225-8)
2968 [015-1225-8](http://doi.org/10.1007/s00531-015-1225-8)

1
2
3
4
5
6
7
8
9
10
11
12
13
14
15
16
17
18
19
20
21
22
23
24
25
26
27
28
29
30
31
32
33
34
35
36
37
38
39
40
41
42
43
44
45
46
47
48
49
50
51
52
53
54
55
56
57
58
59
60
61
62
63
64
65

2969 Ustaömer, T., Ustaömer, P.A., Robertson, A.H.F. and Gerdes, A., 2020. U-Pb-Hf isotopic
2970 data from detrital zircons in late Carboniferous and Mid-Late Triassic sandstones,
2971 and also Carboniferous granites from the Tauride and Anatolide continental units
2972 in S Turkey: implications for Tethyan palaeogeography. *Int. Geol. Rev.* 62, 1159-
2973 1186. <http://doi.org/10.1080/00206814.2019.1636415>

2974 Uzuncimen, S., Tekin, U.K., Bedi, Y., Perincek, D., Varol, E. and Soycan, H., 2011.
2975 Discovery of the Late Triassic (Middle Carnian–Rhaetian) radiolarians in the
2976 volcano-sedimentary sequences of the Kocali Complex, SE Turkey: Correlation
2977 with the other Tauride units. *J. Asian Earth Sci.* 40, 180-200.
2978 <http://doi.org/10.1016/j.jseaes.2010.08.004>

2979 van Hinsbergen, D.J., Torsvik, T.H., Schmid, S.M., Mañenco, L.C., Maffione, M., Vissers,
2980 R.L., Gürer, D. and Spakman, W., 2020. Orogenic architecture of the
2981 Mediterranean region and kinematic reconstruction of its tectonic evolution since
2982 the Triassic. *Gondwana Res.* 81, 79-229. <http://doi.org/10.1016/j.gr.2019.07.009>

2983 Waldron, J., 1984. Structural history of the Antalya Complex in the ‘Isparta Angle’,
2984 Southwest Turkey. In: J.E. Dixon and A.H.F. Robertson (Editors), *Geological*
2985 *Evolution of the Eastern Mediterranean*. Geological Society of London, Special
2986 Publications, pp. 273-286.

2987 Watson, E.B. and Harrison, T.M., 1983. Zircon saturation revisited: temperature and
2988 composition effects in a variety of crustal magma types. *Earth Planet. Sci. Lett.* 64,
2989 295-304. [http://doi.org/10.1016/0012-821X\(83\)90211-X](http://doi.org/10.1016/0012-821X(83)90211-X)

2990 Weiler, Y., 1970. Mode of occurrence of pelites in the Kythrea flysch basin (Cyprus). *J.*
2991 *Sediment. Res.* 40, 1255-1261. [http://doi.org/10.1306/74D7217B-2B21-11D7-](http://doi.org/10.1306/74D7217B-2B21-11D7-8648000102C1865D)
2992 [8648000102C1865D](http://doi.org/10.1306/74D7217B-2B21-11D7-8648000102C1865D)

1
2
3
4
5
6
7
8
9
10
11
12
13
14
15
16
17
18
19
20
21
22
23
24
25
26
27
28
29
30
31
32
33
34
35
36
37
38
39
40
41
42
43
44
45
46
47
48
49
50
51
52
53
54
55
56
57
58
59
60
61
62
63
64
65

2993 Woodcock, N.H. and Robertson, A.H.F., 1977. Origins of some ophiolite-related
2994 metamorphic rocks of the "Tethyan" belt. *Geology* 5, 373-376.
2995 [http://doi.org/10.1130/0091-7613\(1977\)5<373:OOSOMR>2.0.CO;2](http://doi.org/10.1130/0091-7613(1977)5<373:OOSOMR>2.0.CO;2)

2996 Woodside, J., 1977. Tectonic elements and crust of the eastern Mediterranean Sea. *Mar.*
2997 *Geophys. Res.* 3, 317-354. <http://doi.org/10.1007/BF00285658>

2998 Wu, S., Yang, M., Yang, Y., Xie, L., Huang, C., Wang, H. and Yang, J., 2020. Improved in
2999 situ zircon U–Pb dating at high spatial resolution (5–16 μm) by laser ablation–
3000 single collector–sector field–ICP–MS using Jet sample and X skimmer cones. *Int.*
3001 *J. Mass Spectrom.* 456, 116394. <http://doi.org/10.1016/j.ijms.2020.116394>

3002 Xiang, W., Griffin, W.L., Jie, C., Pinyun, H. and Xiang, L., 2011. U and Th contents and
3003 Th/U ratios of zircon in felsic and mafic magmatic rocks: Improved zircon - melt
3004 distribution coefficients. *Acta Geologica Sinica (English Edition)* 85, 164-174.
3005 <http://doi.org/10.1111/j.1755-6724.2011.00387.x>

3006 Xie, L., Zhang, Y., Zhang, H., Sun, J. and Wu, F., 2008. In situ simultaneous determination
3007 of trace elements, U-Pb and Lu-Hf isotopes in zircon and baddeleyite. *Chin. Sci.*
3008 *Bull.* 53, 1565-1573. <http://doi.org/10.1007/s11434-008-0086-y>

3009 Xin, G.-Y., Chu, Y., Su, B.-X., Lin, W., Uysal, I. and Feng, Z.-T., 2021. Rapid transition
3010 from MORB-type to SSZ-type oceanic crust generation following subduction
3011 initiation: insights from the mafic dikes and metamorphic soles in the Pozanti-
3012 Karsanti ophiolite, SE Turkey. *Contrib. Mineral. Petrol.* 176, 64.
3013 <http://doi.org/10.1007/s00410-021-01821-5>

3014 Yılmaz, Y., 1989. An approach to the origin of young volcanic rocks of western Turkey. In:
3015 A.M.C. Şengör (Editor), *Tectonic Evolution of the Tethyan Region*. NATO ASI
3016 Series (Series C: Mathematical and Physical Sciences). Springer, pp. 159-189.

1
2
3
4
5
6
7
8
9
10
11
12
13
14
15
16
17
18
19
20
21
22
23
24
25
26
27
28
29
30
31
32
33
34
35
36
37
38
39
40
41
42
43
44
45
46
47
48
49
50
51
52
53
54
55
56
57
58
59
60
61
62
63
64
65

3017 Yılmaz, Y., 1993. New evidence and model on the evolution of the southeast Anatolian
3018 orogen. *Geol. Soc. Am. Bull.* 105, 251-271. [http://doi.org/10.1130/0016-7606\(1993\)105<0251:NEAMOT>2.3.CO;2](http://doi.org/10.1130/0016-7606(1993)105<0251:NEAMOT>2.3.CO;2)
3019
3020 Yu, Z., Colin, C., Wan, S., Saraswat, R., Song, L., Xu, Z., Clift, P., Lu, H., Lyle, M. and
3021 Kulhanek, D., 2019. Sea level-controlled sediment transport to the eastern Arabian
3022 Sea over the past 600 kyr: Clay minerals and SrNd isotopic evidence from IODP
3023 Site U1457. *Quat. Sci. Rev.* 205, 22-34.
3024 <http://doi.org/10.1016/j.quascirev.2018.12.006>
3025 Zanchi, A., Garzanti, E., Larghi, C., Angiolini, L. and Gaetani, M., 2003. The Variscan
3026 orogeny in Chios (Greece): Carboniferous accretion along a Palaeotethyan active
3027 margin. *Terra Nova* 15, 213-223. <http://doi.org/10.1046/j.1365-3121.2003.00483.x>
3028 Zlatkin, O., Avigad, D. and Gerdes, A., 2013. Evolution and provenance of Neoproterozoic
3029 basement and Lower Paleozoic siliciclastic cover of the Menderes Massif (western
3030 Taurides): coupled U–Pb–Hf zircon isotope geochemistry. *Gondwana Res.* 23,
3031 682-700. <http://doi.org/10.1016/j.gr.2012.05.006>
3032 Zoleikhaei, Y., Amini, A. and Zamanzadeh, S.M., 2015. Integrated provenance analysis of
3033 Zakeen (Devonian) and Faraghan (early Permian) sandstones in the Zagros belt,
3034 SW Iran. *J. Afr. Earth Sci.* 101, 148-161.
3035 <http://doi.org/10.1016/j.jafrearsci.2014.09.012>
3036
3037
3038

3039 Figure Caption

3040 Fig. 1 Outline tectonic map of the Eastern Mediterranean region and its major
3041 tectonic zones, including the main tectonic units mentioned in the text. Main data

1
2
3
4
5
6
7
8
9
10
11
12
13
14
15
16
17
18
19
20
21
22
23
24
25
26
27
28
29
30
31
32
33
34
35
36
37
38
39
40
41
42
43
44
45
46
47
48
49
50
51
52
53
54
55
56
57
58
59
60
61
62
63
64
65

3042 source MTA (2011). Abbreviations: A, Andırın; AB, Adana Basin; AC, Antalya
3043 Complex; AM, Alanya Massif; AMt, Amanos Mountain; An, Anamas; Ak, Akseki;
3044 As, Asi (Orontes); BA, Banias; BB, Baer-Bassit; BHH, Beyşehir-Hoyran-Hadim
3045 (Bözkır) nappes; BM, Bitlis Massif; BO, Bolkar nappe; BoM, Bolu Massif; CB,
3046 Cilicia Basin; Ce, Ceyhan; CyB, Cyprus Basin; D, Divriği; Do, Doğanşehir; E,
3047 Elazığ; EB, Erciyes Basin; Ec, Ecemiş corridor; En, Engizek; F, Feke; GD, Geyik
3048 Dağı; Go, Göksu; HA, Hatay (Kızıldağ); HB, Hekimhan Basin; HeB, Herodotus
3049 Basin; IA, Isparta Angle; K, Kahramanmaraş; KA, Kazdağ; KC, Konya Complex;
3050 KD, Karacahisar dome; KO, Koçali ophiolite; KP, Karaburun Peninsula; LB, Levant
3051 Basin; LnR, Larnaca Ridge; M, Muş; Ma, Malatya; MA, Mamonia Complex; MC,
3052 Maden Complex; Mi, Misis; MM, Mersin Massif; MaM, Malatya Metamorphics; OLB,
3053 Outer Latakia Basin; OR, Orhaneli; PKO, Pozantı-Karsantı ophiolite; PM, Pütürge
3054 Massif; S, Sivas; SD, Sultan Dağı; Se, Seyhan; TM, Troodos Massif; TR, Tartus
3055 Ridge; UB, Ulukışla Basin.

3056 Fig. 2 Simplified stratigraphy of the Kyrenia Range, N Cyprus (modified from
3057 McCay and Robertson, 2012). The paleocurrent data are from McCay (2010).

3058 Fig. 3 (a) Eastward view on the narrow, east-west trending Kyrenia Range, here
3059 dominated by Mesozoic thrust sheets of Trypa Group meta-carbonate rocks, E of
3060 Beylerbeyi, central range; (b) Mesozoic meta-platform carbonates and
3061 unconformably overlying Upper Eocene-Miocene turbidites of the Kythrea Group,
3062 W of Karşıyaka, western range; (c) Irregular unconformity between thick-bedded
3063 marble of the Trypa Group and pinkish basal breccia and pelagic carbonates and
3064 volcanics of the Melounda Formation, S of Karşıyaka, western range; (d) Eocene-

1
2
3
4
5
6
7
8
9
10
11
12
13
14
15
16
17
18
19
20
21
22
23
24
25
26
27
28
29
30
31
32
33
34
35
36
37
38
39
40
41
42
43
44
45
46
47
48
49
50
51
52
53
54
55
56
57
58
59
60
61
62
63
64
65

3065 Miocene turbidites of the Kythrea Group in the northern part of the Mesaoria Basin,
3066 with central Kyrenia Range behind, W of Değirmenlik; (e) Panoramic view of Upper
3067 Eocene-Miocene sandstone turbidites of the Kythrea Group in the northern part of
3068 the Mesaoria Basin, SW of Değirmenlik, central range.

3069 Fig. 4 Outline geological map of the Kyrenia Range (modified from Robertson et
3070 al., 2012b). Sample locations are indicated by coloured numbers.

3071 Fig. 5 Representative photomicrographs of sandstones analysed from the Kyrenia
3072 Range. (a) Medium to coarse-grained sandstone of the Kiparisso Vouno Member
3073 (GC19-09), with angular clasts of chert, recrystallised limestone and muscovite; (b)
3074 Detrital grains of recrystallised chert, basalt (with microphenocrysts) and
3075 metamorphic lithic fragments in the Kalograia-Ardana Formation (GC19-11); (c)
3076 Coarse-grained sandstone with angular grains of quartz (both monocrystalline and
3077 polycrystalline), together with various different rock fragments in a calcite spar
3078 cement (GC19-13; Kythrea Conglomerate); (d) Medium-grained sandstone from
3079 the Bellapais Formation (GC19-12), with abundant angular to sub-angular
3080 serpentinite grains and radiolarian chert in a calcite spar cement; (e) Medium-
3081 grained sandstone with recrystallised micritic carbonate grains, together with
3082 metamorphic lithics (e.g., mica-schist), relatively rounded quartz and feldspar, from
3083 the Klepini Formation (GC19-22); (f) Medium-grained sandstone of the Flamoudi
3084 Formation (GC19-31) showing a mixed assemblage of planktonic and benthic
3085 foraminifera; (g) Fine to medium-grained sandstone of Panagra Formation (GC19-
3086 30), with grains of quartz and carbonate including foraminifera, set in a calcite spar
3087 cement; (h) Medium-grained sandstone of the Trapeza Formation (GC19-06) with

1
2
3
4
5
6
7
8
9
10
11
12
13
14
15
16
17
18
19
20
21
22
23
24
25
26
27
28
29
30
31
32
33
34
35
36
37
38
39
40
41
42
43
44
45
46
47
48
49
50
51
52
53
54
55
56
57
58
59
60
61
62
63
64
65

3088 subangular grains of quartz, feldspar and micritic carbonate; (i) Poorly sorted
3089 sandstone of the Davlos Formation (GC19-33) with grains of serpentinite,
3090 muscovite, redeposited carbonate; (j) Sandstone of Mia Milia Formation (GC19-57)
3091 with redeposited micritic carbonate and biogenic grains including foraminifera; (k)
3092 Gypsiferous sandstone of the Yilmazköy Formation (GC19-53), with small quartz,
3093 metamorphic lithic and biogenic grains; (l) Reworked grains of calcareous red
3094 algae and foraminifera, plus detrital grains of quartz, micritic carbonate and
3095 sedimentary lithic fragments in sandstone of the Athalassa Formation (GC19-17).
3096 Abbreviations: Qz, quartz; RL, recrystallised limestone; Ch, chert; CA, calcite
3097 cement; Ms, muscovite; Md, mudstone; Bs, basalt; C, chert (variably recrystallised,
3098 both primary radiolarian chert and silica-replaced carbonate); Lm, metamorphic
3099 lithics; S, serpentinite (ophiolite-derived rock clast); Lv, volcanic lithics; Mc, micritic
3100 carbonate; F, foraminifera; Fsp, feldspar; Ls, sedimentary lithics; RA, reworked
3101 grain of calcareous red algae.

3102 Fig. 6 Kernel Density Estimation (KDE) plots for detrital zircon U-Pb ages obtained
3103 for the samples from the western (red curve) and central (green curve) Kyrenia
3104 Range (concordant ages only). Bandwidths were set at 5 Ma and 20 Ma, with fixed
3105 binwidths of 10 Ma and 30 Ma for the time windows of 0-541 Ma and 0-4000 Ma,
3106 respectively.

3107 Fig.7 Zircon Th/U ratio versus age plot for the sandstones analysed. The magmatic
3108 and metamorphic zircon fields are from Teipel et al. (2004). The fields for mafic
3109 and felsic melt-sourced zircons are from Linnemann et al. (2011). Separated Th/U
3110 data for each formation are given in Supplementary Figure S5.

1
2
3
4
5
6
7
8
9
10
11
12
13
14
15
16
17
18
19
20
21
22
23
24
25
26
27
28
29
30
31
32
33
34
35
36
37
38
39
40
41
42
43
44
45
46
47
48
49
50
51
52
53
54
55
56
57
58
59
60
61
62
63
64
65

3111 Fig. 8 Kernel Density Estimation (KDE) plots for detrital zircon U-Pb ages obtained
3112 for the samples from the eastern Kyrenia Range (blue curve) and the Karpas
3113 Peninsula (purple curve) (concordant ages only). Bandwidths were set at 5 Ma and
3114 20 Ma, with fixed binwidths of 10 Ma and 30 Ma for the time windows of 0-541 Ma
3115 and 0-4000 Ma, respectively.

3116 Fig. 9 (a-c) U/Yb versus Nb/Yb (Grimes et al., 2015) and (d-f) Nb/Hf versus Th/U
3117 (Hawkesworth and Kemp, 2006) for the zircons analysed.

3118 Fig. 10 $\epsilon\text{Hf}_{(t)}$ versus age plots of the sandstones of the western (a-c), central (d-f),
3119 eastern (g-i) Kyrenia Range and the Karpas Peninsula (j-l) analysed during this
3120 work. Abbreviations: DM, depleted mantle, data after Chauvel et al. (2008); CHUR,
3121 Chondrite Uniform Reservoir, data after Bouvier et al. (2008). The arrows show the
3122 evolutionary trends of the zircons during Late Cretaceous-Pliocene, which reflect
3123 the involvement of juvenile materials which have relatively positive $\epsilon\text{Hf}_{(t)}$ values
3124 (e.g., remnant Neotethys); recycled crustal additions have negative $\epsilon\text{Hf}_{(t)}$ values.

3125 Fig. 11 Simplified sedimentary log of the Middle-Upper Triassic to Pleistocene of
3126 the Kyrenia Range, together with the U-Pb zircon age populations obtained during
3127 this study, combined with published data from Chen et al. (2019), Shaanan et al.
3128 (2021) and Glazer et al. (2021). The dominant zircon morphology is indicated. The
3129 number of zircons in each age category are indicated within the two different boxes
3130 (euhedral/subhedral zircons) and the oval shapes (subrounded/rounded); black for
3131 the main peaks and white for the small peaks. The zircon data are indicated
3132 separately for the western, central and the eastern Kyrenia Range areas and for
3133 the Karpas Peninsula to facilitate regional comparisons.

1
2
3
4
5
6
7
8
9
10
11
12
13
14
15
16
17
18
19
20
21
22
23
24
25
26
27
28
29
30
31
32
33
34
35
36
37
38
39
40
41
42
43
44
45
46
47
48
49
50
51
52
53
54
55
56
57
58
59
60
61
62
63
64
65

3134 Fig. 12 (a) $\epsilon\text{Hf}(t)$ versus U-Pb age plot of zircons from the Triassic Sikhari Formation,
3135 the Upper Cretaceous rhyolite block, the Middle Eocene Kalogaria-Ardana
3136 Formation, the Upper Eocene-Oligocene Bellapais Formation, the Lower Miocene
3137 Flamoudi Formation and the Lower-Upper Miocene Mia Milia Formation; data from
3138 Glazer et al. (2021) and Shaanan et al. (2021); (b) $\epsilon\text{Hf}(t)$ values of Carboniferous-
3139 Recent zircons from the Kyrenia Range, compared with literature data from
3140 possible source rocks in the region. Comparative data from Fu et al. (2015), Lin et
3141 al. (2015), Karslı et al. (2016), Ustaömer et al. (2016, 2020), Tien et al. (2017),
3142 Bingöl et al. (2018), Şengün et al. (2020), Xin et al. (2021). Abbreviations: DM,
3143 depleted mantle, data after Chauvel et al. (2008); CHUR, Chondrite Uniform
3144 Reservoir, data after Bouvier et al. (2008).

3145 Fig. 13 Alternative tectonic models of the Kyrenia Range in the Eastern
3146 Mediterranean region showing sources of detrital zircons. (a) The Kyrenia Range
3147 is restored to the northern margin of Southern Neotethys (Robertson and
3148 Woodcock, 1986; McCay and Robertson, 2012; Robertson et al., 2012a, 2014):
3149 (a1) during rifting and passive margin phase; (a2) during Upper Cretaceous
3150 northward subduction; (a3) during Middle Eocene northward convergence; (a4)
3151 during Upper Miocene convergence to the south of Cyprus; (b) The Kyrenia Range
3152 is restored as part of the distal, N Africa continental margin (Maffione et al., 2017;
3153 McPhee and van Hinsbergen, 2019). This model focusses on the Upper
3154 Cretaceous-Upper Miocene tectonic development, while assuming the prior
3155 existence of an oceanic basin with the Kyrenia Range on its southern, passive
3156 margin (i.e., N Africa-Arabia): (b1) the Upper Cretaceous ophiolites form within S

1
2
3
4
5
6
7
8
9
10
11
12
13
14
15
16
17
18
19
20
21
22
23
24
25
26
27
28
29
30
31
32
33
34
35
36
37
38
39
40
41
42
43
44
45
46
47
48
49
50
51
52
53
54
55
56
57
58
59
60
61
62
63
64
65

3157 Neotethys far to the NE; the subducting slab then rolls back and ‘invades’ the
3158 eastern Mediterranean and is emplaced southwards onto the N Africa-Arabia
3159 continental margin and northwards onto Tauride crust; (b2) the Middle Eocene
3160 remained passive, with the Kyrenia Range still attached to N Africa; (b3) northward
3161 subduction is activated south of Cyprus, similar to (aiv); (c) The Kyrenia Range is
3162 restored as a far-travelled allochthonous unit derived from the southern margin of
3163 Eurasia (Glazer et al., 2021); alternative positions are indicated by dashed circles:
3164 (c1) the model focusses on the Triassic to Mid-Eocene development of the Kyrenia
3165 Range. The Kyrenia Range is located along the Eurasian active margin, with a
3166 setting along the outer north-Gondwana margin (Anatolides) as an alternative; (c2)
3167 zircons were still able to reach the Kyrenia Range in its far-northerly position; (c3)
3168 the entire Kyrenia Range was tectonically transported to near its present position
3169 in the northeastern Mediterranean region, cutting off zircon supply from Eurasia.

3170

3171